FACULTY OF SCIENCE
UNIVERSITY OF COPENHAGEN

Investigating multi-qubit noise in superconducting qubit arrays

Master's Thesis in Physics

Written by *Thomas Schrøder Terneborn*

20-05-2021

Supervised by
Mark Rudner

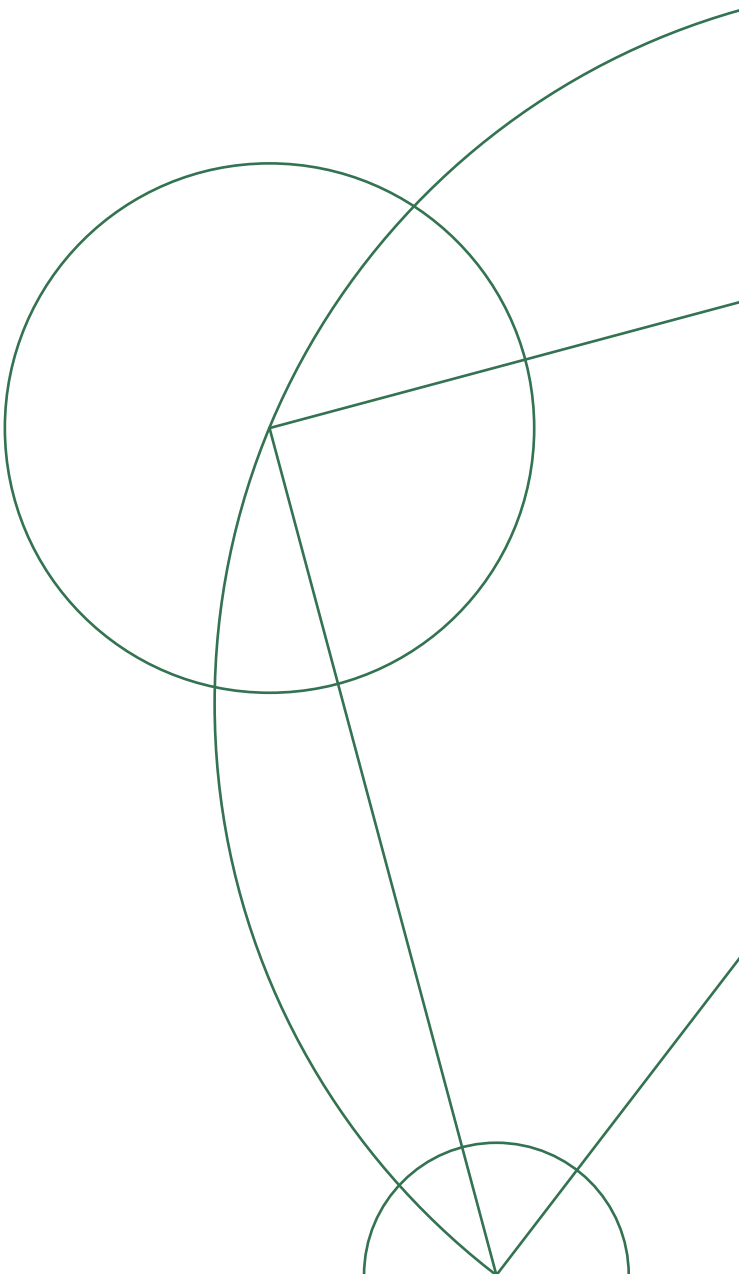

Abstract

The recently developed universal Lindblad equation is employed in predicting and quantizing the noise incumbent upon a system of two coupled superconducting qubits, as well as a system of four qubits modelled as a Heisenberg chain. Additionally the evolution of said systems are numerically simulated using the stochastic Schrödinger equation. The numerical data suggest that the coupling between qubits will cause the noise to spread from qubit to qubit eventually causing errors that are not restricted to affect only one qubit but several qubits at once, depending on the nature of the coupling.

Acknowledgements

Thank you to my supervisor Mark Rudner for making this thesis possible and giving me a chance to understand and learn this much about an interesting subject. Our discussions and his many challenging questions has pushed me beyond my comfort zone and forced me to dive into and get comfortable with subjects I found very difficult.

Thank you to Frederik Nathan for being a tremendous source of information and help. He took much time to answer my pestering questions, and I am much obliged to him as well for all that I have learned throughout this project.

Finally, thank you to Morten Kjaergaard for an insightful discussion and sharing experimental results to compare to the theoretical ones presented in this thesis. This was a great motivation to me in pursuing the final product.

Contents

Chapter 1

Introduction

Over the last couple of decades the publication rate on quantum computing has been steeply increasing, and research within the field is widely supported by government investments and technological businesses[1]. The reason for the ongoing interest in quantum computation can be attributed to different factors. For example, a quantum computer can significantly reduce the complexity of certain computational tasks compared to its classical counterpart[2, 3]. Additionally, the development of quantum computers may even prove a necessity in order to maintain the ongoing progress in computational power. If the number of transistors per square inch on integrated circuits in classical computers continues to grow, then eventually the components will reach such small scales, that quantum effects will start to dominate[2, 4].

The building blocks of quantum computers are the quantum mechanical version of classical bits, called qubits. Whereas a bit can attain either the value 0 or 1, the quantum mechanical phenomenon of superposition enables the qubit to be both 0 and 1 at the same time. This is the main cause for their computational superiority mentioned above. Hence, any quantum system that allows for the isolation of a 2-dimensional subspace qualifies as a qubit, and several candidates for a working qubit have been suggested so far. Among these are trapped ions [5] and electron spins in quantum dots [6].

Another type of qubit which will be at the focus of this thesis is the superconducting circuit qubit. While the Hamiltonians describing the qubit system in principle can be effectively the same for different types of qubits, the sources of noise incumbent upon the different types of systems presumably differ in general. When noise from the environment is taken into account in the study of a quantum system it is usually referred to as an open quantum system. For reasons that will be clarified in Sec. 3.2 an efficient description of the evolution of open quantum systems is the equation of motion for the density matrix describing the system, otherwise known as a master equation. The most general form of a master equation describing a system undergoing Markovian evolution (to be defined in Sec. 3.1) is the Lindblad form which employs the so-called "jump operators" (to be further described in Chapter 4) which describes the dissipation of the system[7, 13]. Up until recently there was no known viable Lindblad form master equation to describe systems with a very fine energy level structure. For instance, the quantum optical master equation (QOME) imposes stringent conditions on the level structure of the system for which it acts as a good description of the system dynamics[12, 14]. In the case of coupled qubits it is easy to conceive of an energy level structure similar to that of a Heisenberg model spin chain, which has the implication that the energy level spacing is exponentially suppressed in the number of spins (or qubits). Hence, the QOME might not be a viable option for the description of coupled qubits. Luckily, in [8] they derive a Lindblad form master equation which they refer to as the universal Lindblad equation (ULE), due to the fact that no assumption about

the system is made throughout its derivation. Hence the ULE can safely be applied to any system regardless of its energy level structure, as long as its evolution is Markovian. As such the ULE will be employed in the study of the superconducting qubits in this thesis. The objective is to ascertain the nature of the noise incumbent on a small system of two coupled superconducting qubits as well as the evolution this noise gives rise to as predicted by the ULE. Such a system was recently experimentally realized in [29], where they among other things attempt to estimate the "jump operators" that arise from various noise channels ("noise channels" will be defined in Chapter 3).

The thesis is structured accordingly: in Chapter 2 a general description of qubits and the noise and errors they may experience is presented, along with how a multi-qubit system may be programmed conveniently. Additionally, superconducting qubits are expounded upon more particularly with how they may be engineered physically. Chapter 3 concerns the evolution of open quantum systems. Specifically Markovian evolution is in focus and the requirements necessary for the evolution to be considered Markovian. Chapter 4 provides a thorough review of the results pertaining to the ULE derived in [8]. It also presents the QOME and compares these two Lindblad master equations. Finally, there is a demonstration of how the evolution of a quantum system according to the ULE may be efficiently simulated using the stochastic Schrödinger equation (SSE). Chapter 5 presents several results of a simulation of two coupled superconducting qubits, and Chapter 6 presents a few results of a simulation of a system of four qubits modelled as a closed Heisenberg chain. Finally, Chapter 7 concludes the thesis. Besides the main text there are two appendixes. App. A provides some of the minute details of the derivations of the master equations presented in the main text, and App. B contains a derivation of the correlation and spectral functions for a bath of electromagnetic modes of both discrete and continuous spectra.

Chapter 2

Generally on qubits

A qubit is simply a two-level system such as a spin-1/2 particle, where the ground state and excited state will be denoted $|0\rangle$ and $|1\rangle$ respectively. Hence, the most general normalized pure state for a qubit can be expressed as $\alpha|0\rangle + \beta|1\rangle$, with $|\alpha|^2 + |\beta|^2 = 1$. The matrix representation of these states is chosen such that:

$$|0\rangle = \begin{pmatrix} 1 \\ 0 \end{pmatrix} \text{ and } |1\rangle = \begin{pmatrix} 0 \\ 1 \end{pmatrix}. \tag{2.1}$$

Evidently the Hilbert space of a single qubit is 2-dimensional, and so its density matrix ρ is a 2×2-matrix. The density matrix will be more closely defined in Sec. 3.2. Suffice it say now that it is a Hermitian matrix describing the state of a system. Observe that any Hermitian 2×2-matrix has four real parameters, so generally this density matrix can be expressed:

$$\rho = \begin{bmatrix} a & c - id \\ c + id & b \end{bmatrix}, \text{ with } a, b, c, d \in \mathbb{R}. \tag{2.2}$$

As such it can be expanded in terms of the identity and the Pauli matrices: $\{\mathbb{1}, \sigma_x, \sigma_y, \sigma_z\}$[30]. Recalling that the trace of the density matrix is 1, the general expansion can be written:

$$\rho = \frac{1}{2}\left(\mathbb{1} + \mathbf{P} \cdot \vec{\sigma}\right), \text{ where } \mathbf{P} = \begin{pmatrix} P_x \\ P_y \\ P_z \end{pmatrix} \text{ and } \vec{\sigma} = \begin{pmatrix} \sigma_x \\ \sigma_y \\ \sigma_z \end{pmatrix}, \tag{2.3}$$

because the trace of each Pauli matrix is zero ($\mathbb{1}$ being the identity matrix). The vector $\mathbf{P}$ has real entries and is often referred to as the Bloch vector. It can be used as a visual representation of the quantum state of the two-level system as is shown in Fig. 2.1. For pure states the Bloch vector has unit length and points onto the Bloch sphere. In this case the pure state $|\psi\rangle$ can be expressed in terms of the polar angle θ and azimuthal angle ϕ (see Fig. 2.1 for reference) as such:

$$|\psi\rangle = \cos\left(\frac{\theta}{2}\right)|0\rangle + \mathrm{e}^{i\phi}\sin\left(\frac{\theta}{2}\right)|1\rangle. \tag{2.4}$$

For mixed states the Bloch vector points inside the Bloch sphere, and hence its length is a measure of the purity of the state.

The matrix representation of the Pauli matrices is:

$$\sigma_x = \begin{bmatrix} 0 & 1 \\ 1 & 0 \end{bmatrix}, \sigma_y = \begin{bmatrix} 0 & -i \\ i & 0 \end{bmatrix} \text{ and } \sigma_z = \begin{bmatrix} 1 & 0 \\ 0 & -1 \end{bmatrix}. \tag{2.5}$$

Sometimes the subscripts $(1, 2, 3)$ are used instead of (x, y, z), and the subscript 0 signifies the identity $\sigma_0 = \mathbb{1}$. Hence it follows that $\sigma_a\sigma_b = \delta_{ab}\mathbb{1} + i\varepsilon_{abc}\sigma_c$, where δ_{ab} is

the Kronecker delta defined as: $\delta_{ab} = 1$ for $a = b$ and $\delta_{ab} = 0$ otherwise. ε_{abc} is the Levi-Civita symbol defined as: $\varepsilon_{abc} = 1$ if (a, b, c) is an even permutation of $(1, 2, 3)$, $\varepsilon_{abc} = -1$ if (a, b, c) is an odd permutation of $(1, 2, 3)$, and $\varepsilon_{abc} = 0$ for repeated indices. With this, and observing that the trace of the Pauli matrices is zero, it further follows:

$$\langle \sigma_i \rangle = \mathrm{tr}\left[\sigma_i \rho\right] = P_i. \tag{2.6}$$

Since P_i is real, the Pauli operators represent observables of the system and so they can conveniently be used to construct the Hamiltonian of the system. Usually the Pauli operators represent the observable spin of a spin-1/2 particle, but as has just been shown they are convenient to use for any general two-level system.

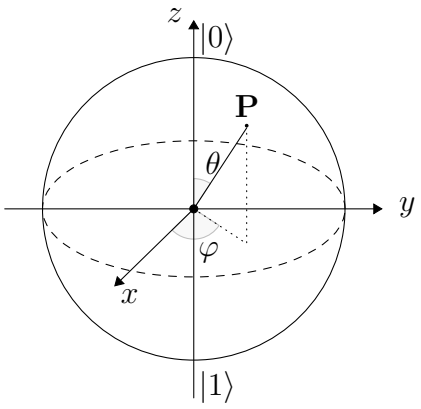

Figure 2.1: The Bloch vector **P** represents the state of a two-level system, where for pure states it has unit length and points onto the Bloch sphere and for mixed states it points inside the Bloch sphere. The point of the sphere's intersection with the z-axis at $z = 1$ represents the state $|0\rangle$, and the opposite point at $z = -1$ represents $|1\rangle$ (this defines the axis of quantization, and the z-axis is the common choice). Hence, all other points on and inside the Bloch sphere not on the z-axis represents states in a superposition of $|0\rangle$ and $|1\rangle$. The state represented by **P** in the figure is $\cos(\theta/2)\,|0\rangle + \mathrm{e}^{i\phi}\sin(\theta/2)\,|1\rangle$ [23]. The code for this figure is provided at [27].

2.1 Programming qubits and qubit Hamiltonians

When programming a system consisting of several qubits there is a choice as to, how the multi-qubit state is represented by a vector. In this thesis, the choice is as follows: for a system of N qubits in the multi-qubit state $|n_0 n_1 n_2 ... n_i ... n_{N-1}\rangle$ (where each n_i is either 0 or 1 corresponding to the single qubit state $|0\rangle$ or $|1\rangle$ respectively) an integer p is defined:

$$p = 1 + \sum_{i=0}^{N-1} 2^i n_i. \tag{2.7}$$

Then this state is represented by a $2^N \times 1$ vector, where the pth entry is 1 and all other entries are 0. For example, the state $|110\rangle$ has $p = 4$ and so:

$$|110\rangle = \begin{pmatrix} 0 \\ 0 \\ 0 \\ 1 \\ 0 \\ 0 \\ 0 \\ 0 \end{pmatrix}.$$

This definition determines how the multi-qubit Pauli matrices are defined. If $\sigma_a^{(j)}$ represents the Pauli operator σ_a acting on the jth qubit (counting from the left in the multi-qubit state ket) then this operator is given by the tensor product:

$$\sigma_a^{(j)} = \underset{N}{\mathbb{1}} \otimes \cdots \otimes \underset{j}{\sigma_a} \otimes \cdots \otimes \underset{3}{\mathbb{1}} \otimes \underset{2}{\mathbb{1}} \otimes \underset{1}{\mathbb{1}}.$$

Notice that the order of the operators in the tensor product is reversed compared to the order of the multi-qubit state ket. This is a result of the choice of the vector representation of the states. As an example, notice the difference between the matrix representations of $\sigma_x^{(1)}$ and $\sigma_x^{(2)}$ for a system of two qubits:

$$\sigma_x^{(1)} = \mathbb{1} \otimes \sigma_x = \begin{bmatrix} 1 & 0 \\ 0 & 1 \end{bmatrix} \otimes \begin{bmatrix} 0 & 1 \\ 1 & 0 \end{bmatrix} = \begin{bmatrix} 0 & 1 & 0 & 0 \\ 1 & 0 & 0 & 0 \\ 0 & 0 & 0 & 1 \\ 0 & 0 & 1 & 0 \end{bmatrix}.$$

$$\sigma_x^{(2)} = \sigma_x \otimes \mathbb{1} = \begin{bmatrix} 0 & 1 \\ 1 & 0 \end{bmatrix} \otimes \begin{bmatrix} 1 & 0 \\ 0 & 1 \end{bmatrix} = \begin{bmatrix} 0 & 0 & 1 & 0 \\ 0 & 0 & 0 & 1 \\ 1 & 0 & 0 & 0 \\ 0 & 1 & 0 & 0 \end{bmatrix}.$$

This can be verified by using that the action of $\sigma_x^{(j)}$ is to "flip" the state of the jth qubit. Hence, $\sigma_x^{(1)}|00\rangle = |10\rangle$ and $\sigma_x^{(2)}|00\rangle = |01\rangle$, which indeed is the case with the definition above.

With that it is straight forward to define any Hamiltonian in terms of the Pauli matrices, and most programming software has inbuilt functions for diagonalizing square matrices and finding eigenvectors thereof.

2.2 Superconducting qubits

A superconducting qubit can be engineered as a small circuit consisting of a Josephson junction running in parallel with a capacitor (see Fig. 2.2). A Josephson junction is

made of two superconducting electrodes separated by a thin barrier, which give rise to a current and voltage given by the Josephson equations[9, 23]:

$$I = I_c \sin(\phi) \text{ and } V = \frac{\hbar}{2e}\partial_t \phi, \tag{2.8}$$

where ϕ is referred to as the superconducting phase, and the critical current I_c is the maximum supercurrent the junction can support before losing its superconducting properties. The superconducting phase is given by the reduced flux $\phi = 2\pi\Phi/\Phi_0$, where Φ is the flux due to the circuit, and $\Phi_0 = h/2e$ is the superconducting magnetic flux quantum[23]. Here the $2e$ reflects the Cooper-pair particles consisting of two bound electrons (e being the elementary charge, the charge of an electron), which emerge when the metal passes into the superconducting phase. The two relations above result in the Hamiltonian:

$$H = 4E_C n^2 - E_J \cos(\phi), \tag{2.9}$$

where $E_C = e^2/2C_\Sigma$, with $C_\Sigma = C_s + C_J$ being the total capacitance of the circuit, and $E_J = I_c\Phi_0/2\pi$. The energy E_C is the charging energy required to add each electron of the Cooper-pair to the island, and E_J is the Josephson energy[23]. The charge number n is the number of Cooper-pairs on the island, given by $Q/2e$ with Q being the total charge on the island (the caption to Fig. 2.2 explains what is meant by "the island").

In connection with the quantum harmonic oscillator, as discussed in App. B.1, the operators n and ϕ can be regarded as canonically conjugate variables, and so the first term in the Hamiltonian Eq. (2.9) can be regarded as the kinetic energy, and the second term the potential energy. The introduction of the Josephson junction has caused this potential energy to take a cosinusoidal rather than a parabolic form, which means that the energy levels are not equidistant, as shown in Fig. 2.2. The difference between the ground state and the first excited state, ω_{01}, is greater than the difference between the first excited state and the second excited state, ω_{12}. This anharmonicity of the energy levels makes it possible to isolate the two lowest levels $|0\rangle$ and $|1\rangle$, forming a computational subspace that effectively behaves as a qubit, simplyfing the Hamiltonian to:

$$H = \frac{\omega_q}{2}\sigma_z, \text{ where } \omega_q = \frac{\sqrt{8E_J E_C} - E_C}{\hbar}. \tag{2.10}$$

and $\omega_q = \omega_{01}$ is the qubit frequency, otherwise known as the splitting of the qubit[23].

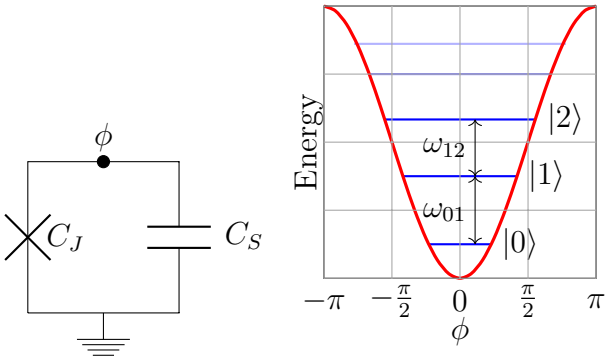

Figure 2.2: **Left:** a schematic of an example of a simple qubit circuit. The bottom of the circuit is connected to the ground, and on the left is a Josephson junction symbolized by a cross, and on the right is a capacitor symbolized by to parallel lines. The Josephson junction and capacitor isolates the top of the circuit from the part connected to the ground, forming an island with superconducting phase ϕ. **Right:** a sketch of the potential energy spectrum due to the circuit on the left. The Josephson junction causes the potential to have a cosinusoidal shape, making the energy levels anharmonically spaced. This provides a computational subspace consisting of the two lowest energy states $|0\rangle$ and $|1\rangle$ which effectively can be treated as a qubit. This figure is inspired by [23].

In order to implement high-fidelity gate operations and store quantum information in the qubit, it is favourable to be able to tune the qubit splitting[23, 26]. One way of doing this is by replacing the single Josephson junction in the circuit in Fig. 2.2 with a loop consisting of two parallel Josephson junctions as shown in Fig. 2.3, and threading the loop with an external magnetic field resulting in a flux Φ_{ext}. This external flux reduces the effective critical current shared by the two Josephson junctions, and so by varying Φ_{ext} the Josephson energy E_J can be tuned. This makes it possible to control the qubit splitting, and so an array of qubits can be brought into resonance with one another allowing them to interchange energies when needed[23]. It can also be used to implement a detuning between qubits in order to keep them out of resonance to avoid this type of interaction. This tuning of the qubit frequency emulates the behavior of a spin-1/2 particle in a magnetic field. By varying the strength of the magnetic field the energy splitting between the spin-up and spin-down state of the particle can be controlled. Specifically, the Josephson energy in Eqs. (2.9) and (2.10) is replaced by the tunable effective Josephson energy[23]:

$$E'_J(\phi_e) = 2E_J \left|\cos(\phi_e)\right|, \text{ where } \phi_e = \frac{\pi\Phi_{\text{ext}}}{\Phi_0}. \tag{2.11}$$

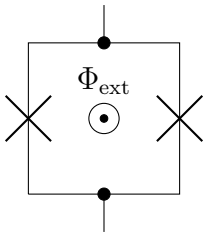

Figure 2.3: In order to tune the qubit splitting of the superconducting circuit qubit in Fig. 2.2, the single Josephson junction can be replaced by a loop of two parallel Josephson junctions as shown here. By threading the loop with a magnetic field the splitting is decreased, and so by varying the magnetic flux Φ_{ext} through the loop the splitting can be controlled.

Another property of spin-1/2 particles, that it is favourable to have qubits emulating, is the coupling of their spin[15]. There are different ways in which to couple superconducting circuit qubits that lead to coupling along different axes, distinguishing between longitudinal and transverse coupling compared to the quantization axis. One way to achieve coupled circuit qubits is by connecting the islands of the qubits through a capacitor C_g, as shown in Fig. 2.4 (a). This will give rise to a Hamiltonian of three parts: $H = H_1 + H_2 + H_{\text{int}}$, where H_1 and H_2 are the separate Hamiltonians of the two qubits given by Eq. (2.9) or effectively Eq. (2.10), and H_{int} is the Hamiltonian describing the interaction of the two qubits given by[23]:

$$H_{\text{int}} = C_g V_1 V_2, \tag{2.12}$$

where V_1 and V_2 are the voltage operators of the respective qubit islands. In the weak coupling limit $C_g \ll C_1, C_2$, where C_1 and C_2 are the shunt capacitance for the respective qubits, the interaction Hamiltonian effectively takes the form:

$$H_{\text{int}} = g\sigma_x^{(1)}\sigma_x^{(2)}, \tag{2.13}$$

where g is the qubit-qubit coupling energy. This can be tuned by altering the geometry of the capacitor, i.e. by changing its size or the distance between the capacitor plates. The capacitive coupling may as well be chosen along the y-direction as long as it is transverse to the axis of quantization, but an additional coupling of the qubits by means of induction makes it possible to have the qubits coupled along both transverse directions. Inductive coupling is achieved by moving two looped circuit qubits into close proximity of each other, such that the magnetic field due to the looped current in the one circuit induces a current in the other circuit and vice versa (see Fig. 2.4 (b)). This gives rise to an interaction term in the Hamiltonian given by $H_{\text{int}} = M_{12} I_1 I_2$, where M_{12} is the mutual inductance due to the two inductances L_1 and L_2, and I_1 and I_2 are the current operators of the respective circuits given by the Josephson current in Eq. (2.8). Similarly to capacitive coupling in the weak coupling limit this Hamiltonian effectively takes the form of Eq. (2.13), alternatively with the coupling along the y-direction. The inductive coupling can also be tuned by moving the qubit circuits closer or farther apart. The circuit loops may even be brought to overlap to further increase the coupling.

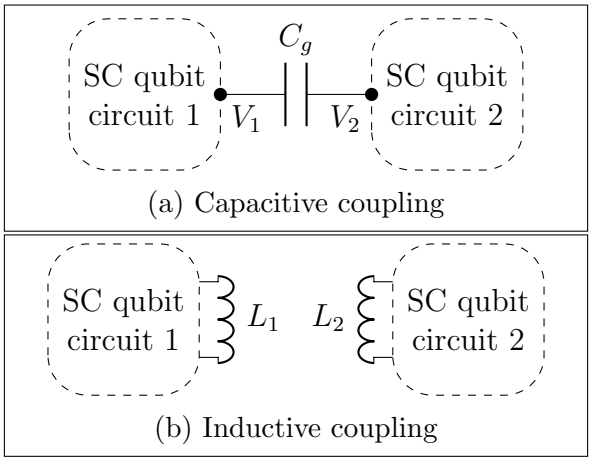

Figure 2.4: This figure illustrates how superconducting qubits can be coupled both (a) capacitively and (b) inductively. Take note that L_1 and L_2 do not represent coils in the circuits but simply the inductance due to the looped currents in the circuits.

2.3 Noise and errors on qubits

A quantum computer will inevitably interact with its environment which leads to the decay of the quantum information stored in the qubits making up the device[31]. This coupling of the qubits to the environment is what is referred to as noise, and noise leads to logical errors in the information stored in the qubits. For examble, a qubit in the state $|0\rangle$ can undergo a bit flip error when it experiences a certain type of noise which takes it to the state $|1\rangle$, thus disrupting the information.

With the Bloch vector picture (see Fig. 2.1) of the state of a qubit it is convenient to distinguish the types of noise that induce errors in the qubit state. In the qubit frame the z-axis is longitudinal, and so *longitudinal noise* corresponds to errors acting with σ_z on the qubit. The $x-y$ plane is transverse in the qubit frame, and so *transverse noise* corresponds to errors with σ_x or σ_y acting on the qubit[23]. Longitudinal noise leads to pure dephasing of the qubit state, as the action of a noise operator proportional to σ_z on the qubit destroys the information stored in the phase of the qubit state. Observe for instance the action of the error operator σ_z on the state in Eq. (2.4):

$$\begin{aligned}\sigma_z |\psi\rangle &= \cos\left(\frac{\theta}{2}\right)|0\rangle - \mathrm{e}^{i\phi}\sin\left(\frac{\theta}{2}\right)|1\rangle \\ &= \cos\left(\frac{\theta}{2}\right)|0\rangle + \mathrm{e}^{i(\phi+\pi)}\sin\left(\frac{\theta}{2}\right)|1\rangle .\end{aligned}$$

Hence, longitudinal noise causes the Bloch vector to precess about the z-axis as depicted on the Bloch sphere in Fig. 2.5 (a). The polar angle θ, however, is left undisturbed by longitudinal noise, and so the qubit's polarization along the z-axis is intact.

Transverse noise, on the contrary, causes depolarization along the z-axis. This occurs due to energy exchange with the bath and results in transitions between the states $|0\rangle$ and $|1\rangle$. This is evident when considering a noise operator of the simple form σ_x acting on the state $|1\rangle$: $\sigma_x |1\rangle = |0\rangle$ (also depicted on the Bloch sphere in Fig. 2.5

(b)). In [23] the provide a more thorough revision of noise on superconducting qubits which has also been the main inspiration for this section.

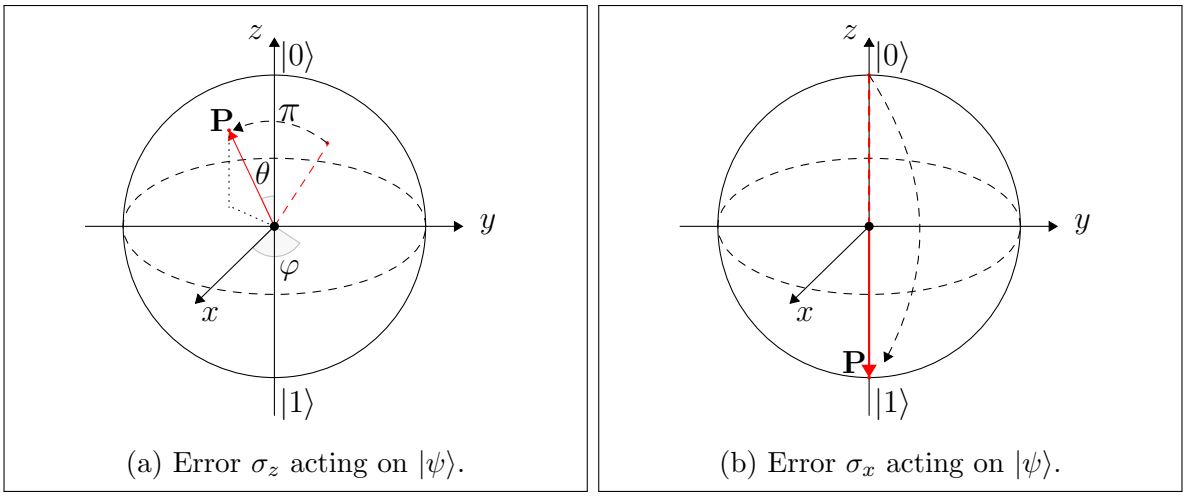

(a) Error σ_z acting on $|\psi\rangle$.

(b) Error σ_x acting on $|\psi\rangle$.

Figure 2.5: The error operators σ_z (a) and σ_x (b) acting on the state $|\psi\rangle$ in Eq. (2.4) represented on the Bloch sphere.

Chapter 3

Evolution of open quantum systems

When constructing quantum systems to be used for logical computations, they should ideally be closed systems so as to avoid unwanted correlations between the system and its environment, which ultimately leads to logical errors. However, as it is not possible to have local systems that are completely isolated from its surroundings, it is necessary to understand how a system develops under the influence of uncontrolled interactions with its environment, which will often be denoted the bath.

If $\mathcal{H}_\mathcal{S}$ and $\mathcal{H}_\mathcal{B}$ represent the Hilbert spaces of the system and the bath respectively, then the Hilbert space of the composite system (otherwise referred to as the bipartite system) is given by the tensor product $\mathcal{H}_\mathcal{S} \otimes \mathcal{H}_\mathcal{B}$.

3.1 Open quantum systems and Markovian evolution

In this section, general open quantum systems will be studied using as the foundation a Hamiltonian that incorporates an entirely general system and bath:

$$H(t) = H_\mathcal{S}(t) + H_\mathcal{B} + H_{\mathcal{SB}}. \tag{3.1}$$

Here $H_\mathcal{S}(t)$ and $H_\mathcal{B}$ are the Hamiltonians for the system and bath respectively, and $H_{\mathcal{SB}}$ describes the interactions between the system and bath. This part can be decomposed as:

$$H_{\mathcal{SB}} = \sqrt{\gamma} \sum_\alpha X_\alpha B_\alpha, \tag{3.2}$$

where X_α is a dimensionless Hermitian operator acting on the Hilbert space of the system $\mathcal{H}_\mathcal{S}$, and B_α is a Hermitian operator with units of $[\text{energy}]^{1/2}$ acting on the Hilbert space of the bath $\mathcal{H}_\mathcal{B}$. The α-s label the different noise channels through which the system and bath interact, and γ is an energy scale parametrizing the coupling strength of these noise channels.The coupling is chosen to appear in a square root in the Hamiltonian for convenience, because later $\sqrt{\gamma}$ will appear in only even powers in the master equations to be derived. This choice in turn means that the bath operators have dimensions of $[\text{Energy}]^{1/2}$, but this is a natural choice for a bath of a continuous energy spectrum such as an Ohmic bath[8]. More information on Ohmic baths is provided in Sec. 3.5.

There is a particular type of evolution of open quantum systems that will be the cornerstone for all the systems that are studied in this thesis, and that is Markovian evolution. Markovian evolution describes a process, where the future state of a system is entirely determined by its present state, without reference to the system's past. This imposes some restrictions on the bath that the system is connected to, as will be shown presently. Fig. 3.1 at the end of this section presents an example of two cases, where a two-level system is connected to a bath of photonic modes, and at some distance

from the system a mirror that perfectly reflects photons is located. In the one case the bath consists of such a small number of photons, that a photon emitted from the system can pass through the bath, be reflected on the mirror, and return to the system re-exciting it to its prior state. If the system decays and emits a photon at time t_i and reabsorbs the same photon at time t_f, then only knowing the state of the system at a time t between t_i and t_f will not provide the information, that the system is about to reabsorb a photon it emitted in the past. In that case it is necessary to know the history of the system in order to make predictions about its future, and so this case does not present a system described by Markovian dynamics.

In the other case the bath is full of photons, such that when the system decays at the emission of a photon, there is a large probability that the system will have absorbed a different photon from the bath, before the emitted photon has returned. Hence, in this case it is possible to make predictions about the future of the system without knowing its state in the past, as long as the statistical properties of the bath are available.

The only thing distinguishing the two cases is the statistics of the bath. From this example one property that is instrumental to providing a "good" Markovian bath can be inferred, namely that the correlations of the bath should decay rapidly on the timescale of system-bath interactions[8]. In the case of the "bad" Markovian bath the characteristic decay time of the bath correlations τ is comparable to or longer than the time interval $t_f - t_i$, whereas in the other case it is much shorter $\tau \ll t_f - t_i$. More generally, the inequality $\tau \ll \Gamma^{-1}$ should be fulfilled, where Γ is the rate of system-bath interactions. The parameters τ and Γ will be accurately defined later in Sec. 3.4.

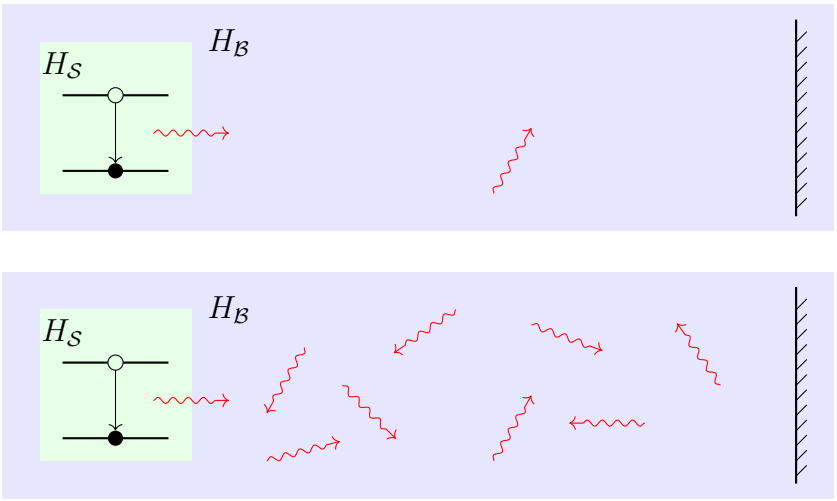

Figure 3.1: **Top:** a two-level system (green) decays at the emission of a photon (red arrow) into a bath (blue) consisting of a small number of photons. On the far right at some distance from the system is located a mirror that perfectly reflects incoming photons. Since there are only a few photons in the bath, there is a very small probability that any of these photons will re-excite the system, before the particular photon emitted by the system will have travelled to the mirror and back to the system again, re-exciting it itself. Hence, in this case the information stored in the system is not lost to the bath but returns at a later time. This does not constitute Markovian evolution. **Bottom:** here everything is the same except that there is a much larger number of photons in the bath. Hence, the probability for any of these photons to re-excite the system is large, and this essentially means that the information stored in the system is lost to the bath.

3.2 The density matrix and its evolution

The density matrix is an efficient choice for monitoring the evolution of an open quantum system, because in addition to the information kept in a state ket it also incorporates information about how much is known about the system, and whether the system is entangled with its environment. Entanglement of the system and bath makes the state kets of the system and bath inseparable, such that the state ket of the system cannot be isolated from the state ket of the bath. However, the bath can always be traced out of the density matrix of the bipartite system, such that the reduced density matrix of the system alone is given by $\rho = \mathrm{tr}_{\mathcal{B}}[\rho_{\mathcal{SB}}]$. The state ket would be a sufficient choice, if the system was guaranteed to be always in a pure state, but since that is only truly possible for closed systems it is necessary to understand the behavior of mixed ensembles.

A mixed ensemble denotes an ensemble where a fraction of the members are characterized by $|\phi^{(i)}\rangle$ with relative population w_i, and so the density matrix is constructed as:

$$\rho(t) = \sum_i w_i \, |\phi^{(i)}(t)\rangle \, \langle \phi^{(i)}(t)| \, , \tag{3.3}$$

with the fractional populations obeying $\sum_i w_i = 1$. Eq. (3.3) is the most general form of a density matrix representing an ensemble that is undisturbed, and if for instance $w_k = 1$ and $w_i = 0$ for all $i \neq k$ then it is a pure ensemble. That the ensemble is left undisturbed is manifested in the fractional populations being time-independent, because they cannot change in this case ([10] p. 185). This is indeed the case when the ensemble is the aforementioned bipartite system of the system and bath, because there is nothing beyond that to influence the composite system. Note that the definition Eq. (3.3) ensures that $\mathrm{tr}(\rho) = 1$, and $\langle\psi|\,\rho\,|\psi\rangle \geq 0$ for any state $|\psi\rangle$, which is to say that the density matrix is positive[30]. Furthermore, expectation values of an observable A can be found as $\langle A\rangle = \mathrm{tr}(A\rho)$.

To establish the evolution of the density matrix the time-derivative of Eq. (3.3) is taken, using that the states $|\phi^{(i)}\rangle$ obey the Schrödinger equation:

$$\begin{aligned}\partial_t\rho &= \sum_i w_i \left(\left(\partial_t\,|\phi^{(i)}\rangle\right)\langle\phi^{(i)}| + |\phi^{(i)}\rangle\left(\partial_t\,\langle\phi^{(i)}|\right)\right)\\ &= -\,i\sum_i w_i\left(H\,|\phi^{(i)}\rangle\langle\phi^{(i)}| - |\phi^{(i)}\rangle\langle\phi^{(i)}|\,H\right).\end{aligned}$$

This leads to the von Neumann equation:

$$\partial_t\rho(t) = -i\,[H(t),\rho(t)]\,. \tag{3.4}$$

In the framework of the open quantum system discussed above the density matrix in Eq. (3.4) is the one for the bipartite system $\rho_{\mathcal{SB}}$, and the Hamiltonian is the composite one in Eq. (3.1).

3.3 The Bloch-Redfield equation

The Bloch-Redfield (BR) equation is the first equation of motion for a density matrix representing and open quantum system to be investigated in this thesis. For simplicity, the derivation of the BR equation is made for only one noise channel such that there is only one term in Eq. (3.2). The derivation is largely based on [8].

It is easiest to derive it in the interaction picture, where states and operators are transformed by a rotation of frame according to the non-interacting part of the Hamiltonian $H_{\mathcal{S}}(t) + H_{\mathcal{B}}$. Then, in the interaction picture, the bipartite system evolves only according to the interacting part of the full Hamiltonian ([11] p. 82):

$$\tilde{H}(t) = \sqrt{\gamma}\tilde{X}(t)\tilde{B}(t). \tag{3.5}$$

To make this transformation explicit it is given here for the system and the bath operator respectively:

$\tilde{X}(t) = \mathrm{e}^{iH_{\mathcal{B}}t}U^\dagger(t)XU(t)\mathrm{e}^{-iH_{\mathcal{B}}t}$, where $U(t) = \mathcal{T}\mathrm{e}^{-i\int_0^t \mathrm{d}t' H_{\mathcal{S}}(t')}$ ([10] p. 71 and [11] p. 83),

with $\mathcal{T}$ denoting time ordering. Since $H_{\mathcal{S}}(t)$ and X act on a different Hilbert space than $H_{\mathcal{B}}$ they obey $[H_{\mathcal{S}}(t), H_{\mathcal{B}}] = [X, H_{\mathcal{B}}] = 0$, and so the above reduces to:

$$\tilde{X}(t) = U^\dagger(t)XU(t). \tag{3.6}$$

For the same reason:

$$\tilde{B}(t) = \mathrm{e}^{iH_{\mathcal{B}}t} B \mathrm{e}^{-iH_{\mathcal{B}}t}.$$

As observed, in the interaction picture the bipartite system evolves according to (3.5) which means that its density matrix obeys the following von Neumann equation:

$$\partial_t \tilde{\rho}_{\mathcal{SB}}(t) = -i \left[\tilde{H}(t), \tilde{\rho}_{\mathcal{SB}}(t) \right]. \tag{3.7}$$

Integration of this and plugging back in gives:

$$\partial_t \tilde{\rho}_{\mathcal{SB}}(t) = -\int_{t_0}^{t} \mathrm{d}t' \left[\tilde{H}(t), \left[\tilde{H}(t'), \tilde{\rho}_{\mathcal{SB}}(t') \right] \right] - i \left[\tilde{H}(t), \tilde{\rho}_{\mathcal{SB}}(t_0) \right]. \tag{3.8}$$

Now the Born approximation is employed by setting $\tilde{\rho}_{\mathcal{SB}}(t') \approx \tilde{\rho}(t') \otimes \rho_{\mathcal{B}}$ inside the integral. This ensures that the system and bath are allowed to develop correlations to first order in the spin-bath coupling parameter γ, but beyond that they are assumed to be disentangled. The inclusion of higher order correlations is obtained by repeatedly integrating Eq. (3.7) and plugging into the above, but by keeping the coupling sufficiently small the higher order correlations become negligible [12].

To obtain the master equation for the reduced density matrix of the system $\tilde{\rho}(t)$ the bath degrees of freedom are to be traced over, but first some assumptions about the bipartite system are made. It assumed that at some arbitrary time in the remote past the bath was in a steady state independent of the system. Choosing t_0 to be in this regime then $\rho_{\mathcal{SB}}(t_0) = \rho(t_0) \otimes \rho_{\mathcal{B}}$. Secondly, it is observed that each bath operator B_α in Eq. (3.2) can, without loss of generality, be assumed to have vanishing expectation values in the bath state $\rho_{\mathcal{B}}$, because any nonzero expectation values can be eliminated by appropriate redefinition of $H_{\mathcal{S}}$ and B_α [8]. With these assumptions it follows that:

$$\partial_t \tilde{\rho}(t) = -\gamma \int_{t_0}^{t} \mathrm{d}t' J(t-t') \left[\tilde{X}(t), \tilde{X}(t') \tilde{\rho}(t') \right] + H.c., \tag{3.9}$$

where $J(t-t') = \mathrm{tr}_{\mathcal{B}}[\tilde{B}(t)\tilde{B}(t')\rho_{\mathcal{B}}]$ is the two-point bath correlation function, and $H.c.$ implies addition of the Hermitian conjugate of the preceding. A proof of the above is given in App. A.1.

The final step is to replace $\tilde{\rho}(t')$ in the integral by $\tilde{\rho}(t)$, under the assumption that the characteristic decay time of the bath correlation function is so short, that the density matrix of the system is approximately stationary over this time, and taking the limit $t_0 \to -\infty$. The result of this is the BR equation:

$$\partial_t \tilde{\rho}(t) = -\gamma \int_{-\infty}^{t} \mathrm{d}t' J(t-t') \left[\tilde{X}(t), \tilde{X}(t') \tilde{\rho}(t) \right] + H.c. \tag{3.10}$$

This last approximation is referred to as the Markov approximation [8], because another way to state the assumption is, that the evolution of the system at a given point in time only depends upon the state of the system at the same time, and not the previous history of the system. This is what is called Markovian evolution as described in the

end of Sec. 3.1, and Eq. (3.10) is an example of this, as the density matrix on the right-hand side is referred to only at the same time as that on the left-hand side. The two approximations employed for the derivation above is collectively referred to as the Born-Markov approximation, and this gives rise to a correction $\xi(t)$ to Eq. (3.10). In the next section it will be shown that this correction has a bound that is controlled by the properties of the bath and the system-bath coupling γ.

Notice that Eq. (3.10) is an equation of motion for $\rho(t)$ which depends only on an observable system operator, the system Hamiltonian and the statistical properties of the bath. Such an equation is often referred to as a master equation [8], and later a particular form of Markovian master equations will be discussed. But first some important properties of the bath will be investigated as these are necessary for the discussion to follow.

3.4 Statistical properties of the bath

Aside from the system-bath coupling the most important factor in determining whether or not the evolution of the system is well-described by Eq. (3.10) is the bath itself. As long as the system-bath coupling is small, the BR equation is independent of the configuration of the system, and so the only requirement for this master equation to be valid (besides a small system-bath coupling) is that the bath is well-behaved from a Markovian point of view. The main point of this section is to quantify what a well-behaved bath constitutes.

The necessary statistical properties of the bath are all incorporated in the bath correlation function:

$$J(t-t') = \mathrm{tr}_{\mathcal{B}}\left(\tilde{B}(t)\tilde{B}(t')\rho_{\mathcal{B}}\right), \tag{3.11}$$

or equivalently its Fourier transform, the bath spectral function:

$$J(\omega) = \frac{1}{2\pi}\int_{-\infty}^{\infty}\mathrm{d}t J(t)\mathrm{e}^{i\omega t}. \tag{3.12}$$

The bath correlation function has a useful symmetric property that will be exploited in the derivations to come. Consider its complex conjugate:

$$\begin{aligned} J^*(t-t') &= \mathrm{tr}_{\mathcal{B}}\left(\left[\tilde{B}(t)\tilde{B}(t')\rho_{\mathcal{B}}\right]^\dagger\right) \\ &= \mathrm{tr}_{\mathcal{B}}\left(\rho_{\mathcal{B}}\tilde{B}(t')\tilde{B}(t)\right) \\ &= \mathrm{tr}_{\mathcal{B}}\left(\tilde{B}(t')\tilde{B}(t)\rho_{\mathcal{B}}\right) \\ &= J(t'-t). \end{aligned}$$

Here the cyclic property of the trace has been used along with the fact, that all the operators above are Hermitian. This symmetry of the correlation function means that

the spectral function is purely real. Observe:

$$\begin{aligned} J^*(\omega) &= \frac{1}{2\pi}\int_{-\infty}^{\infty} \mathrm{d}t J^*(t)\mathrm{e}^{-i\omega t} \\ &= \frac{1}{2\pi}\int_{-\infty}^{\infty} \mathrm{d}t J(-t)\mathrm{e}^{-i\omega t}. \end{aligned}$$

Now changing the variable of integration $t \to -t$:

$$\begin{aligned} J^*(\omega) &= -\frac{1}{2\pi}\int_{\infty}^{-\infty} \mathrm{d}t J(t)\mathrm{e}^{i\omega t} \\ &= \frac{1}{2\pi}\int_{-\infty}^{\infty} \mathrm{d}t J(t)\mathrm{e}^{i\omega t} \\ &= J(\omega). \end{aligned}$$

Hence, its imaginary part must be zero.

Another function that stores all the same information as either of the above but will prove to be more convenient is the jump correlator. The jump correlator is defined by its Fourier transform $g(\omega) = \sqrt{J(\omega)/2\pi}$ which in the time domain gives[8]:

$$g(t) = \frac{1}{\sqrt{2\pi}}\int_{-\infty}^{\infty} \mathrm{d}\omega \sqrt{J(\omega)}\mathrm{e}^{-i\omega t}, \tag{3.13}$$

and hence:

$$g(\omega) = \frac{1}{2\pi}\int_{-\infty}^{\infty} \mathrm{d}t g(t)\mathrm{e}^{i\omega t}. \tag{3.14}$$

Now that the spectral function is proven to be real it is straight forward to see, that the jump correlator has the same symmetric property as the correlation function: $g^*(t) = g(-t)$. With this function two important quantities that characterize the evolution of the system and bath can be defined. One of them is the energy scale

$$\Gamma = 4\gamma\left[\int_{-\infty}^{\infty} \mathrm{d}t\,|g(t)|\right]^2, \tag{3.15}$$

which sets an upper bound for the rate of bath-induced evolution of the system. Another way to view this quantity is as the timescale of system-bath interaction Γ^{-1} as discussed in the end of Sec. 3.1 in connection with Fig. 3.1. The other quantity is another timescale:

$$\tau = \frac{\int_{-\infty}^{\infty}\mathrm{d}t\,|g(t)t|}{\int_{-\infty}^{\infty}\mathrm{d}t\,|g(t)|}, \tag{3.16}$$

which provides a measure for the characteristic correlation time of the bath observable, also discussed in Sec. 3.1. It can be thought of more intuitively as the memory time of the bath, and as such a "good" Markovian bath is one with a "bad" memory, where the correlation between bath observables decay rapidly with time(see Fig. 3.1 for a

discussion of this). Hence, a small τ compared to Γ^{-1} is closely connected to the Markov approximation employed between Eqs. (3.9) and (3.10).

In fact, these two quantities together provide a bound for the correction to the BR equation, namely

$$||\xi(t)|| \leq \Gamma^2 \tau, \tag{3.17}$$

where $||\cdot||$ denotes the spectral norm(see [8] for a proof of this bound). Notice that the right-hand side of Eq. (3.10) scales linearly with γ whereas $\Gamma^2\tau$ scales as γ^2. This means that if the integral over the jump correlator converges, it is in principle always possible to find a small enough value of γ to keep the system's evolution Markovian, making Eq. (3.10) a good description of its dynamics. In [8] they also show that the rate of change of $\tilde{\rho}(t)$ in Eq. (3.10) with the correction $\xi(t)$ is bounded according to

$$||\partial_t \tilde{\rho}(t)|| \leq \Gamma/2. \tag{3.18}$$

Hence, Γ is strictly speaking not the rate of system-bath interactions but rather an upper bound for this. Holding this together with the bound on $\xi(t)$ suggests that a sufficient condition for the Born-Markov approximation to be justified is $\Gamma\tau \ll 1$. Hence, the dimensionless parameter $\Gamma\tau$ provides a measure of "Markovianity" for the bath in question.

3.5 Examples of bath correlation and spectral functions

The bath correlation function (and hence the spectral function) can often be computed for a specific bath with appropriate bath operators $\tilde{B}$. App. B is devoted to finding the bath correlation and spectral function for an electromagnetic vacuum. This is accomplished by first quantizing the electromagnetic field in order to find appropriate bath operators to plug into Eq. (3.11), which turns out to be given by the electric field operators in Eq. (B.18). For a continuous spectrum of electromagnetic modes this leads to the following correlation and spectral function:

$$J(t-t') = -\frac{\pi}{\beta^2 \hbar \epsilon_0 c} \frac{1}{\sinh^2\left(\frac{\pi}{\beta\hbar}[t-t']\right)}, \text{ and} \tag{3.19}$$

$$J(\omega) = \frac{\hbar}{\pi \epsilon_0 c} \frac{\omega}{1 - \mathrm{e}^{-\beta\hbar\omega}}. \tag{3.20}$$

Here $\beta = 1/k_B T$ with k_B being the Boltzmann constant and T the temperature of the bath, ϵ_0 is the vacuum permittivity, and c is the speed of light.

Notice that for large temporal separation the correlation function decays exponentially on the characteristic time scale $\tau = \beta\hbar/2\pi$. This suggests that as a rule of thumb the characteristic correlation time of the bath is inversely proportional to the bath's temperature. There is some intuition to this when once again interpreting τ as the memory time of the bath. At small temperatures the bath is frozen, and few things happen, and so each event stands out more clearly, and the bath is more likely to "remember" what happens. On the other hand, at higher temperatures it is natural

to expect the bath to be sort of chaotic with many things happening, and so it gets harder to distinguish the events from each other, and the bath quickly "forgets" what has happened.

The bath spectral function $J(\omega)$ provides a measure of how well the bath exchanges energy with the system, where ω is the amount of energy absorbed by the bath. Hence, negative values of ω represents emission of energy from the bath into the system. Since the expression above for $J(\omega)$ is injective and grows with increasing ω, then generally for finite temperature the bath is more likely to receive energy than emit energy. This asymmetry is due to the fact, that the system may spontaneously emit energy into the bath, which is clearly not symmetric in frequency. This quantum mechanical effect distinguishes the spectral functions of quantum mechanical systems from that of classical systems, for which the spectral function is symmetric in frequency[23]. Notice specifically, that:

$$\frac{J(\omega)}{J(-\omega)} = \mathrm{e}^{\beta\hbar\omega}.$$

For positive ω this ratio is clearly larger than 1, but observe that for $T \to \infty$ the above goes towards 1, and so for very hot baths it is equally likely to receive as to emit energy. On the other hand, for $T \to 0$ the ratio above diverges, suggesting that for a very cold bath it is highly unlikely that it should emit any energy.

The bath described by Eqs. (3.19) and (3.20) is an example of an Ohmic bath, as generally an Ohmic bath consists of a continuum of bosonic modes, where for large frequencies the spectral function is linear in the frequency of the bosonic modes[25]. Hence, a more general spectral function for an Ohmic bath is:

$$J(\omega) = \frac{1}{\omega_0} \frac{\omega}{1 - \mathrm{e}^{-\beta\omega}}, \tag{3.21}$$

where the energy scale ω_0 is there to keep the spectral function dimensionless[8]. In order to find the characteristic correlation time of the bath as in Eq. (3.16) it is necessary to first find the jump correlator using Eq. (3.13). However, since the spectral function above goes like ω for large frequencies, its Fourier transform will not converge. This can be managed by introducing a cutoff frequency ω_c (often denoted the ultraviolet cutoff) under the assumption, that modes with frequencies above the cutoff frequency interact very weakly with the system. This is not only analytically convenient but also physically justified, as modes with a wavelength much short than the extent of the system will interact very weakly with it. See Fig. 3.2 for a visual representation of this. Consider for example a bath of phononic modes interacting with a superconducting qubit. In a typical superconducting metal such as aluminum the speed of sound is on the order of $v = 5000$ m/s, and a qubit can have an extent on the order of a few micrometers[26]. Hence, the ultraviolet cutoff can be estimated as $\omega_c = 2\pi v/a$, with a being the extent of the qubit, giving a frequency cutoff of approximately 31 GHz.

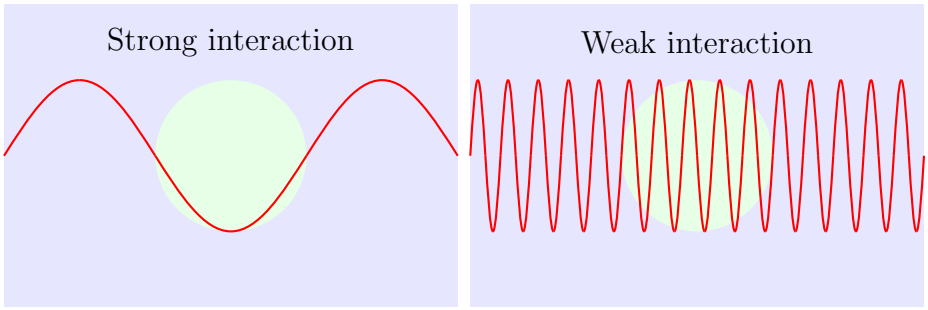

Figure 3.2: This figure depicts a bosonic mode (red wave) interacting with a system (green circle). The left side represents the situation, where the wavelength of the bosonic mode is similar to or larger than the extent of the system resulting in a strong interaction, whereas the right side represents the situation where the wavelength is much shorter than the extent of the system resulting in a weak interaction.

There are different ways to introduce this cutoff. In the derivation of the correlation function for the bath of electromagnetic modes in App. B.4 a polynomial suppression is used in Eq. (B.29). In [8] it is introduced as a Gaussian decay, such that:

$$J(\omega) = \frac{1}{\omega_0} \frac{\omega \mathrm{e}^{-\frac{\omega^2}{2\omega_c^2}}}{1 - \mathrm{e}^{-\beta\omega}}. \tag{3.22}$$

Both of these models ensures that the spectral function goes smoothly to zero as the magnitude of the frequency exceeds ω_c. This also provides a well-behaved Fourier transform, whereas a sharp cutoff at $\omega = \omega_c$ will result in long non-zero "tails" in the jump correlator making it a bad description of a Markovian bath.

The jump correlator can now be found numerically as a discrete Fourier transform of $g(\omega) = \sqrt{J(\omega)/2\pi}$, where $J(\omega)$ is given by the spectral function above, by generating a large set of data points of ω and corresponding $g(\omega)$, where the frequencies are linearly spaced within an interval $[-\omega_{\max}; \omega_{\max}]$, with $\omega_{\max} \gg \omega_c$, such that $g(\omega_{\max}) \ll 1$. This ensures that most of the contribution from the integral in Eq. (3.13) is included in the discrete Fourier transform.

In Fig. 3.3 numerically generated data show the relationship between various Markovianity parameters and the temperature of the bath. The solid lines are with the ultraviolet cutoff set to $\omega_c = 50\omega_0$ and the dashed lines with $\omega_c = 200\omega_0$. The data confirms that the correlation time τ decays, as the temperature of the bath increases. However, the energy scale Γ only decays up until some temperature where it starts to increase (observe that the spectral function grows linearly with the temperature for large T). Comparing the solid and dashed lines suggests, that this turning point is governed by the ultraviolet cutoff, and that the increase starts to happen as the temperature approaches the cutoff. In fact the quantity $\Gamma\tau$ will eventually also start to increase as the temperature grows, meaning that for a very hot bath the system-bath coupling needs to be kept very small in order to keep the evolution of the system Markovian.

Notice that for large temperatures $T \gg \omega$ the bath spectral function is approxi-

mately given by:

$$J(\omega) = \frac{T}{\omega_0} \mathrm{e}^{-\frac{\omega^2}{2\omega_c^2}}.$$

Hence it follows, that the temperature appears in first order in the expression for Γ Eq. (3.15), which explains why Fig. 3.3 (a) exhibits a linear behavior of Γ as a function of the temperature for large temperatures.

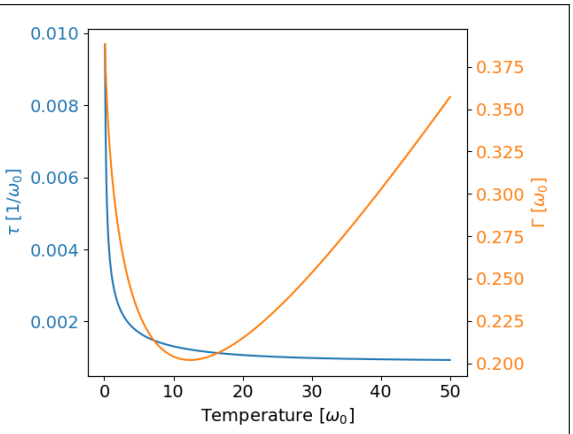

(a) Cutoff frequency $\omega_c = 50\omega_0$

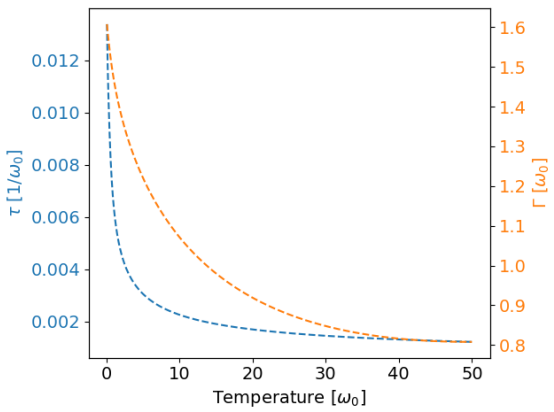

(b) Cutoff frequency $\omega_c = 200\omega_0$

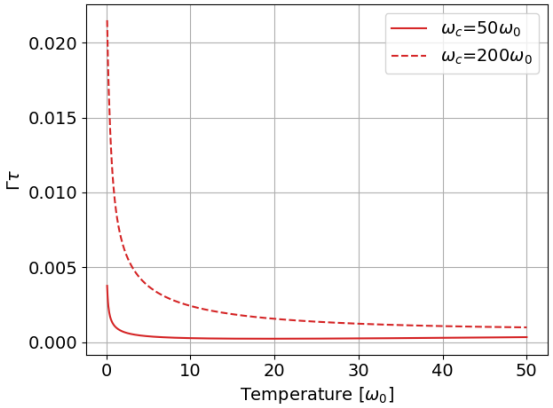

(c) Markovianity $\Gamma\tau$ of the bath as a function of the temperature for cutoff frequency $\omega_c = 50\omega_0$ (solid) and $\omega_c = 200\omega_0$ (dashed).

Figure 3.3: These plots show the relationship between various Markovianity parameters and the temperature of the bath. The solid curves are for $\omega_c = 50\omega_0$ and the dashed curves are for $\omega_c = 200\omega_0$.

Chapter 4

Master equation in the Lindblad form

For a quantum system that is described by Markovian evolution the most general form of its equation of motion that is guaranteed to preserve the trace and positivity of the density matrix is the so-called Lindblad form[13]:

$$\partial_t \rho = -i\left[H_{\mathcal{S}} + \Lambda, \rho\right] + \sum_i \gamma_i \left(L_i \rho L_i^\dagger - \frac{1}{2}\left\{ L_i^\dagger L_i, \rho \right\} \right). \tag{4.1}$$

Here Λ is the Lamb shift that renormalizes the system Hamiltonian due to the interaction with the bath [8, 12], and L_i is known as a jump operator with corresponding energy scale γ_i parametrizing the coupling strength between the system and bath i. Hence, the i-s here label the baths or equivalently the noise channels as the α-s in Eq. (3.2). The jump operators are what govern the dissipation in the system's evolution[8], and comparison with the von Neumann equation (3.4) distinguishes the sum in the above as what indeed describes the dissipation of the information stored in the system.

The above claims that since the BR equation (3.10) is a Markovian master equation it can be cast in the Lindblad form, and there indeed exist different approximation schemes that can be employed to this to obtain a master equation in the Lindblad form. These different approximations may impose different restrictions on the system that the resulting master equation can be applied to, and the main thing that distinguishes different Lindblad master equations are the jump operators, as will be shown.

In the next section the well studied quantum optical master equation[13] will be reviewed to show its limitations and to emphasise the benefit of the recently developed universal Lindblad equation[8], which will be the subject of the following section and the equation of motion on which the quantum systems studied in this thesis will be modelled.

4.1 The quantum optical master equation

This section is reserved only for the presentation of the quantum optical master equation for a single noise channel, and the approximation that is employed leading to it. The explicit derivation of the equation is pushed to App. A.2.

The QOME in the Lindblad form for a single noise channel as derived in App. A.2 is given by:

$$\partial_t \tilde{\rho} = -i\left[\Lambda, \tilde{\rho}\right] + L_{ph}\tilde{\rho}L_{ph}^\dagger - \frac{1}{2}\left\{ L_{ph}^\dagger L_{ph}, \tilde{\rho} \right\} + \sum_{m\neq n} \left(L_{mn}\tilde{\rho}L_{mn}^\dagger - \frac{1}{2}\left\{ L_{mn}^\dagger L_{mn}, \tilde{\rho} \right\} \right), \tag{4.2}$$

Here there are two types of jump operators: the dephasing jump operator:

$$L_{ph} = \sqrt{2\pi\gamma J(0)} \sum_m X_{mm} \left|m\right\rangle \left\langle m\right|, \tag{4.3}$$

and the decay jump operators:

$$L_{mn} = \sqrt{2\pi\gamma J(E_n - E_m)} X_{mn} \left|m\right\rangle \left\langle n\right|, \tag{4.4}$$

with $X_{mn} = \left\langle m\right| X \left|n\right\rangle$. The action of the dephasing jump operator on the system corresponds to noise disturbing the phase of the wave function describing the state of the system, whereas the decay operators disturb the energy state of the system. In language of qubit noise in Sec. 2.3 the dephasing operator causes pure dephasing, and the decay operators cause depolarization of the qubit state.

Eq. (4.2) is derived from the BR equation (3.10), so aside from the implications of the Born-Markov approximation, the rotating wave approximation (RWA) imposes strict conditions on the systems for which Eq. (4.2) is a good model. By switching the system operators back into the Schrödinger picture in the BR equation, the equation of motion for the density matrix can be expressed as:

$$\partial_t \tilde{\rho} = -\gamma \sum_{mnpq} \Gamma_{pq} \mathrm{e}^{i(E_m - E_n + E_p - E_q)t} \left[\hat{X}_{mn}, \hat{X}_{pq}\tilde{\rho}\right] + H.c.,$$

$$\text{where } \Gamma_{mn} \equiv \int_0^\infty \mathrm{d}t J(t) \mathrm{e}^{-i(E_m - E_n)t},$$

and $\hat{X}_{mn} = \left|m\right\rangle \left\langle m\right| X \left|n\right\rangle \left\langle n\right|$. The RWA is then invoked to discard the terms in the sum where $E_m - E_n + E_p - E_q \neq 0$, under the assumption that these terms oscillate so fast that over the relaxation time of the bath they average out[12]. Another way to state this is, that the smallest difference between energy differences of the system is assumed to be much larger than the relaxation rate. Hence, the terms that remain for the development of Eq. (4.2) are the ones where either $m = n$ and $p = q$ or $m = q$ and $n = p$. However, there may exist distinct m, n, p and q for which $E_m - E_n + E_p - E_q = 0$, depending on the system under investigation. For such a system there is no good argument as to why only the terms discussed above should be kept, and it is necessary to be more careful when discarding terms from the sum. But this requires information about the specific system in question and would often be a problematic procedure for large systems. Besides, the resulting master equation will in general be specific only to the system for which it is derived, whereas Eq. (4.2) has a more general use. However, its application is restricted to systems where no two distinct transitions give rise to the same energy exchange. In other words, if a photon is observed to be emitted from the system, it should be possible to tell exactly what decay occurred.

There are systems to which the QOME cannot be applied even with a rigorous employment of the RWA, because when the energy levels become too dense, the rate of system-bath interactions cannot be said to be much smaller than the energy spacing of the system. An example of this is a spin-1/2 Heisenberg chain, as its level spacing is exponentially suppressed in the number of spins[8]. This motivates the development of a Lindblad master equation that does not impose any requirements on the structure of the system in question.

4.2 Derivation of the universal Lindblad equation

This section reviews the derivation of the ULE as it is presented in [8] while emphasizing certain calculations and approximations. In addition to this, a comparison to the QOME will be made that is not provided in [8].

This Lindblad master equation is accurate on the same level of approximation as the BR equation (3.10) (i.e. in the Markovian limit $\Gamma\tau \ll 1$), but unlike the QOME (4.2), its validity does not depend upon the structure of the energy levels of the system. As such it is referred to as the universal Lindblad equation. Once again the derivation begins with the BR equation but provides a different approximation scheme that induces errors of the same magnitude as the Born-Markov approximation used in deriving Eq. (3.10)[8]. Starting from Eq. (3.10) means that the derivation will once again be for a single noise channel (i.e. there is only one system-bath coupling term in Eq. (3.2)), but later it will be generalized to an arbitrary number of noise channels.

The first step is to decompose the bath correlation function as a convolution in terms of the jump correlator:

$$J(t-t') = \int_{-\infty}^{\infty} \mathrm{d}s g(t-s)g(s-t'), \tag{4.5}$$

With the definition of the jump correlator Eq. (3.13) it is straight forward to verify the above simply by inserting. Hence, Eq. (3.10) can be expressed as:

$$\begin{aligned}\partial_t\tilde{\rho}(t) &\approx -\gamma \int_{-\infty}^{t} \mathrm{d}t' \int_{-\infty}^{\infty} \mathrm{d}s g(t-s)g(s-t') \left[\tilde{X}(t), \tilde{X}(t')\tilde{\rho}(t)\right] + H.c. \\ &\approx -\gamma \int_{-\infty}^{\infty} \mathrm{d}t' \int_{-\infty}^{\infty} \mathrm{d}s \theta(t-t')g(t-s)g(s-t') \left[\tilde{X}(t), \tilde{X}(t')\tilde{\rho}(t)\right] + H.c.\end{aligned}$$

Here the Heaviside step function $\theta(t)$ (defined as $\theta(t) = 1$ for $t > 0$, $\theta(t) = 0$ for $t < 0$, and $\theta(t) = 1/2$ for $t = 0$) has been introduced to extend the integral to infinity. The following function is introduced for convenience:

$$\mathcal{F}(t,s,t')[\tilde{\rho}] \equiv -\gamma\theta(t-t')g(t-s)g(s-t') \left[\tilde{X}(t), \tilde{X}(t')\tilde{\rho}\right] + H.c. \tag{4.6}$$

With that, integration of the master equation over a finite time interval from t_1 to t_2, chosen such that $t_2 - t_1 \gg \tau$, leads to:

$$\tilde{\rho}(t_2) - \tilde{\rho}(t_1) \approx \int_{t_1}^{t_2} \mathrm{d}t \int_{-\infty}^{\infty} \mathrm{d}t' \int_{-\infty}^{\infty} \mathrm{d}s \mathcal{F}(t,s,t') \left[\tilde{\rho}(t)\right]. \tag{4.7}$$

The bound on the rate of change of $\tilde{\rho}(t)$ in Eq. (3.18) means that for $|t-s| \lesssim \tau$, in the Markovian limit $\Gamma\tau \ll 1$, the density matrix in the integral above can with good approximation be replaced with $\tilde{\rho}(s)$, as long as the magnitude of the difference of t and s does not exceed τ considerably. This condition is supported by the fact, that the jump correlator $g(t-s)$ in Eq. (4.6) is strongly suppressed, when the magnitude of its argument exceeds τ. In fact, for the same reason $\mathcal{F}(t,s,t')$ is strongly suppressed when the difference of any of its arguments exceeds τ. Hence, by the assumption that

$t_2 - t_1 \gg \tau$, it is fairly justified to exchange the limits of integration on t and s. Fig. 4.1 provides a visual representation supporting this argument.

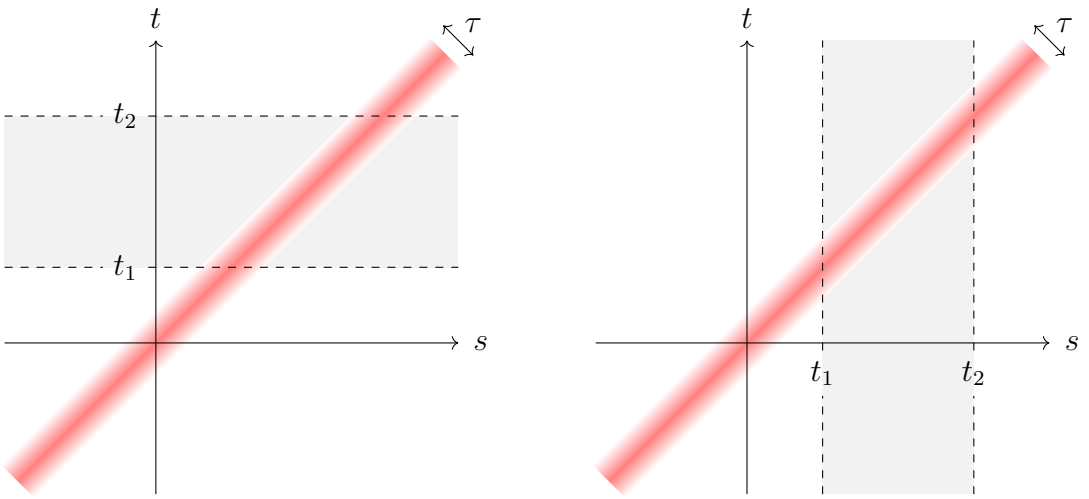

Figure 4.1: This figure provides two pictures of the same coordinate system of the temporal variables t and s. The faded red area is centered around $t = s$ and its width in the t-s plane is τ. When the distance to the line $t = s$ increases, the red color fades into white, representing the strong suppression of $g(t - s)$ as $|t - s|$ exceeds τ. The shaded gray area is the region of integration for the two variables. On the left the limits of integration are from t_1 to t_2 for t, and $-\infty$ to ∞ for s, whereas on the right the limits have been interchanged. Because of the strong suppression of $g(t - s)$ outside the shaded red area the main contribution to the integration is the red area within the two dashed lines, and this area is approximately the same in both cases. Hence, interchanging the limits of integration results in approximately the same value of the integrals.

Accordingly, in the Markovian limit Eq. (4.7) can with good approximation be rewritten as:

$$\tilde{\rho}(t_2) - \tilde{\rho}(t_1) \approx \int_{t_1}^{t_2} \mathrm{d}s \int_{-\infty}^{\infty} \mathrm{d}t' \int_{-\infty}^{\infty} \mathrm{d}t \mathcal{F}(t, s, t') \left[\tilde{\rho}(s)\right].$$

Taking the derivative with respect to t_2 and relabelling the variables results in:

$$\begin{aligned}\partial_t \tilde{\rho}(t) &\approx \int_{-\infty}^{\infty} \mathrm{d}s \int_{-\infty}^{\infty} \mathrm{d}s' \mathcal{F}(s, t, s') \left[\tilde{\rho}(t)\right] \\ &\approx -\gamma \int_{-\infty}^{\infty} \mathrm{d}s \int_{-\infty}^{\infty} \mathrm{d}s' \theta(s - s') g(s - t) g(t - s') \left[\tilde{X}(s), \tilde{X}(s')\tilde{\rho}(t)\right] + H.c.\end{aligned}$$

Notice now, that the density matrix on the right-hand side enters as $\rho(t)$ and not $\rho(t')$. As such the equation is now Markovian, and the derivation of the ULE is nearly complete; all that remains is to rewrite the above in the Lindblad form. This is rigorously done in App. A.3, and the result is:

$$\partial_t \tilde{\rho}(t) = -i \left[\tilde{\Lambda}(t), \tilde{\rho}(t)\right] + \tilde{L}(t)\tilde{\rho}(t)\tilde{L}^\dagger(t) - \frac{1}{2}\left\{\tilde{L}^\dagger(t)\tilde{L}(t), \tilde{\rho}(t)\right\}, \tag{4.8}$$

where the jump operator is given by:

$$\tilde{L}(t) = \sqrt{\gamma}\int_{-\infty}^{\infty} \mathrm{d}s g(t-s)\tilde{X}(s), \tag{4.9}$$

and the Lamb shift:

$$\tilde{\Lambda}(t) = \frac{\gamma}{i2}\int_{-\infty}^{\infty}\mathrm{d}s\int_{-\infty}^{\infty}\mathrm{d}s'\tilde{X}(s)g(s-t)g(t-s')\tilde{X}(s')\mathrm{sgn}(s-s'). \tag{4.10}$$

The Schrödinger picture equation can be found by transforming the above as in Eq. (3.6). Notice that the left-hand side can be rewritten as:

$$\begin{aligned}\partial_t\tilde{\rho}(t) &= \partial_t\left(U^\dagger(t)\rho(t)U(t)\right)\\ &= U^\dagger(t)\partial_t\rho U(t) + iU^\dagger(t)\left[H_{\mathcal{S}}(t),\rho(t)\right]U(t).\end{aligned}$$

Hence, applying the transformation gives:

$$\partial_t\rho(t) = -i\left[H_{\mathcal{S}}(t)+\Lambda(t),\rho(t)\right] + L(t)\rho(t)L^\dagger(t) - \frac{1}{2}\left\{L^\dagger(t)L(t),\rho(t)\right\}. \tag{4.11}$$

Here it has been used that $\tilde{\rho}(t) = U^\dagger(t)\rho(t)U(t)$ along with the unitarity of the time evolution operator: $U^\dagger(t)U(t) = U(t)U^\dagger(t) = 1$. Hence, in the Schrödinger picture the jump operator is given by:

$$L(t) = \sqrt{\gamma}\int_{-\infty}^{\infty}\mathrm{d}s g(t-s)U(t,s)XU^\dagger(t,s). \tag{4.12}$$

Here it has been used that $U(t)U^\dagger(s) = U(t,s)$. In a similar manner the Lamb shift Eq. (4.10) can be expressed in the Schrödinger picture.

Before moving on there is an interesting thing to notice here, namely that there is only one jump operator for the single noise channel in the ULE, whereas there are as many jump operators as there are transitions in the QOME in Eqs. (4.3) and (4.4). In order to further compare the two Lindblad master equations, the jump operator for the ULE should be expressed in terms of a time independent system Hamiltonian:

$$L(t) = \sqrt{\gamma}\int_{-\infty}^{\infty}\mathrm{d}s g(t-s)\mathrm{e}^{-iH_{\mathcal{S}}(t-s)}X\mathrm{e}^{iH_{\mathcal{S}}(t-s)}.$$

By inserting two complete sets of eigenstates of $H_{\mathcal{S}}$ on either side of X, the above can be rewritten as:

$$L(t) = \sqrt{\gamma}\sum_{mn}\int_{-\infty}^{\infty}\mathrm{d}s g(t-s)\mathrm{e}^{i(E_n-E_m)(t-s)}X_{mn}\left|m\right\rangle\left\langle n\right|, \text{ where } X_{mn} = \left\langle m\right|X\left|n\right\rangle.$$

The integral above is just the Fourier transform of the jump correlater Eq. (3.14), so:

$$L = 2\pi\sqrt{\gamma}\sum_{mn} g\left(E_n - E_m\right)X_{mn}\left|m\right\rangle\left\langle n\right|. \tag{4.13}$$

This shows explicitly that the single jump operator for the ULE incorporates all the transitions that the system operator X makes available, whereas there are individual jump operators for each transition in the QOME. This emphasizes the issue with the RWA used to derive Eq. (4.2) that makes this QOME a bad model for systems, where the structure of the energy levels have distinct transitions of equal energy. Consider a system of an energy level structure as in Fig. 4.2, where the difference of the two lower levels is equal to the difference of the two upper levels: $E_1 - E_0 = E_3 - E_2 \equiv \Delta E$. If this systems starts out in a superposition of the two upper levels $(|2\rangle + |3\rangle)/\sqrt{2}$, and a photon is observed with the energy $\omega_\gamma = E_3 - E_1 = E_2 - E_0$, then the system will have decayed, and the wavefunction collapses into the state $(|0\rangle + |1\rangle)/\sqrt{2}$. The action of the jump operators for the ULE will correctly capture this behavior, whereas the jump operators for the QOME will collapse the wavefunction into either $|0\rangle$ or $|1\rangle$, losing the superposition.

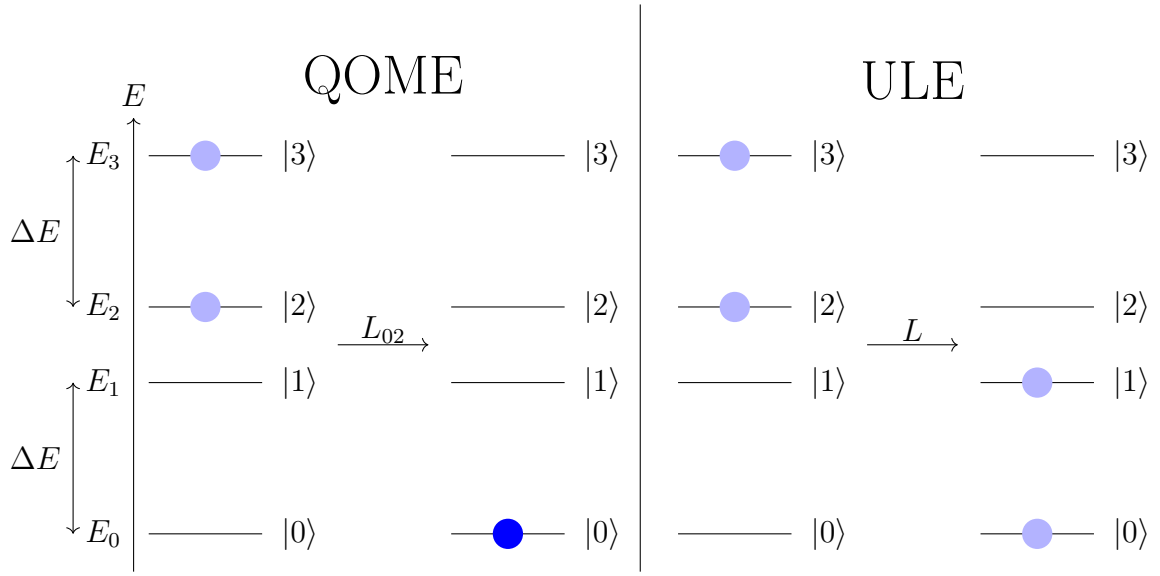

Figure 4.2: This figure depicts the difference between the QOME and the ULE, when jump operators from each master equation are applied to a specific system, consisting of four energy states, starting in a superposition of the two upper energy levels, symbolized by two fuzzy blue points. On the far left an energy scale shows, that the structure of the energy levels is such, that the difference between the two lower levels is equal to the difference between the two upper levels. In both cases the process depicted is the emission of a photon with energy $\omega_\gamma = E_3 - E_1 = E_2 - E_0$, which will cause the system to decay into a superposition of the two lower levels. **QOME:** the decay of the system can be effected by either of the jump operators L_{02} or L_{13}, given by Eq. (4.4). In this example L_{02} is arbitrarily chosen, causing the system to decay into the ground state, symbolized by a deep blue point. **ULE:** the jump operator L, given by Eq. (4.13), effects the decay into a superposition of the two lower levels, as is physically accurate.

4.3 The universal Lindblad equation for arbitrary number of noise channels

In this section, the ULE will be generalized to an arbitrary number of noise channels N. This is once again a review of some of the results derived in [8].

First of all, for N noise channels there are N^2 bath correlation functions making up an $N \times N$ matrix $\mathbf{J}(t)$ with elements:

$$J_{\alpha\beta}(t-t') = \mathrm{tr}_{\mathcal{B}}\left(\tilde{B}_\alpha(t)\tilde{B}_\beta(t')\rho_{\mathcal{B}}\right). \tag{4.14}$$

This is the generalization of Eq. (3.11), where α and β label the N noise channels. This gives rise to another matrix comprising the different bath spectral functions:

$$\mathbf{J}(\omega) = \frac{1}{2\pi}\int_{-\infty}^{\infty} \mathrm{d}t \mathbf{J}(t)\mathrm{e}^{i\omega t}. \tag{4.15}$$

Hence, each element $J_{\alpha\beta}(\omega)$ is the Fourier transform of the corresponding element in $\mathbf{J}(t)$. In the same way, the matrices comprising the different jump correlators and their Fourier transforms can be constructed, generalizing Eq. (3.13):

$$\mathbf{g}(t) = \frac{1}{\sqrt{2\pi}}\int_{-\infty}^{\infty} \mathrm{d}\omega \sqrt{\mathbf{J}(\omega)}\mathrm{e}^{-i\omega t} \text{ and } \mathbf{g}(\omega) = \sqrt{\frac{\mathbf{J}(\omega)}{2\pi}}, \tag{4.16}$$

where the square root denotes the matrix square root, because the elements in $\mathbf{J}(\omega)$ are given by the matrix product: $J_{\alpha\beta}(\omega) = \frac{1}{2\pi}\sum_\lambda g_{\alpha\lambda}(\omega)g_{\lambda\beta}(\omega)$.

The quantities Γ and τ are defined from the generalized multi-channel jump correlater as:

$$\Gamma = 4\gamma\left[\int_{-\infty}^{\infty}\mathrm{d}t||\mathbf{g}(t)||_{2,1}\right] \text{ and } \tau = \frac{\int_{-\infty}^{\infty}\mathrm{d}t||\mathbf{g}(t)t||_{2,1}}{\int_{-\infty}^{\infty}\mathrm{d}t||\mathbf{g}(t)||_{2,1}}, \tag{4.17}$$

where $||\cdot||_{2,1}$ denotes the $L_{2,1}$ matrix norm[16]. In the case of a single noise channel, where $N = 1$, the equations above reduce to the ones in Eqs. (3.15) and (3.16) as required.

When the Markovianity parameters given by Eq. (4.17) obeys $\Gamma\tau \ll 1$, the density matrix of the system evolves according to:

$$\partial_t\tilde{\rho}(t) = -i\left[\tilde{\Lambda}(t), \tilde{\rho}(t)\right] + \sum_\lambda\left(\tilde{L}_\lambda(t)\tilde{\rho}(t)\tilde{L}_\lambda^\dagger(t) - \frac{1}{2}\left\{\tilde{L}_\lambda^\dagger(t)\tilde{L}_\lambda(t), \tilde{\rho}(t)\right\}\right) + \xi'(t), \tag{4.18}$$

where the correction is bounded according to $||\xi'(t)|| \leq 2\Gamma^2\tau$. The jump operators are given by:

$$\tilde{L}_\lambda(t) = \sqrt{\gamma}\sum_\alpha\int_{-\infty}^{\infty}\mathrm{d}s g_{\lambda\alpha}(t-s)\tilde{X}_\alpha(s). \tag{4.19}$$

Hence, the jump operator associated with noise channel λ is given by a sum over all the noise channels. Finally, the lamb shift is given by:

$$\tilde{\Lambda}(t) = \frac{\gamma}{i2}\int_{-\infty}^{\infty} \mathrm{d}s \int_{-\infty}^{\infty} \mathrm{d}s' \sum_{\alpha\beta} \tilde{X}_\alpha(s)\tilde{X}_\beta(s')\phi_{\alpha\beta}(s-t, t-s'), \tag{4.20}$$

where $\phi_{\alpha\beta}(t,s)$ are the matrix elements of $\phi(t,s) = \mathbf{g}(t)\mathbf{g}(-s)\mathrm{sgn}(t-s)$.

The sum over noise channels in the jump operator Eq. (4.19) considerably complicates the expression compared to that of a single noise channel. Especially because the Fourier transform of the jump correlator $g_{\alpha\beta}(\omega)$ can generally no longer be found as simply the square root of the corresponding bath spectral function $J_{\alpha\beta}(\omega)$. However, if α and β label baths of different noise sources (such as charge noise and flux noise in the case of superconducting qubits[23]) it is fairly justified to assume that the baths or uncorrelated such that the their mutual correlation function $J_{\alpha\beta}(t) = 0$. α and β may also label different noise channels to the same bath, in which case there is no immediate reason to expect their correlation to be zero. Consider for example a system of two qubits, where α labels a noise channel between the one qubit and the bath, and β labels a noise channel between the other qubit and the bath. In that case the correlation function is for the bath operators $\tilde{B}(x_\alpha, t)$ and $\tilde{B}(x_\beta, t')$. Thus α and β respectively label the position of the qubits, and the correlation function does now not only depend upon the temporal separation of the bath operators but also their spatial separation: $J(x_\alpha - x_\beta, t-t')$. In App. B.4 it is explained that this correlation function can with good approximation be assumed to decay very rapidly with the separation $x_\alpha - x_\beta$. On the basis of these arguments it will be assumed that all the baths labelled by the noise channels are independent, such that the matrix of correlation functions $\mathbf{J}(t)$ is diagonal. This in turn means that $\mathbf{g}(t)$ is also diagonal, and so the sum over α in the jump operator $\tilde{L}_\lambda$ Eq. (4.19) only has the one term where $\alpha = \lambda$. I.e. the term associated with the noise channel that the jump operator itself is representing.

4.4 Simulating open quantum systems using the ULE

As the ULE has now been obtained it is in principle possible to numerically simulate the dynamics of open quantum systems using Eq. (4.18). As was pointed out in connection with the QOME, the motivation for deriving the ULE was to develop a model for predicting the behavior of systems like a spin-1/2 Heisenberg chain, where the level spacing is exponentially suppressed in the number of spins, making the QOME invalid for such a system. However, the Hilbert space of a system of N spins has a dimension of 2^N, which means that the simulation requires evolving a $2^N \times 2^N$ density matrix. Even for moderately sized systems such numerical computations become inconceivable for most of today's computers. Luckily, master equations in the Lindblad form can be conveniently integrated using the stochastic Schrödinger equation, which merely requires the evolution of a $2^N \times 1$ state vector[8].

The SSE is a numerical technique for simulating open quantum systems described by a Lindblad master equation. It is also referred to as the quantum trajectory or Monte Carlo wavefunction method, because the objective is to propagate pure states in time according to an effective Hamiltonian incorporating the dissipative process combined

with quantum jumps described by the jump operators. The evolution of each of these pure states gives rise to a collection of quantum trajectories, and by taking an average of these trajectories, expectation values propagated by the Lindblad master equation can be reconstructed[24].

The ULE in the Schrödinger picture can be expressed as (the dependence on time is suppressed to avoid clutter):

$$\partial_t \rho = -i \left(H_{\text{eff}} \rho - \rho H_{\text{eff}}^\dagger \right) + \sum_\lambda L_\lambda \rho L_\lambda^\dagger, \tag{4.21}$$

with the effective Hamiltonian given by:

$$H_{\text{eff}} = H_{\mathcal{S}} + \Lambda - \frac{i}{2} \sum_\lambda L_\lambda^\dagger L_\lambda. \tag{4.22}$$

Please take note, that in all the simulations to be presented in Chapters 5 and 6 the effect of the Lamb shift in the equation above has been ignored.

Now the pure state $|\psi(t)\rangle$ can be evolved a time step δt according to the effective Hamiltonian. For a small enough time step this evolution can be expanded to first order in δt:

$$|\psi(t+\delta t)\rangle \approx (1 - i H_{\text{eff}} \delta t) \, |\psi(t)\rangle \, . \tag{4.23}$$

Since H_{eff} is non-Hermitian the new state $|\psi(t+\delta t)\rangle$ is not normalized, and so its norm is given by:

$$\begin{aligned} \langle \psi(t+\delta t) | \psi(t+\delta t) \rangle &\approx \langle \psi(t)| \left(1 + i H_{\text{eff}}^\dagger \delta t \right) (1 - i H_{\text{eff}} \delta t) \, |\psi(t)\rangle \\ &\approx 1 - \delta t \, \langle \psi(t)| \, i \left(H_{\text{eff}} - H_{\text{eff}}^\dagger \right) |\psi(t)\rangle \, , \end{aligned}$$

where the expression has been kept to first order in δt. From the above can be defined:

$$\delta p \equiv \delta t \, \langle \psi(t)| \, i \left(H_{\text{eff}} - H_{\text{eff}}^\dagger \right) |\psi(t)\rangle = \delta t \, \langle \psi(t)| \sum_\lambda L_\lambda^\dagger L_\lambda \, |\psi(t)\rangle \equiv \delta t \sum_\lambda \delta p_\lambda. \tag{4.24}$$

Effectively, δp_λ can be interpreted as the probability that the action described by the jump operator L_λ occurs in the time interval from t to $t+\delta t$. Hence, δp is the probability that any kind of quantum jump will occur in the time interval.

Now the procedure is to initiate a large number of systems in the same state $\psi(t=0)$, and for each of these realizations a random number r_1 is generated from a uniform distribution in the interval $[0;1]$. If $r_1 > \delta p$ then no jump occurs for the particular trajectory in the particular time step, and the state is evolved according to the effective Hamiltonian:

$$|\psi(t+\delta t)\rangle = \frac{\mathrm{e}^{-i H_{\text{eff}} \delta t} \, |\psi(t)\rangle}{\mathcal{N}}, \text{ where } \mathcal{N} = \sqrt{\langle \psi(t)| \, \mathrm{e}^{i H_{\text{eff}}^\dagger \delta t} \mathrm{e}^{-i H_{\text{eff}} \delta t} \, |\psi(t)\rangle},$$

keeping the state normalized.

If on the other hand $r_1 \leq \delta p$ then a jump occurs, and another random number r_2 is generated in the same way as r_1. This time the interval $[0; 1]$ is divided into sub-intervals labeled by the noise channels λ, where the size of each section is proportional to $\delta p_\lambda / \delta p$. If r_2 falls into the sub-interval labelled by m, then the quantum jump corresponding to L_m occurs within the time step, and hence:

$$|\psi(t + \delta t)\rangle = \frac{L_m |\psi(t)\rangle}{\sqrt{\delta p_m / \delta t}}. \tag{4.25}$$

Once again $\sqrt{\delta p_m / \delta t}$ is there to keep the state normalized, and that this is so can be inferred from Eq. (4.24).

This procedure is thus repeated an arbitrary number of times, and then expectation values can be found for a particular time step by averaging over the states of the different trajectories at that time step. Hence, the dynamics of the system can be predicted.

As an illustrative example, consider a single spin in a Zeeman field of strength B:

$$H = -BS_z, \tag{4.26}$$

with ground state $|g\rangle = |\uparrow\rangle$ and energy $E_g = -B/2$ and excited state $|e\rangle = |\downarrow\rangle$ and energy $E_e = B/2$. The system is prepared in the spin-down state and connected to an Ohmic bath as in Eq. (3.22) via the Pauli operator σ_x. This noise channel opens for transitions between the spin-up and spin-down state of the system. Hence, a single one of the trajectories described by the SSE will eventually decay into the spin-down state either spontaneously or stimulated by the bath, but then there is a probability that the bath will later stimulate an excitation of the system back into the spin-up state. This behaviour will go on indefinitely for as long as the system is left alone. Fig. 4.3 (a) shows a sketch of how a single trajectory might have evolved under the SSE, and Fig. 4.3 (b) shows how the average of many such trajectories might look.

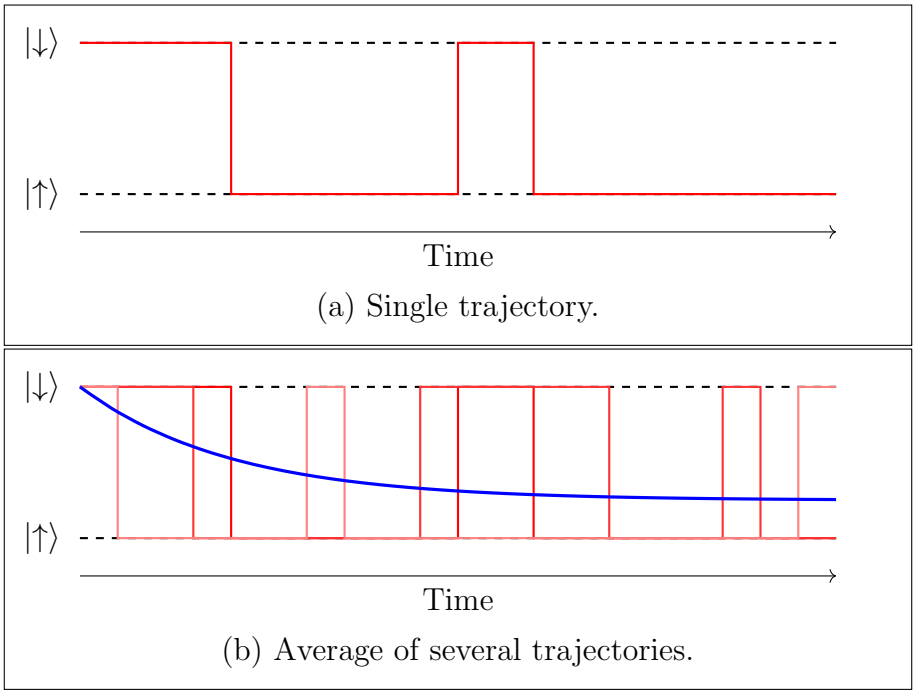

Figure 4.3: **(a)** A sketch of a single quantum trajectory evolving under the SSE. **(b)** A sketch of many quantum trajectories evolving independently under the SSE with their average shown in blue.

For a two-level system like that described by Eq. (4.26) it is no problem to compute its evolution directly according to the ULE because of its small dimension. Fig. 4.4 shows the evolution of the expectation value of the Pauli operator σ_z for a system prepared in its excited state and connected to a bath via the σ_x Pauli operator. The parameters of the system are chosen accordingly: the strength of the Zeeman field is $B = 8\omega_0$, the temperature of the bath is $T = 2\omega_0$, the ultraviolet cutoff is $\omega_c = 100\omega_0$, and the system-bath coupling is $\gamma = 0.02\omega_0$. This leads to the values $\tau = 0.0034\omega_0^{-1}$ and $\Gamma = 1.3\omega_0$, meaning that $\Gamma\tau = 0.0043$ ensuring Markovianity and the validity of the ULE. The blue line is the evolution according to the SSE using the jump operator of the ULE and it is the average of $10,000$ trajectories, and the red line is directly according to the ULE. The curves agree very well upon visual inspection following an exponential decay from the initial value towards its steady state population. However, there is some discrepancy between the rate of relaxation and steady state population of the two curves. The direct ULE gives $\Gamma_{\text{ULE}} = 1.04\omega_0$ as the relaxation rate, where the SSE gives $\Gamma_{SSE} = 1.06\omega_0$, and for the steady state population the ULE yields $p_{\text{ULE}} = 0.964$, whereas the SSE yields $p_{\text{SSE}} = 0.963$. This slight discrepancy can be attributed to the fact, that whereas the direct application of the ULE results in a curve that truly follows an exponential decay, the stochastic element of the SSE will cause the population to saturate the steady state population at a finite time. After this saturation point has been reached, the quantum jumps generated by the SSE on the individual trajectories will cause small fluctuations of the average about the steady state population. The values pertaining to the curve generated by the direct ULE are extracted from an exponential fit, but due to this saturation caused by the SSE the curve generated hence

has been truncated in order to provide better estimates for the relaxation rate and the steady state population. The data of the SSE for times before $3\omega_0^{-1}$ (ensuring only data from before the saturation point) are used to extract the relaxation rate by finding the logarithm of the expectation values and fitting to a straight line. Hence, the slope of the line is the relaxation rate. The steady state population is found as the average of the expectation values for times after $7\omega_0^{-1}$, ensuring that the saturation point is passed.

Another statistical error in the SSE arises from the fact that for a given time step δt for a single trajectory, only the probability δp of a single quantum jump occurring within δt is considered. The probability for two or more quantum jumps occurring within δt is not taken into account, or rather it is assumed that δp is so small, that δp^2 is negligible in comparison. Thus it is vital to keep δp sufficiently small in order to have the SSE provide reliable results. The magnitude of δp is controlled by the system-bath coupling γ but also the size of the time step δt. Hence, the smaller δt is chosen, the more reliable are the results obtained from the SSE. On the other hand, the smaller δt is, the higher the computational cost is. The data generated via the SSE in Fig. 4.4 is for 10,000 time steps, hence the step size is roughly $10^{-3}\omega_0^{-1}$.

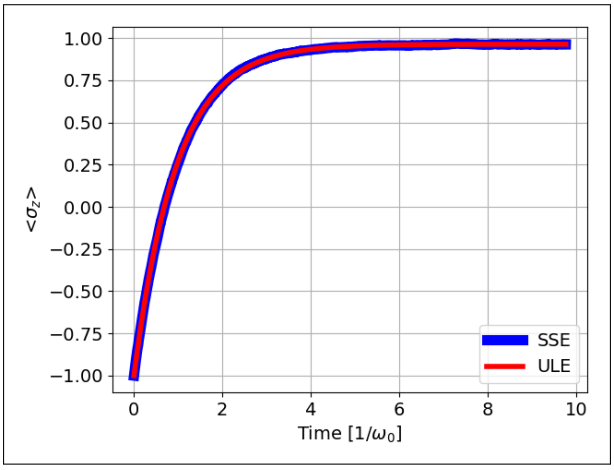

Figure 4.4: This figure shows the similarity of data generated by direct application of the ULE (red) and data generated by the SSE using the jump operators of the ULE (blue).

Chapter 5

Two coupled superconducting qubits

This section presents the simulation of two coupled superconducting qubits modelled on the ULE. Particularly the jump operators will be investigated to determine the type of errors the bath induces on the qubits. In a conversation with one of the authors of [29] the following model was suggested to represent the experimental setup used in that work. Furthermore, some typical values for the different parameters of the model were discussed.

The two circuit qubits can be set up and coupled, such that the effective Hamiltonian describing the system can be written:

$$H_{\mathcal{S}} = -\frac{\omega_q}{2}\sigma_z^{(1)} - \frac{\omega_q + d}{2}\sigma_z^{(2)} - g\left(\sigma_x^{(1)}\sigma_x^{(2)} + \sigma_y^{(1)}\sigma_y^{(2)}\right), \tag{5.1}$$

where the splitting of the second qubit $\omega_2 = \omega_q + d$ has a detuning d compared to the first qubit $\omega_1 = \omega_q$. This detuning can be achieved by threading the loop of Josephson junctions of each qubit by differing external fields as shown in Fig. 2.3. The tuning of the qubit frequency is further discussed above Eq. (2.11). The coupling along the two transverse axes x and y can be achieved by a combination of capacitive and inductive coupling of the qubits as discussed in Sec. 2.2. The subscript on the Hamiltonian $H_{\mathcal{S}}$ is to emphasize, that the Hamiltonian above plays the role of the system Hamiltonian in the framework of Eqs. (3.1) and (3.2). The suggested values for the parameters of this model are: $\omega_q \approx 3-6$ GHz, $d \approx 0.7-1$ GHz, and $g \approx 10-20$ MHz. In the simulations to follow they are chosen in various combinations with a little more freedom.

The situation under investigation for this system is, when the first qubit is coupled to an Ohmic bath through a noise channel coupling transversely to the qubit, namely σ_x. Hence, the system operator X in Eq. (4.19) is given by $X = \sigma_x^{(1)} = \mathbb{1} \otimes \sigma_x$. Since the Hamiltonian is time independent the jump operator can be found using Eq. (4.13):

$$L = 2\pi\gamma \sum_{m,n=0}^{4} g(E_n - E_m) \langle m| \sigma_x^{(1)} |n\rangle |m\rangle \langle n|, \tag{5.2}$$

where the eigenstates $\{|0\rangle, |1\rangle, |2\rangle, |3\rangle\}$ and corresponding energies can be found by

diagonalization of $H_{\mathcal{S}}$:

$$
\begin{aligned}
|0\rangle &= |00\rangle && \text{with } E_0 = -\omega_q - \frac{d}{2}, \\
|1\rangle &= \frac{1}{\sqrt{1+\left(\frac{E_1+d/2}{2g}\right)^2}}\left(|10\rangle - \frac{E_1+d/2}{2g}|01\rangle\right) && \text{with } E_1 = -\sqrt{4g^2+\frac{d^2}{4}}, \\
|2\rangle &= \frac{1}{\sqrt{1+\left(\frac{E_2+d/2}{2g}\right)^2}}\left(|10\rangle - \frac{E_2+d/2}{2g}|01\rangle\right) && \text{with } E_2 = \sqrt{4g^2+\frac{d^2}{4}}, \\
|3\rangle &= |11\rangle && \text{with } E_3 = \omega_q + \frac{d}{2}.
\end{aligned}
$$

Here the eigenstates are expressed in terms of the multi-qubit basis states defined in Sec. 2.1.

5.1 Hypothesis

A somewhat naïve expectation would be that the jump operator is confined to only induce errors on the system on the first qubit alone and just through the transverse coupling $\sigma_x^{(1)}$. However, considering the expression for the jump operator in Eq. (4.19) there is reason expect the jump operator might be given by other types of coupling and even two-qubit errors. This is because the system operator enters into the expression for the jump operator as its interaction picture Heisenberg evolution $\tilde{X}(s) = U^\dagger(s)XU(s)$, and with the coupling term in $H_{\mathcal{S}}$ this suggests that the system operator $\sigma_x^{(1)}$ will evolve into other Pauli operators. The Heisenberg equation of motion in the interaction picture is given by $\partial_t X = i[H_{\mathcal{S}}, X]$([10] p. 83), hence:

$$\partial_t \sigma_x^{(1)} = \omega_q \sigma_y^{(1)} - 2g\sigma_z^{(1)}\sigma_y^{(2)}. \tag{5.3}$$

Here the commutation relation for the Pauli operators has been used([10] p. 169): $[\sigma_a, \sigma_b] = i2\varepsilon_{abc}\sigma_c$. Since the system operator X enters into Eq. (4.19) in the integral with the jump correlator $g(t)$ it is only really evolved a short amount of time set by the timescale τ, because beyond this the jump operator is strongly suppressed by assumption, Hence, the integral hardly contributes when the magnitude of the argument of $g(t)$ is larger than τ. Because τ is assumed small, the equation of motion above suggests that $\sigma_x^{(1)}(\tau)$ can be approximated as:

$$\sigma_x^{(1)}(\tau) = \sigma_x^{(1)} + \omega_q \tau \sigma_y^{(1)} - 2g\tau\sigma_z^{(1)}\sigma_y^{(2)}. \tag{5.4}$$

Eqs. (5.3) and (5.4) indeed suggest, that the jump operator will be a mix of different types of errors, both single-qubit and two-qubit. They even suggest, that the amount of two-qubit error relative to single-qubit error is approximately proportional to ω_q/g.

In order to investigate exactly what kind of errors that the jump operator comprises, and to which extent the different errors are represented in the jump operator,

it is convenient to expand the jump operators in terms of all possible combinations of products of the Pauli matrices and the identity acting on the two qubits:

$$L = \sum_{i,j=0}^{4} \chi_{ij} \sigma_i \otimes \sigma_j. \tag{5.5}$$

As explained in Sec. 2.1 the first Pauli matrix from the right is the one acting on the first qubit, and the next Pauli matrix from the right is acting on the second qubit, etc. Hence, χ_{ij} is the generally complex coefficient for $\sigma_j^{(1)}\sigma_i^{(2)}$. This is the operator analogue of expanding the state ket of the system in terms of some basis (usually the eigenbasis), and so by normalizing these coefficients such that:

$$\sum_{ij} c_{ij} = 1, \text{ where } c_{ab} = \frac{|\chi_{ab}|^2}{\sum_{ij} |\chi_{ij}|^2}, \tag{5.6}$$

then the c_{ij} can be interpreted as the probability with which the jump operator acts like the corresponding combination of Pauli matrices on the system. It is straight forward to generalize this to more qubits, but for two qubits these coefficients can be expressed as a matrix. Fig. 5.1 shows, what kind of Pauli operator acting on the first qubit each column of this matrix corresponds to, and what kind of Pauli operator acting on the second qubit each row corresponds to. Furthermore, the blue areas comprise coefficients corresponding to single-qubit errors, and the green area comprises coefficients corresponding to two-qubit errors. With this grouping of the coefficients it is straight forward to define the relative coefficient of single-qubit error and the relative coefficient of two-qubit error as:

$$\kappa_1 = \sum_{i=1}^{3} (c_{0i} + c_{i0}) \text{ and } \kappa_2 = \sum_{i,j=1}^{3} c_{ij} \tag{5.7}$$

respectively.

	$\mathbb{1}^{(1)}$	$\sigma_x^{(1)}$	$\sigma_y^{(1)}$	$\sigma_z^{(1)}$
$\mathbb{1}^{(2)}$	c_{00}	c_{01}	c_{02}	c_{03}
$\sigma_x^{(2)}$	c_{10}	c_{11}	c_{12}	c_{13}
$\sigma_y^{(2)}$	c_{20}	c_{21}	c_{22}	c_{23}
$\sigma_z^{(2)}$	c_{30}	c_{31}	c_{32}	c_{33}

Figure 5.1: This figure shows, that each column of the coefficient matrix corresponds to a certain Pauli operator acting on the first qubit, and each row corresponds to a certain Pauli operator acting on the second qubit. The blue areas comprise coefficient corresponding to single-qubit errors, and the green area comprises coefficients corresponding to two-qubit errors.

Now a generalization of what was used in Eq. (2.6) can be employed to find expressions for the coefficients χ_{ij}:

$$\chi_{ij} = \frac{1}{4}\mathrm{tr}\left[\sigma_i \otimes \sigma_j L\right]. \tag{5.8}$$

Hence, it is straight forward to numerically find the relationship between the coefficients c_{ij} and different parameters of the system and bath, such as the qubit-qubit coupling or the temperature of the bath.

Using the above it can be shown that the only non-zero coefficients for the jump operator in Eq. (5.2) are:

$$\begin{aligned}
\chi_{01} &= \frac{\pi\sqrt{\gamma}}{4}\left(g_{01} + g_{02} + g_{10} + g_{20} + g_{13} + g_{23} + g_{31} + g_{32}\right), \\
\chi_{02} &= i\frac{\pi\sqrt{\gamma}}{4}\left(-g_{01} - g_{02} + g_{10} + g_{20} - g_{13} - g_{23} + g_{31} + g_{32}\right), \\
\chi_{13} &= \frac{\pi\sqrt{\gamma}}{4}\left(g_{01} - g_{02} + g_{10} - g_{20} - g_{13} + g_{23} - g_{31} + g_{32}\right), \\
\chi_{23} &= i\frac{\pi\sqrt{\gamma}}{4}\left(-g_{01} + g_{02} + g_{10} - g_{20} + g_{13} - g_{23} - g_{31} + g_{32}\right),
\end{aligned}$$

where the $g_{ij} = g(E_i - E_j)$ are the jump correlators. In the weak coupling limit $g \ll \omega_q$ and for zero detuning it can be shown, that the ratio of two-qubit error to single-qubit error inherent in the jump operator is approximately:

$$\frac{\kappa_2}{\kappa_1} \approx \left(\frac{g}{\omega_q}\right)^2. \tag{5.9}$$

This concurs with Eqs. (5.3) and (5.4) and the intuition that the stronger the qubits are coupled to each other the faster they will mix with each other, and so the error on the first qubit gets mixed into the second qubit. However, with a small coupling between the qubits this effect is expected to be very subtle, since in that case $g/\omega_q \ll 1$.

5.2 Jump operator coefficients

Fig. 5.2 provides four plots showing the relationship between the coefficients κ_1 and κ_2 and different parameters of the system and bath. In order to keep the Markovianity of the evolution sufficiently small, the system-bath coupling is chosen as $\gamma = 0.1$ kHz. In all cases the cutoff frequency is chosen as 31 GHz, and in Figs. 5.2 (a), (b) and (c) the temperature of the bath is set to 20 mK. This gives a Markovianity of $\Gamma\tau \approx 0.008$ ensuring the validity of the ULE. In Fig. 5.2 (d), however, the Markovianity varies with the temperature. The largest value it attains is $\Gamma\tau \approx 0.01$ keeping the evolution fairly Markovian.

All the plots unanimously confirm the expectation, that as the ratio g/ω_q grows, the part of the jump operator that acts as a single-qubit error κ_1 decreases, and the part acting as a two-qubit error κ_2 increases. Observe additionally in Fig. 5.2 (a), that for $g = 100$ MHz and zero detuning the ratio κ_2/κ_1 agrees well with the prediction in Eq.

(5.9), as $(g/\omega_q)^2 \approx 0.0004$ for these parameters. As expected the effect of two-qubit error is very subtle, and the largest value of κ_2 of all the data collected in the four figures (which occurs in the extreme case of $\omega_q = 0$ and $g = 100$ MHz in Fig. 5.2 (b)) does not even exceed 1.5 %. In [29] (although they do not show this explicitly) they do extract some jump operators that exhibit two-qubit noise even for such a small coupling. They provide data for some experimentally extracted jump operators for which κ_2 is on the order of 10^{-5}, which is in the same region as what has been numerically generated here for the qubit frequency $\omega_q = 5$ GHz and qubit-qubit coupling $g = 20$ MHz. For instance, in Fig. 5.2 (a) the entire data series for κ_2 with $g = 20$ MHz lie within the range $1.46 \cdot 10^{-5} - 1.60 \cdot 10^{-5}$.

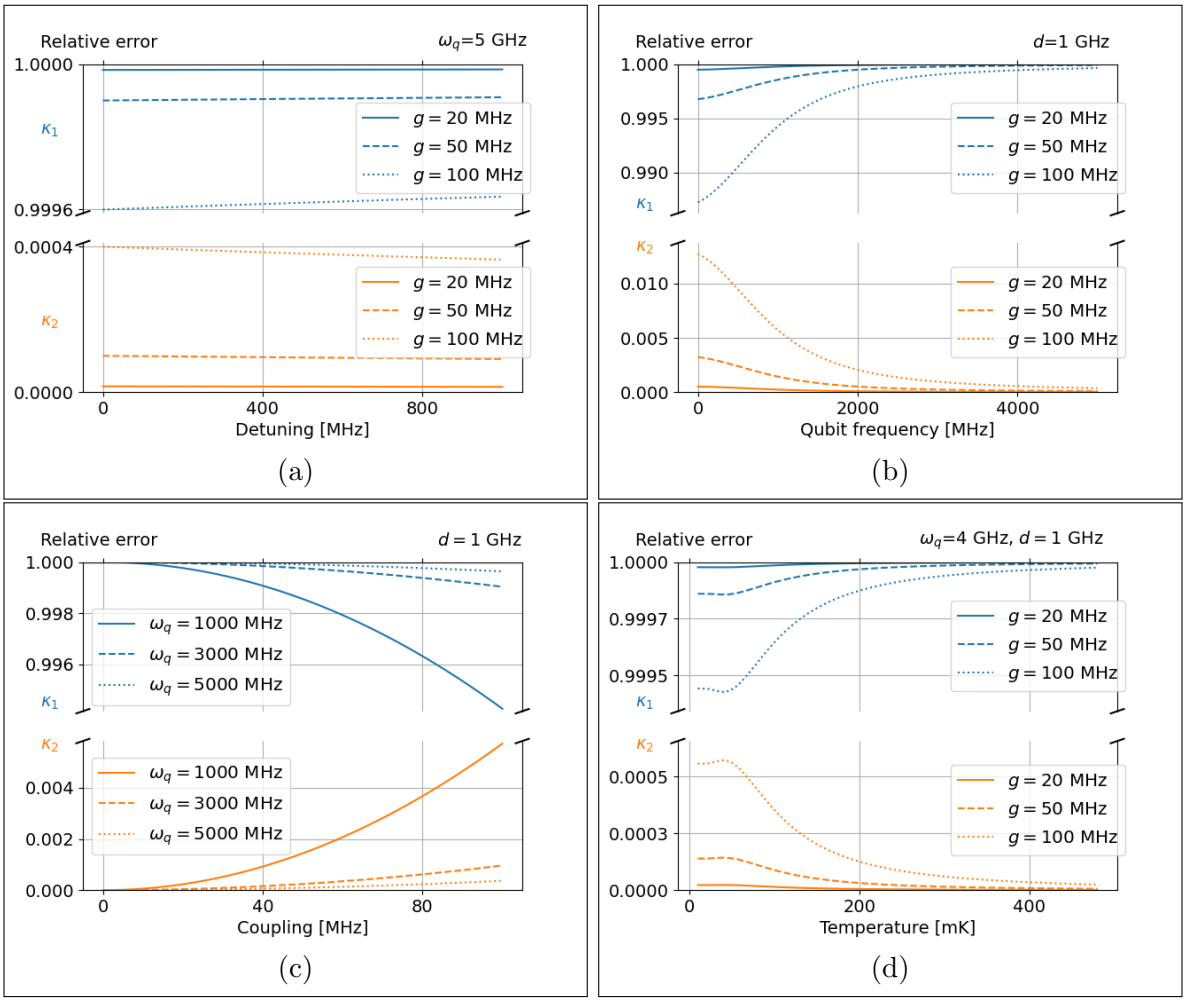

Figure 5.2: The coefficients κ_1 (blue) and κ_2 (orange) characterizing the proportions of single- and two-qubit errors respectively (as defined in Eq. (5.7)) as a function of: **(a)** detuning d, **(b)** qubit frequency ω_q, **(c)** qubit-qubit coupling g, and **(d)** temperature of the bath T.

A particularly interesting detail is the small kink in Fig. 5.2 (d), where for very small temperatures the ratio κ_2/κ_1 grows with increasing temperature before it peaks and then diminishes for still larger temperatures. The decrease is expected because as

seen in Fig. 3.3 the characteristic bath correlation time τ is inversely proportional to the temperature. Hence for growing temperature, τ decreases which gives the single-qubit operator $\sigma_x^{(1)}$ less time to evolve into a two-qubit operator as discussed above (see Eqs. (5.3) and (5.4)). A possible explanation for this peak can be realized when considering the plot for high temperatures and approaching $T = 0$, or in other words, considering the behavior of the system as τ grows. For large T and small τ the operator $\tilde{\sigma}_x^{(1)}(t)$ has little time to develop into a two-qubit operator, but as the temperature decreases and τ grows, $\tilde{\sigma}_x^{(1)}$ has more and more time to develop into a two-qubit operator. However, after some time the evolution will reach a turning point, at which $\tilde{\sigma}_x^{(1)}$ will start to evolve back into a single-qubit operator, before the jump correlator is sufficiently suppressed, and it might be this turning point that the kink in Fig. 5.2 (d) reflects.

The validity of this explanation can be assessed by considering the interaction picture Heisenberg evolution of $\sigma_x^{(1)}$:

$$\tilde{\sigma}_x^{(1)}(t) = \mathrm{e}^{iH_{\mathcal{S}}t}\sigma_x^{(1)}\mathrm{e}^{-iH_{\mathcal{S}}t}, \tag{5.10}$$

where $H_{\mathcal{S}}$ is given by Eq. (5.1). Once again, this can be expanded in terms of the Pauli matrices as in Eq. (5.5), only now the coefficients are time dependent. Thus the evolution of $\kappa_1(t)$ and $\kappa_2(t)$ for $\tilde{\sigma}_x^{(1)}$ can be found, and Fig. 5.3 (a) shows that these coefficients have a sinusoidal evolution. The hypothesis is then, that there is a directly proportional correlation between the time of the first peak in their evolution, which is given by half of the period of the oscillation $P_{1/2}$ (shown in red in the figure), and the value of τ corresponding to the temperature of the peak, T_{peak}, in Fig. 5.3 (b), which shows the same data for the jump operator coefficients as Fig. 5.2 (d).

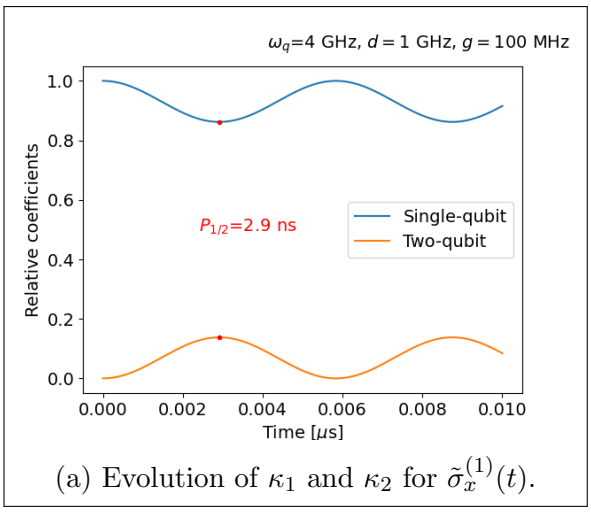

(a) Evolution of κ_1 and κ_2 for $\tilde{\sigma}_x^{(1)}(t)$.

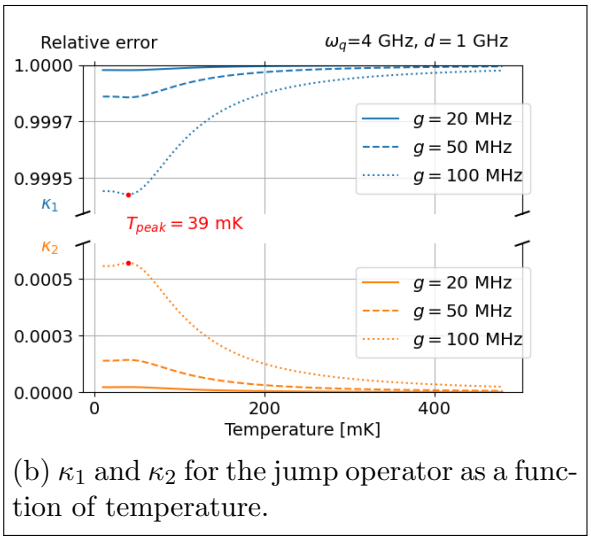

(b) κ_1 and κ_2 for the jump operator as a function of temperature.

Figure 5.3: **(a)** This shows the evolution of the single- and two-qubit error coefficients κ_1 and κ_2 for $\tilde{\sigma}_x^{(1)}$ with the time of the first peak indicated in red which is equal to half of the period of the oscillation $P_{1/2}$. **(b)** This presents the same data as Fig. 5.2 (d) with the temperature of the peak T_{peak} indicated in red. The hypothesis is, that this peak is due to the first peak in the evolution on the left, and the effect of the subsequent peaks in that evolution are suppressed by the decay of the jump correlator.

The data shown in blue in Fig. 5.4 is generated by finding the temperature of the peak in Fig. 5.3 (b) for different coupling strengths between the qubits, and then converting this temperature to τ_{peak} using Eq. (3.16). The data shown in orange is found by fitting either of the sinusoidal curves in Fig. 5.3 (a) and extracting the period of the oscillation. The time of the first peak is then half of this period $P_{1/2}$, which is also found for different coupling strengths between the qubits. The behavior of these two sets of data contradicts the hypothesis, that the peak in Fig. 5.2 (d) is due to the first peak in Fig. 5.3 (a). Additionally, the value of the τ_{peak} is so much smaller than the corresponding value of $P_{1/2}$, that the jump correlator should have decayed sufficiently to suppress any effect caused by the peak at $P_{1/2}$. Hence it is concluded, that the origin of this peak has a different explanation, as of yet unknown.

Since the coupling between the qubits is what motivated the expectation, that $\tilde{\sigma}_x^{(1)}(t)$ would evolve into two-qubit Pauli operators, it may be surprising to see, that the period of the oscillation (or equivalently the frequency) in Fig. 5.3 (a) seemingly has a finite limit for $g \to 0$ as suggested by the data in Fig. 5.4. The expansion of $\tilde{\sigma}_x^{(1)}(t)$ has the same non-zero coefficients as the jump operator, and those corresponding to two-qubit Pauli operators are given by:

$$c_{13} = \frac{1}{2}(\alpha - \beta)\left[\cos(\{E_0 - E_1\}t) - \cos(\{E_0 - E_2\}t)\right], \text{ and}$$
$$c_{23} = \frac{1}{2}(\alpha - \beta)\left[\sin(\{E_1 - E_0\}t) + \sin(\{E_0 - E_2\}t)\right],$$

where

$$\alpha = \frac{a}{a^2+1} \text{ with } a = \frac{E_1 + d/2}{2g}, \text{ and}$$
$$\beta = \frac{b}{b^2+1} \text{ with } b = \frac{E_2 + d/2}{2g}.$$

In the small coupling limit where $g \ll d$ the energies E_1 and E_2 can be approximated as:

$$E_1 = -E_2 \approx -\frac{d}{2} - 4\frac{g^2}{d}.$$

Plugging this into the coefficients above and employing some further simple approximations due to the small coupling limit leads to:

$$\kappa_2 = 8\left(\frac{g}{d}\right)^2\left[1 - \cos\left(\left\{d + 8\frac{g^2}{d}\right\}t\right)\right]. \tag{5.11}$$

This shows that the frequency of the oscillation in Fig. 5.3 (a) does indeed have a finite limit for $g \to 0$ given by the detuning d. However, the amplitude vanishes as $g \to 0$ which confirms the expectation, that $\tilde{\sigma}_x^{(1)}(t)$ only develops two-qubit Pauli operators for non-zero coupling between the qubits.

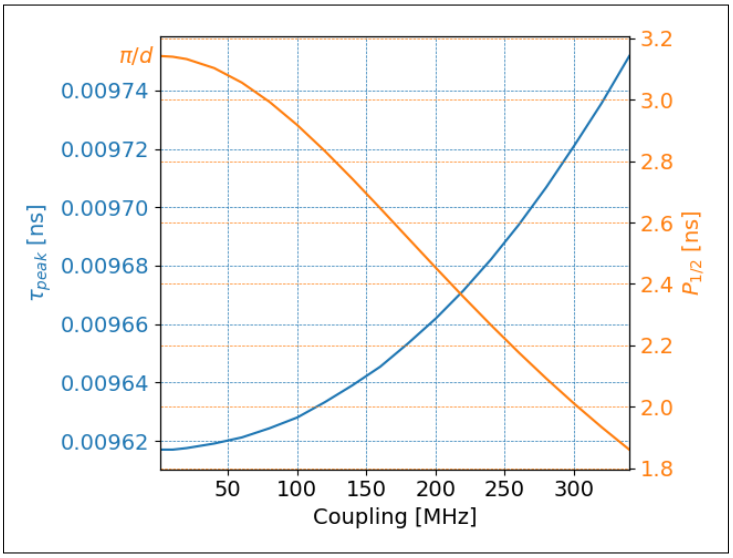

Figure 5.4: The blue data show the relationship between the value of τ corresponding to the temperature of the peak in Fig. 5.3 (b) and the qubit-qubit coupling. The orange data show the relationship between the time of the first peak in Fig. 5.3 (a) and the qubit-qubit coupling. The limit of $P_{1/2}$ for $g \to 0$ is indicated: π/d.

5.3 Evolution according to the SSE

For the simulations shown here the following parameters of the model are used (unless otherwise stated): $\omega_q = 4$ GHz, $d = 1$ GHz, and $g = 20$ MHz. The temperature of the bath is 20 mK, the cutoff frequency is $\omega_c = 31$ GHz, and the system-bath coupling is $\gamma = 0.1$ kHz. This gives $\Gamma\tau \approx 0.008$, indicating that the evolution of the system is well described by the ULE.

Two qubits located in the same quantum device are expected to be subjected to the same sources of noise. Hence in this section the two qubits will be connected via their respective σ_x Pauli operators to the same bath (with the assumption that the bath operators at the location of the respective qubits are uncorrelated by virtue of the arguments stated at the end of Sec. 4.3). Hence, the jump operators are given by:

$$L_1 = 2\pi\gamma \sum_{m,n=0}^{4} g(E_n - E_m) \langle m| \sigma_x^{(1)} |n\rangle |m\rangle \langle n| \,, \text{ and} \tag{5.12}$$

$$L_2 = 2\pi\gamma \sum_{m,n=0}^{4} g(E_n - E_m) \langle m| \sigma_x^{(2)} |n\rangle |m\rangle \langle n| \,. \tag{5.13}$$

The energy level structure due to the Hamiltonian in Eq. (5.1) is similar to that depicted in Fig. 4.2, so here the expectation that the ULE will preserve superpositions between eigenstates will be tested. This is conveniently done by monitoring the expectation value of the following operators throughout the evolution:

$$O_{01} = |0\rangle \langle 1| + |1\rangle \langle 0| \,, \text{ and} \tag{5.14}$$

$$O_{23} = |2\rangle \langle 3| + |3\rangle \langle 2| \,. \tag{5.15}$$

The operator O_{01} is sensitive to superpositions between eigenstates $|0\rangle$ and $|1\rangle$, and O_{23} is sensitive to superpositions between eigenstates $|2\rangle$ and $|3\rangle$.

Fig. 5.5 shows the evolution of the expectation value of these two operators along with the energy for the system starting in the eigenstate of O_{23} with eigenvalue 1:

$$|\psi_{23}\rangle = \frac{1}{\sqrt{2}}\left(|2\rangle + |3\rangle\right).$$

As the plot in the figure shows, the expectation value of O_{23} indeed starts at 1 before oscillating between 1 and -1 while decaying towards 0 (the time series here does not show the decay so well). Interestingly, the expectation value of O_{01} starts to develop small oscillations as the system evolves. This suggests that the coherence of the state is preserved across the transitions. This indeed confirms the expectation for the ULE stated above, which is something that is not expected for the QOME as discussed in connection with Fig. 4.2.

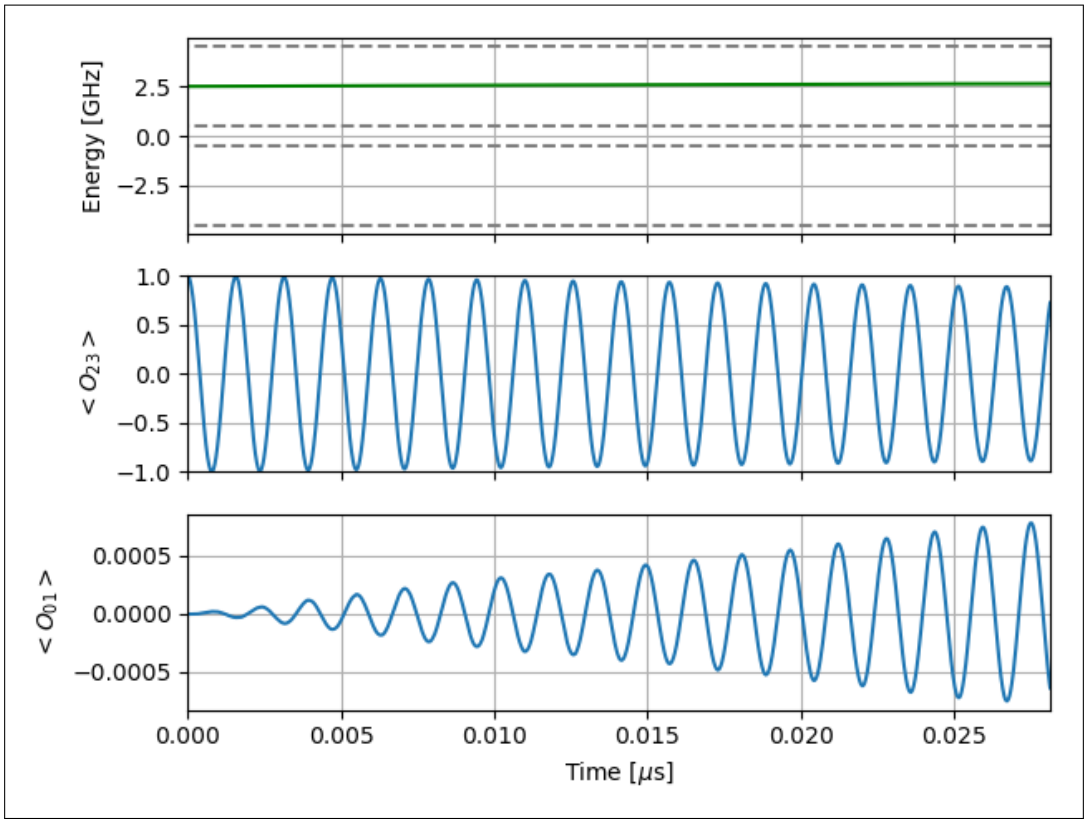

Figure 5.5: This is an average of 10,000 trajectories. It shows the evolution of different expectation values of the system starting in the state $|\psi_{23}\rangle = \frac{1}{\sqrt{2}}\left(|2\rangle + |3\rangle\right)$. In the top plot the eigenenergies of the system are indicated with dashed lines, and the green curve shows the evolution of the expectation value $\langle H\rangle$.

Looking closely at Fig. 5.5 it appears that the energy increases which may be surprising. The longer time series in Fig. 5.6 shows this initial increase as well but eventually it decays all the way towards the ground state energy (not visible in the

figure). This increase occurs because the action of either of the jump operators L_1 and L_2 on the initial state $|\psi_{23}\rangle$ puts the system into a higher energy state. This is confirmed by comparing the values of (see Eq. (4.25)):

$$\langle\psi_{\text{init}}|\, H\, |\psi_{\text{init}}\rangle \text{ and } \frac{\langle\psi_{\text{init}}|\, L_m^\dagger H L_m\, |\psi_{\text{init}}\rangle}{\delta p_m/\delta t},$$

where m is either 1 or 2. This means that each individual trajectory will most likely receive energy from the bath at the beginning of their evolution. There is no physical reason that it should be so, it may simply be the effect of the noise channels being connected to the σ_x Pauli operator of each qubit. By introducing additional noise channels to the qubits' other Pauli operators a more truthful prediction of the system's evolution may be realized.

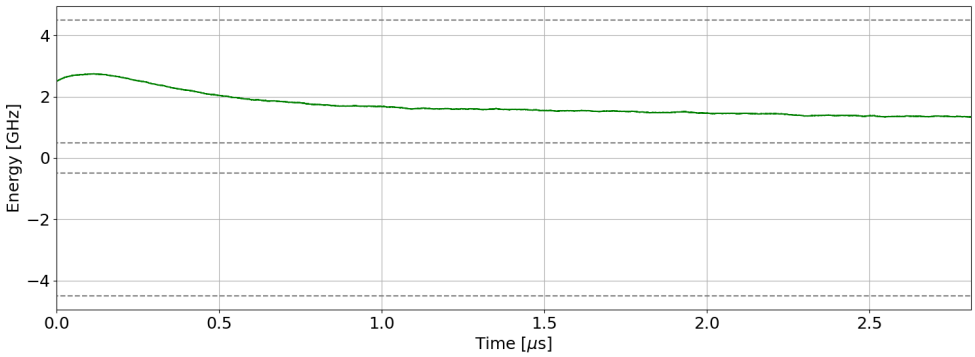

Figure 5.6: This shows the evolution of the energy of the system for the initial state $|\psi_{23}\rangle$. It is not visible here, but the energy eventually decays all the way to the ground state energy.

Chapter 6

Heisenberg chain of four spins

As a final demonstration this chapter presents some data generated according to the ULE and SSE for a system of qubits modelled as a Heisenberg chain of four spins with periodic boundary conditions and no splitting at each site. Hence, the Hamiltonian is given by:

$$H_{\mathcal{S}} = -g \sum_{i}^{4} \vec{\sigma}_i \cdot \vec{\sigma}_{i+1}. \tag{6.1}$$

Here $\vec{\sigma}_5 = \vec{\sigma}_1$, such that the chain forms a closed loop. This ensures translational symmetry from site to site such that a bath connected via a single noise channel to the σ_x Pauli operator at a particular site will affect the overall evolution of the system in the same way as if it had been connected to any other site.

Once again the noise channel is chosen as an Ohmic bath connected to $\sigma_x^{(1)}$. Since all spins are in some way coupled to each other (either directly or via their neighboring spins) it is expected that the jump operator will exhibit not only single- and two-qubit errors but also three- and four-qubit errors. This is based on the intuition that when the error has developed into the neighboring spins (as was seen in the preceding chapter) it is from there developed into the last spin in the chain opposite to the one connected to the bath. This can be ascertained by once again expanding the jump operator in terms of combinations of Pauli operators and the identity as in Eq. (5.5), only this time with tensor products of four Pauli operators, one for each site. Hence, κ_1, κ_2, κ_3, and κ_4 can be defined similarly to Eq. (5.7) representing single-, two-, three-, and four-qubit error respectively.

The data in Fig. 6.1 is simulated with spin-bath coupling given by $\gamma = 0.01\omega_0$, bath temperature $T = 2\omega_0$, and cutoff frequency $\omega_c = 100\omega_0$. This yields $\Gamma\tau \approx 0.002$ ensuring that the evolution is in the ULE regime. Fig. 6.1 (a) indeed shows that as the coupling g between the qubits increases, the jump operator develops more multi-qubit and less single-qubit error. In this setup the jump operator even comprises more two-qubit than single-qubit error for large coupling. There is a considerable amount of three-qubit error for larger coupling ending at 8.7 % for $g = 40\omega_0$. The amount of four-qubit error is scarce but non-zero and reaches 0.99 % for large coupling.

Fig. 6.1 (b) shows the evolution of the expectation value of the projection operator on the single-qubit state $|0\rangle$. This projection operator for the ith qubit is given by[28]:

$$P_0^{(i)} = \frac{\mathbb{1} + \sigma_z^{(i)}}{2}. \tag{6.2}$$

Hence, $p_0^{(i)} = \left\langle P_0^{(i)} \right\rangle$ is the probability for finding the ith qubit in the state $|0\rangle$. The evolution in Fig. 6.1 (b) is for $g = 5\omega_0$ and starts in the system's most excited eigenstate

which evidently is $|1100\rangle$. All four expectation values appear to oscillate about 0.5 with diminishing amplitude as the qubits mix with each other.

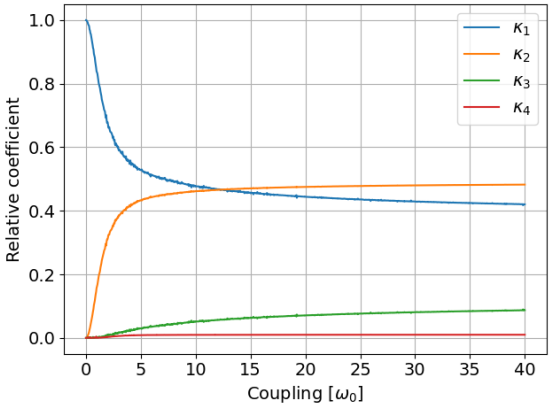

(a) The coefficients κ_1, κ_2, κ_3, and κ_4 as a function of qubit-qubit coupling.

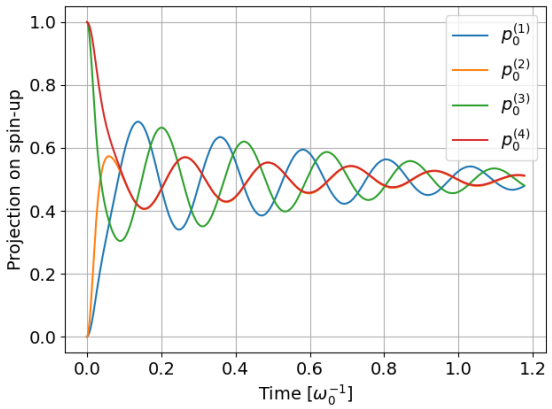

(b) Evolution of the expectation value of the projection operator on the single-qubit state $|0\rangle$ for all four qubits starting in the system's most excited eigenstate $|1100\rangle$.

Figure 6.1: These data are generated according to the ULE for a closed Heisenberg chain of four spins. In (b) the coupling is $g = 5\omega_0$.

Fig. 6.1 (a) shows that outside of the small coupling regime the ULE suggests that the effect of multi-qubit noise is certainly not negligible. This could also have been shown in Sec. 5.2 by allowing the qubit-qubit coupling g to approach or even exceed the qubit frequency ω_q, but then the results obtained might not have provided a truthful picture of the model in Eq. (5.1). The argumentation for the structure of this Hamiltonian was precisely based on the small coupling limit as discussed in connection with Eq. (2.13). Hence, there is presently nothing that suggests that the Hamiltonian in Eq. (5.1) would keep its form for large coupling. However, this does not eliminate the suggestion that the more dramatic effects shown in Fig. 6.1 (a) actually occurs in nature.

Chapter 7

Conclusion

In this thesis, the recently developed ULE was employed in predicting the evolution of a system of coupled superconducting qubits and particularly the noise and errors incumbent upon the qubits. It was shown that when a noise channel connects the environment to a specific qubit in the system, then the ULE predicts that a coupling between the qubits causes the noise to spread to the other qubits in the system. This means that any error in the multi-qubit state caused by the noise is not restricted to the one qubit connected to the bath. There is a probability that the noise channel will cause errors that affect the neighboring qubits as well. In Secs. 5.1 and 5.2 it was shown how the probability for various error events to occur can be quantified, and numerical data were generated for a system of two coupled superconducting qubits. These data indeed confirmed the intuition that when the coupling between the qubits increased, the probability for an error event to be affecting the state of both qubits increased as well. This prediction was further solidified by the numerical data generated for a system of four qubits modelled as a closed Heisenberg chain in Chapter 6.

The evolution of the two-qubit system as predicted by the ULE was also numerically simulated using the SSE, and the results obtained played a part in confirming the superiority of the ULE to the QOME in describing the evolution of particular systems. It was shown in Sec. 5.3 that the jump operators of the ULE preserves the coherence of a superposition state across transitions, whereas the jump operators of the QOME are expected to lose this information immediately due to their structure. This expected behavior due to the QOME, however, remains to be shown. It is possible to numerically simulate this in the same way as for the ULE, but take note of the increased intricacy of applying the jump operators of the QOME to the SSE. As discussed in Sec. 4.2 there emerges only one jump operator in the ULE per noise channel, whereas there emerges as many jump operators as there are energy transitions in the system in the QOME per noise channel. These many jump operators due to the QOME make the programming of the SSE considerably more laborious even for a small system of two qubits. Hence, not only is the ULE superior in its universality, it even simplifies the simulation of quantum systems using the SSE compared to the QOME.

While studying the theoretical effect of noise on superconducting qubits according to the ULE in this thesis, only transverse noise due to an Ohmic bath has been considered. A more complete picture can obtained by considering more carefully the type of noise that is usually present in superconducting systems, and how this noise couples to the qubits. In [23] they provide several examples of noise on superconducting qubits such as charge noise and magnetic flux noise. They also suggest different spectral densities as models for the baths that are the sources of the different types of noise, and whether each type of noise couples transversely or longitudinally to the qubits (transverse and longitudinal noise is discussed in Sec. 2.3).

Within the field of quantum error correction (QEC), which is the study of the pro-

tection of quantum information from logical errors[31], there is the concept of noise (or error) models. A noise model is a description of how a source of noise introduces logical errors onto an array of qubits. For example, in [32] (where they analyze correlated noise on a surface code) they define the *ballistic* noise model, which is where an error event introduces logical errors on qubits in a straight line on a toric code. However, the qubits on a toric code are not merely coupled along straight lines but in a much more complicated fashion. It has been shown in this thesis, that the ULE predicts that errors on an array of qubits will spread via the coupling between the qubits. Hence, more realistic noise models may be achieved by tailoring it according to the jump operators due to the ULE. The ULE is thus suggested as a tool for the future study of noise models in QEC.

Bibliography

[1] Elsevier (2021) *Quantum computing research trends report.* Available at: https://www.elsevier.com/solutions/scopus/who-uses-scopus/research-and-development/quantum-computing-report. (Accessed 07-05-2021).

[2] Eisert, J., Wolf, M.M. (2006) 'Quantum computing', *Handbook of Nature-Inspired and Innovative Computing*, [Online]. Available at: https://arxiv.org/abs/quant-ph/0401019v3. (Accessed 07-05-2021).

[3] Shor, P.W. (1996) 'Polynomial-Time Algorithms for Prime Factorization and Discrete Logarithms on a Quantum Computer', *SIAM J.Sci.Statist.Comput.*, 26, 1484 [Online]. Available at: https://arxiv.org/abs/quant-ph/9508027. (Accessed 07-05-2021).

[4] Moore, G.E. (1965) 'Cramming more components onto integrated circuits', *Electronics*, 38, 8 [Online]. Available at: https://newsroom.intel.com/wp-content/uploads/sites/11/2018/05/moores-law-electronics.pdf. (Accessed 07-05-2021).

[5] Steane, A. (2021) *Introduction to Ion Trap Quantum Computing*, University of Oxford, Department of Physics. Available at: https://www2.physics.ox.ac.uk/research/ion-trap-quantum-computing-group/intro-to-ion-trap-qc. (Accessed 07-05-2021).

[6] Hanson, R., Elzerman, J.M., Willems van Beveren, L.H. et al (2004) 'Electron spin qubits in quantum dots', *IEDM Technical Digest. IEEE International Electron Devices Meeting*, 2004, pp. 533-536. Available at: https://ieeexplore.ieee.org/document/1419211. (Accessed 07-05-2021).

[7] Lindblad, G. (1976) 'On the generators of quantum dynamical semigroups', *Communications in Mathematical Physics*, 48, [Online]. Available at: https://link.springer.com/article/10.1007/BF01608499. (Accessed 07-05-2021).

[8] Nathan, F., Rudner, M. (2020) 'Universal Lindblad equation for open quantum systems', *Phys. Rev. B*, 120, [Online]. Available at: https://arxiv.org/abs/2004.01469. (Accessed 20-05-2021).

[9] Sólyom, J. (2007) Chapter 26 - Superconductivity. In: Sólyom, J., *Fundamentals of the Physics of Solids*, pp. 449-515.

[10] Sakurai, J.J., Napolitano, J. (2017) *Modern quantum mechanics*, 2nd ed. Cambridge: Cambridge University Press

[11] Bruus, H., Flensberg, K. (2004) *Many-body quantum theory in condensed matter physics: an introduction*, Oxford: Oxford University Press

[12] Manzano, D. (2020) 'A short introduction to the Lindblad Master Equation', [Online]. Available at: `https://arxiv.org/abs/1906.04478`. (Accessed 20-05-2021).

[13] Breuer, H.-P., Petruccione, F. (2003) 'Concepts and methods in the theory of open quantum systems', [Online]. Available at: `https://arxiv.org/abs/quant-ph/0302047v1`. (Accessed 20-05-2021).

[14] Wikiversity (2020) *Open Quantum Systems/The Quantum Optical Master Equation*. Available at: `https://en.wikiversity.org/wiki/Open_Quantum_Systems/The_Quantum_Optical_Master_Equation`. (Accessed 09-05-2021).

[15] Casparis, L., Larsen, T.W., Olsen, M.S. et al. (2015) 'Gatemon Benchmarking and Two-Qubit Operation', *Physical Review Letters*, 116, [Online]. Available at: `https://arxiv.org/abs/1512.09195`. (Accessed 20-05-2021).

[16] Wikipedia (2021) *Matrix norm*. Available at: `https://en.wikipedia.org/wiki/Matrix_norm#L2,1_and_Lp,q_norms`. (Accessed 03-05-2021).

[17] Griffiths, D.J. (2014) *Introduction to electrodynamics*, 4th ed., Pearson new international ed., Edinburgh Gate: Pearson Education Limited.

[18] Fetter, A.L., Walecka, J.D., (2003) *Theoretical mechanics of particles and continua*, Mineola, New York: Dover Publications, Inc.

[19] Hedegård, P. (2018) *Statistisk fysik: forår 2018*, Copenhagen: Polyteknisk Boghandel.

[20] Simon, S.H. (2013) *The Oxford solid state physics*, 1st ed., Oxford: Oxford University Press.

[21] Riley, K.F., Hobson, M.P., (2011) *Essential mathematical methods: for the physical sciences*, Cambridge: Cambridge University Press.

[22] Grainger, R.G. (2013) Chapter 5 - Electromagnetic Scattering. In: Grainger, R.G., *An atmospheric radiative transfer primer* pp. 101-113.
Available at: `http://eodg.atm.ox.ac.uk/user/grainger/research/book/protected/Chapter5.pdf` (Accessed 31-03-2021).

[23] Krantz, P., Kjaergaard, M., Yan, F., et al (2019) 'A quantum engineer's guide to superconducting qubits', *Applied Physics Review 6*, issue 2, June [Online]. Available at: `https://arxiv.org/abs/1904.06560`. (Accessed 31-03-2021).

[24] Daley, A.J., (2014) 'Quantum trajectories and open many-body quantum systems', *Advances in Physics 63*, issue 2 [Online]. Available at: `https://arxiv.org/abs/1405.6694`. (Accessed 02-04-2021).

[25] Ingold, G.-L., (1998) Chapter 4 - Dissipative Quantum Systems. In: Dittrich, T., Hänggi, P., Ingold, G.-L. et al. *Quantum transport and dissipation*, pp. 213-248, [Online]. Available at: `https://www.physik.uni-augsburg.de/theo1/hanggi/Chapter_4.pdf`. (Accessed: 16-04-2021).

[26] Vion, D., Aassime, A., Cottet, A. et al. (2002) 'Manipulating the Quantum State of an Electrical Circuit', *Science*, 296, pp. 886-889. Available at: https://arxiv.org/abs/cond-mat/0205343. (Accessed 11-05-2021).

[27] Stack Exchange (2018) *How to draw a Bloch sphere*. Available at: https://tex.stackexchange.com/questions/345420/how-to-draw-a-bloch-sphere. (Accessed 12-05-2021).

[28] Greiner, W. (1990) Chapter 7 - Projection Operators for Energy and Spin. In: Relativistic Quantum Mechanics. Springer, Berlin, Heidelberg. Available at: https://link.springer.com/chapter/10.1007%2F978-3-662-02634-2_7. (Accessed 17-05-21).

[29] Samach, G.O., Greene, A., Borregaard, J., et al. (2021) 'Lindblad Tomography of a Superconducting Quantum Processor', [Online]. Available at: https://arxiv.org/abs/2105.02338. (Accessed 17-05-2021).

[30] Preskill, J. (2015) Chapter 2 - Foundations I: States and Ensembles. In: Physics 219/Computer Science 219 Quantum Computation lecture notes, [Online]. Available at: http://theory.caltech.edu/~preskill/ph219/index.html#lecture. (Accessed 20-05-2021).

[31] Preskill, J. (1999) Chapter 7 - Quantum Error Correction. In: Physics 219/Computer Science 219 Quantum Computation lecture notes, [Online]. Available at: http://theory.caltech.edu/~preskill/ph219/index.html#lecture. (Accessed 18-05-2021).

[32] Nickerson, N.H., Brown, B.J. (2019) 'Analysing correlated noise on the surface code using adaptive decoding algorithms', *Quantum 3*, 131, [Online]. Available at: https://arxiv.org/abs/1712.00502. (Accessed 18-05-2021).

[33] Wikipedia (2021) *L'Hôpital's rule*. Available at: https://en.wikipedia.org/wiki/L%27H%C3%B4pital%27s_rule. (Accessed 18-05-2021).

Appendix A

Derivations of master equations

This appendix provides some of the smaller and more tedious details of the derivations of the master equations presented in the main text of this thesis.

A.1 Derivation of the Bloch-Redfield equation

This section shows a part of the derivation of the Bloch-Redfield equation, specifically how to get from Eq. (3.8) to Eq. (3.9).

The second term in Eq. (3.8) vanishes when inserting $\tilde{\rho}_{\mathcal{SB}}(t_0) = \tilde{\rho}(t_0) \otimes \rho_{\mathcal{B}}$ (as assumed for t_0 being some arbitrary time in the remote past) and tracing over the bath:

$$\mathrm{tr}_{\mathcal{B}}\left(\left[\tilde{H}(t), \tilde{\rho}(t_0) \otimes \tilde{\rho}_{\mathcal{B}}\right]\right) = \sqrt{\gamma}\left[\tilde{X}(t), \tilde{\rho}(t_0)\right] \mathrm{tr}_{\mathcal{B}}\left(\tilde{B}(t)\rho_{\mathcal{B}}\right).$$

Here the cyclic property of the trace has been exploited, and by assumption each bath operator has vanishing expectation value, and so the above vanishes. What is left is:

$$\begin{aligned}\partial_t\tilde{\rho}(t) &= -\int_{t_0}^{t} \mathrm{d}t' \mathrm{tr}_{\mathcal{B}}\left(\left[\tilde{H}(t), \left[\tilde{H}(t'), \tilde{\rho}_{\mathcal{SB}}(t')\right]\right]\right) \\ &= -\gamma\int_{t_0}^{t} \mathrm{d}t' \mathrm{tr}_{\mathcal{B}}\left(\left[\tilde{X}(t)\tilde{B}(t), \left[\tilde{X}(t')\tilde{B}(t'), \tilde{\rho}(t') \otimes \rho_{\mathcal{B}}\right]\right]\right).\end{aligned}$$

Here the Born approximation has been employed, and on the left-hand side it was used that $\tilde{\rho} = \mathrm{tr}_{\mathcal{B}}(\tilde{\rho}_{\mathcal{SB}})$. Now begins the simplification of the commutator:

$$\begin{aligned}&\left[\tilde{X}(t)\tilde{B}(t), \left[\tilde{X}(t')\tilde{B}(t'), \tilde{\rho}(t') \otimes \rho_{\mathcal{B}}\right]\right] \\ =&\left[\tilde{X}(t)\tilde{B}(t), \tilde{X}(t')\tilde{\rho}(t')\tilde{B}(t')\rho_{\mathcal{B}} - \tilde{\rho}(t')\tilde{X}(t')\rho_{\mathcal{B}}\tilde{B}(t')\right] \\ =&\tilde{X}(t)\tilde{X}(t')\tilde{\rho}(t')\tilde{B}(t)\tilde{B}(t')\rho_{\mathcal{B}} - \tilde{X}(t)\tilde{\rho}(t')\tilde{X}(t')\tilde{B}(t)\rho_{\mathcal{B}}\tilde{B}(t') \\ &- \tilde{X}(t')\tilde{\rho}(t')\tilde{X}(t)\tilde{B}(t')\rho_{\mathcal{B}}\tilde{B}(t) + \tilde{\rho}(t')\tilde{X}(t')\tilde{X}(t)\rho_{\mathcal{B}}\tilde{B}(t')\tilde{B}(t) \\ =&\tilde{X}(t)\tilde{X}(t')\tilde{\rho}(t')\tilde{B}(t)\tilde{B}(t')\rho_{\mathcal{B}} - \tilde{X}(t')\tilde{\rho}(t')\tilde{X}(t)\tilde{B}(t')\rho_{\mathcal{B}}\tilde{B}(t) \\ &+ \left(\tilde{X}(t)\tilde{X}(t')\tilde{\rho}(t')\tilde{B}(t)\tilde{B}(t')\rho_{\mathcal{B}}\right)^{\dagger} - \left(\tilde{X}(t')\tilde{\rho}(t')\tilde{X}(t)\tilde{B}(t')\rho_{\mathcal{B}}\tilde{B}(t)\right)^{\dagger}\end{aligned}$$

Here it has been used that operators acting on different Hilbert spaces commute, and that all of the operators above are Hermitian. Notice that the last two terms are just the Hermitian conjugate of the first two terms which means that they can conveniently be expressed as *H.c.* Now taking the trace over the bath and once again using the its cyclic property reduces the above to:

$$\left[\tilde{X}(t), \tilde{X}(t')\tilde{\rho}(t')\right] \mathrm{tr}_{\mathcal{B}}\left(\tilde{B}(t)\tilde{B}(t')\rho_{\mathcal{B}}\right) + H.c.$$

Plugging this back in to Eq. (3.8) immediately leads to Eq. (3.9).

A.2 Derivation of the quantum optical master equation

Starting from the Bloch-Redfield equation in Eq. (3.10) the first step is to switch the system operators back to the Schrödinger picture and inserting two complete sets in the eigenbasis of the system Hamiltonian ($\mathbb{1} = \sum_m |m\rangle \langle m|$, where $H_\mathcal{S} |m\rangle = E_m |m\rangle$), which for simplicity will be assumed time-independent:

$$\begin{aligned}\tilde{X}(t) =& \mathrm{e}^{iH_\mathcal{S}t} X \mathrm{e}^{-iH_\mathcal{S}t} \\ =& \sum_{mn} \mathrm{e}^{iH_\mathcal{S}t} |m\rangle \langle m| X |n\rangle \langle n| \mathrm{e}^{-iH_\mathcal{S}t} \\ =& \sum_{mn} \mathrm{e}^{i(E_m - E_n)t} \hat{X}_{mn}, \text{ where } \hat{X}_{mn} \equiv |m\rangle \langle m| X |n\rangle \langle n| .\end{aligned}$$

Plugging this into Eq. (3.10) gives:

$$\partial_t \tilde{\rho} = -\gamma \int_{-\infty}^{t} \mathrm{d}t' J(t-t') \sum_{mnpq} \left[\mathrm{e}^{i(E_m - E_n)t} \hat{X}_{mn}, \mathrm{e}^{i(E_p - E_q)t'} \hat{X}_{pq} \tilde{\rho} \right] + H.c.$$

Here and in the following $\tilde{\rho} \equiv \tilde{\rho}(t)$ to avoid clutter. Changing the variable of integration from $t' \to t - t'$ leads to:

$$\begin{aligned}\partial_t \tilde{\rho} =& -\gamma \sum_{mnpq} \Gamma_{pq} \mathrm{e}^{i(E_m - E_n + E_p - E_q)t} \left[\hat{X}_{mn}, \hat{X}_{pq} \tilde{\rho} \right] + H.c., \text{ where} \\ \Gamma_{mn} \equiv& \int_0^\infty \mathrm{d}t J(t) \mathrm{e}^{-i(E_m - E_n)t}.\end{aligned}$$

Now the rotating wave approximation is invoked by discarding terms in the sum where $E_m - E_n + E_p - E_q \neq 0$. This is based on the assumption, that the relaxation rate of the bath is much smaller than both the temperature of the bath and the smallest difference between energy levels of the system. The relaxation rate is governed by the system-bath coupling parameter γ, so when this is sufficiently small the terms where $E_m - E_n + E_p - E_q \neq 0$ average to zero. The remaining terms are the ones where either $m = n$ and $p = q$, or $m = q$ and $n = p$. Here it is assumed that no two distinct transitions occur at the same frequency. Discarding the rest is easily done by replacing the exponential in the sum with $\delta_{mn}\delta_{pq} + \delta_{mq}\delta_{np} - \delta_{mn}\delta_{np}\delta_{pq}$, where δ_{mn} is the Kronecker delta. The term $\delta_{mn}\delta_{np}\delta_{pq}$ is subtracted to avoid counting the case where $m = n = p = q$ twice. Hence:

$$\begin{aligned}\partial_t \tilde{\rho} =& -\gamma \sum_{mnpq} \left(\delta_{mn}\delta_{pq} + \delta_{mq}\delta_{np} - \delta_{mn}\delta_{np}\delta_{pq} \right) \Gamma_{pq} \left[\hat{X}_{mn}, \hat{X}_{pq} \tilde{\rho} \right] + H.c. \\ =& -\gamma \left(\sum_{mn} \Gamma_{nn} \left[\hat{X}_{mm}, \hat{X}_{nn} \tilde{\rho} \right] + \sum_{mn} \Gamma_{nm} \left[\hat{X}_{mn}, \hat{X}_{nm} \tilde{\rho} \right] - \sum_{m} \Gamma_{mm} \left[\hat{X}_{mm}, \hat{X}_{mm} \tilde{\rho} \right] \right) \\ &+ H.c.\end{aligned}$$

The last sum can be cancelled with the terms in the second sum where $m = n$:

$$\partial_t \tilde{\rho} = -\gamma \left(\sum_{mn} \Gamma_{nn} \left[\hat{X}_{mm}, \hat{X}_{nn} \tilde{\rho} \right] + \sum_{m \neq n} \Gamma_{nm} \left[\hat{X}_{mn}, \hat{X}_{nm} \tilde{\rho} \right] \right) + H.c.$$

Now it is convenient to split Γ_{mn} in to its real and imaginary part such that $\Gamma_{mn} = \frac{1}{2}J_{mn} + iS_{mn}$. With this definition, consider the terms of the second sum above and its Hermitian conjugate counterpart:

$$\begin{aligned}
&\left(\frac{1}{2}J_{nm} + iS_{nm}\right)\left[\hat{X}_{mn}, \hat{X}_{nm}\tilde{\rho}\right] + \left(\frac{1}{2}J_{nm} - iS_{nm}\right)\left[\tilde{\rho}\hat{X}^\dagger_{nm}, \hat{X}^\dagger_{mn}\right] \\
=&\frac{1}{2}J_{nm}\left(\hat{X}_{mn}\hat{X}_{nm}\tilde{\rho} - \hat{X}_{nm}\tilde{\rho}\hat{X}_{mn} + \tilde{\rho}\hat{X}^\dagger_{nm}\hat{X}^\dagger_{mn} - \hat{X}^\dagger_{mn}\tilde{\rho}\hat{X}^\dagger_{nm}\right) \\
&+ iS_{nm}\left(\hat{X}_{mn}\hat{X}_{nm}\tilde{\rho} - \hat{X}_{nm}\tilde{\rho}\hat{X}_{mn} - \tilde{\rho}\hat{X}^\dagger_{nm}\hat{X}^\dagger_{mn} + \hat{X}^\dagger_{mn}\tilde{\rho}\hat{X}^\dagger_{nm}\right).
\end{aligned}$$

The definition of $\hat{X}_{mn}$ ensures that $\hat{X}^\dagger_{mn} = \hat{X}_{nm}$. Thus the above can be rewritten as:

$$\begin{aligned}
&\frac{1}{2}J_{nm}\left(\hat{X}^\dagger_{nm}\hat{X}_{nm}\tilde{\rho} - \hat{X}_{nm}\tilde{\rho}\hat{X}^\dagger_{nm} + \tilde{\rho}\hat{X}^\dagger_{nm}\hat{X}_{nm} - \hat{X}_{nm}\tilde{\rho}\hat{X}^\dagger_{nm}\right) \\
&+ iS_{nm}\left(\hat{X}_{mn}\hat{X}_{nm}\tilde{\rho} - \hat{X}_{nm}\tilde{\rho}\hat{X}^\dagger_{nm} - \tilde{\rho}\hat{X}_{mn}\hat{X}_{nm} + \hat{X}_{nm}\tilde{\rho}\hat{X}^\dagger_{nm}\right) \\
=&J_{nm}\left(\frac{1}{2}\left\{\hat{X}^\dagger_{nm}\hat{X}_{nm}, \tilde{\rho}\right\} - \hat{X}_{nm}\tilde{\rho}\hat{X}^\dagger_{nm}\right) + iS_{nm}\left[\hat{X}_{mn}\hat{X}_{nm}, \tilde{\rho}\right].
\end{aligned}$$

Similarly, consider the terms of the first sum:

$$\begin{aligned}
&\left(\frac{1}{2}J_{nn} + iS_{nn}\right)\left[\hat{X}_{mm}, \hat{X}_{nn}\tilde{\rho}\right] + \left(\frac{1}{2}J_{nn} - iS_{nn}\right)\left[\tilde{\rho}\hat{X}^\dagger_{nn}, \hat{X}^\dagger_{mm}\right] \\
=&\frac{1}{2}J_{nn}\left(\hat{X}^\dagger_{mm}\hat{X}_{nn}\tilde{\rho} - \hat{X}_{nn}\tilde{\rho}\hat{X}^\dagger_{mm} + \tilde{\rho}\hat{X}^\dagger_{nn}\hat{X}_{mm} - \hat{X}_{mm}\tilde{\rho}\hat{X}^\dagger_{nn}\right) \\
&+ iS_{nn}\left(\hat{X}_{mm}\hat{X}_{nn}\tilde{\rho} - \hat{X}_{nn}\tilde{\rho}\hat{X}^\dagger_{mm} - \tilde{\rho}\hat{X}_{nn}\hat{X}_{mm} + \hat{X}_{mm}\tilde{\rho}\hat{X}^\dagger_{nn}\right).
\end{aligned}$$

For every term in the sum where $m = a$ and $n = b$ there is another term where $m = b$ and $n = a$, such that their sum can be rewritten as:

$$\hat{X}^\dagger_{aa}\hat{X}_{bb}\tilde{\rho} + \tilde{\rho}\hat{X}^\dagger_{bb}\hat{X}_{aa} + \hat{X}^\dagger_{bb}\hat{X}_{aa}\tilde{\rho} + \tilde{\rho}\hat{X}^\dagger_{aa}\hat{X}_{bb} = \left\{\hat{X}^\dagger_{aa}\hat{X}_{bb}, \tilde{\rho}\right\} + \left\{\hat{X}^\dagger_{bb}\hat{X}_{aa}, \tilde{\rho}\right\},$$

and similarly for $\hat{X}_{aa}\tilde{\rho}\hat{X}^\dagger_{bb}$ and $[\hat{X}^\dagger_{aa}\hat{X}_{bb}, \tilde{\rho}]$. Additionally, the definition of Γ_{mn} ensures that $J_{aa} = J_{bb}$. Using all this for the master equation gives:

$$\begin{aligned}
\partial_t\tilde{\rho} = -\gamma\Bigg(&\sum_{mn}\left(\frac{1}{2}J_{nn}\left\{\hat{X}^\dagger_{mm}\hat{X}_{nn}, \tilde{\rho}\right\} - J_{nn}\hat{X}_{nn}\tilde{\rho}\hat{X}^\dagger_{mm} + iS_{nn}\left[\hat{X}_{mm}\hat{X}_{nn}, \tilde{\rho}\right]\right) \\
&+ \sum_{m\neq n}\left(\frac{1}{2}J_{nm}\left\{\hat{X}^\dagger_{nm}\hat{X}_{nm}, \tilde{\rho}\right\} - J_{nm}\hat{X}_{nm}\tilde{\rho}\hat{X}^\dagger_{nm} + iS_{nm}\left[\hat{X}_{mn}\hat{X}_{nm}, \tilde{\rho}\right]\right)\Bigg).
\end{aligned}$$

Now observe that

$$J_{mn} = \Gamma_{mn} + \Gamma^*_{mn} = \int_{-\infty}^{\infty} \mathrm{d}t J(t)\mathrm{e}^{i(E_n - E_m)} = 2\pi J(E_n - E_m),$$

by the definition of the bath spectral function Eq. (3.12). Hence $J_{mm} = J(0)$, and so by defining

$$L_{ph} \equiv \sqrt{2\pi\gamma J(0)} \sum_m \hat{X}_{mm}$$

as the dephasing jump operator, and

$$L_{mn} \equiv \sqrt{2\pi\gamma J(E_n - E_m)} \hat{X}_{mn}$$

as the decay jump operators, the QOME can be cast in the Lindblad form:

$$\partial_t \tilde{\rho} = -i\left[\Lambda, \tilde{\rho}\right] + L_{ph}\tilde{\rho}L_{ph}^\dagger - \frac{1}{2}\left\{L_{ph}^\dagger L_{ph}, \tilde{\rho}\right\} + \sum_{m\neq n}\left(L_{mn}\tilde{\rho}L_{mn}^\dagger - \frac{1}{2}\left\{L_{mn}^\dagger L_{mn}, \tilde{\rho}\right\}\right).$$

A.3 Derivation of the universal Lindblad equation

The objective of this section is to express the ULE in Lindblad form starting from:

$$\partial_t \tilde{\rho}(t) = -\gamma \int_{-\infty}^{\infty} \mathrm{d}s \int_{-\infty}^{\infty} \mathrm{d}s' \theta(s-s') g(s-t) g(t-s') \left[\tilde{X}(s), \tilde{X}(s')\tilde{\rho}(t)\right] + H.c.$$

The first step to this is to decompose the Heaviside step function into its symmetric and anti-symmetric parts: $\theta(s-s') = \frac{1}{2} + \frac{1}{2}\mathrm{sgn}(s-s')$, where the sign-function has been introduced: $\mathrm{sgn}(t) = 1$ for $t > 0$, $\mathrm{sgn}(t) = -1$ for $t < 0$, and $\mathrm{sgn}(0) = 0$. To avoid too lengthy equations, in the following the parts of the master equation connected with the symmetric and anti-symmetric parts of $\theta(s-s')$ will be treated separately. First, all that is connected to the sign-function will be written out:

$$\begin{aligned}
&-\frac{\gamma}{2}\int_{-\infty}^{\infty}\mathrm{d}s\int_{-\infty}^{\infty}\mathrm{d}s'\mathrm{sgn}(s-s')\Big[g(s-t)g(t-s')\tilde{X}(s)\tilde{X}(s')\tilde{\rho}(t) \\
&\qquad - g(s-t)g(t-s')\tilde{X}(s')\tilde{\rho}(t)\tilde{X}(s) \\
&\qquad + g^*(s-t)g^*(t-s')\tilde{\rho}(t)\tilde{X}(s')\tilde{X}(s) \\
&\qquad - g^*(s-t)g^*(t-s')\tilde{X}(s)\tilde{\rho}(t)\tilde{X}(s')\Big] \\
&= -\frac{\gamma}{2}\int_{-\infty}^{\infty}\mathrm{d}s\int_{-\infty}^{\infty}\mathrm{d}s'\mathrm{sgn}(s-s')\Big[g(s-t)g(t-s')\tilde{X}(s)\tilde{X}(s')\tilde{\rho}(t) \\
&\qquad - g(s-t)g(t-s')\tilde{X}(s')\tilde{\rho}(t)\tilde{X}(s) \\
&\qquad + g(t-s)g(s'-t)\tilde{\rho}(t)\tilde{X}(s')\tilde{X}(s) \\
&\qquad - g(t-s)g(s'-t)\tilde{X}(s)\tilde{\rho}(t)\tilde{X}(s')\Big].
\end{aligned}$$

Here it has been used that the jump correlator has the symmetric property $g^*(t) = g(-t)$ which is easily verified by complex conjugation of Eq. (3.13), keeping in mind that the bath spectral function is real.

Since the limits of integration of s and s' are the same, these two variables can be interchanged in any of the four terms above. Applying it to the last two terms and using that $\mathrm{sgn}(t'-t) = -\mathrm{sgn}(t-t')$ yields:

$$-\frac{\gamma}{2}\int_{-\infty}^{\infty}\mathrm{d}s\int_{-\infty}^{\infty}\mathrm{d}s'\mathrm{sgn}(s-s')g(s-t)g(t-s')\left[\tilde{X}(s)\tilde{X}(s'),\tilde{\rho}(t)\right] = -i\left[\tilde{\Lambda}(t),\tilde{\rho}(t)\right].$$

Here, the Lamb shift $\tilde{\Lambda}$ is defined as:

$$\tilde{\Lambda}(t) = \frac{\gamma}{i2}\int_{-\infty}^{\infty}\mathrm{d}s\int_{-\infty}^{\infty}\mathrm{d}s'\tilde{X}(s)g(s-t)g(t-s')\tilde{X}(s')\mathrm{sgn}(s-s'). \tag{A.1}$$

Now for the other part of the master equation connected to the symmetric part of $\theta(s-s')$:

$$\begin{aligned}-\frac{\gamma}{2}\int_{-\infty}^{\infty}\mathrm{d}s\int_{-\infty}^{\infty}\mathrm{d}s'\Big[&g(s-t)g(t-s')\tilde{X}(s)\tilde{X}(s')\tilde{\rho}(t)\\ &- g(s-t)g(t-s')\tilde{X}(s')\tilde{\rho}(t)\tilde{X}(s)\\ &+ g^*(s-t)g^*(t-s')\tilde{\rho}(t)\tilde{X}(s')\tilde{X}(s)\\ &- g^*(s-t)g^*(t-s')\tilde{X}(s)\tilde{\rho}(t)\tilde{X}(s')\Big].\end{aligned}$$

Once again using that $g^*(t) = g(-t)$ leads to:

$$\begin{aligned}&-\frac{\gamma}{2}\int_{-\infty}^{\infty}\mathrm{d}sg^*(t-s)\tilde{X}(s)\int_{-\infty}^{\infty}\mathrm{d}s'g(t-s')\tilde{X}(s')\tilde{\rho}(t)\\ &+\frac{\gamma}{2}\int_{-\infty}^{\infty}\mathrm{d}s'g(t-s')\tilde{X}(s')\tilde{\rho}(t)\int_{-\infty}^{\infty}\mathrm{d}sg^*(t-s)\tilde{X}(s')\\ &-\frac{\gamma}{2}\tilde{\rho}(t)\int_{-\infty}^{\infty}\mathrm{d}s'g^*(t-s')\tilde{X}(s')\int_{-\infty}^{\infty}\mathrm{d}sg(t-s)\tilde{X}(s)\\ &+\frac{\gamma}{2}\int_{-\infty}^{\infty}\mathrm{d}sg(t-s)\tilde{X}(s)\tilde{\rho}(t)\int_{-\infty}^{\infty}\mathrm{d}s'g^*(t-s')\tilde{X}(s')\\ &=\tilde{L}(t)\tilde{\rho}(t)\tilde{L}^\dagger(t) - \frac{1}{2}\left\{\tilde{L}^\dagger(t)\tilde{L}(t),\tilde{\rho}(t)\right\},\end{aligned}$$

where the jump operator is defined as:

$$\tilde{L}(t) = \sqrt{\gamma}\int_{-\infty}^{\infty}\mathrm{d}sg(t-s)\tilde{X}(s). \tag{A.2}$$

Putting all this together gives the ULE in the interaction picture for a single noise channel:

$$\partial_t\tilde{\rho}(t) = -i\left[\tilde{\Lambda}(t),\tilde{\rho}(t)\right] + \tilde{L}(t)\tilde{\rho}(t)\tilde{L}^\dagger(t) - \frac{1}{2}\left\{\tilde{L}^\dagger(t)\tilde{L}(t),\tilde{\rho}(t)\right\}. \tag{A.3}$$

Appendix B

Bath of electromagnetic modes

In this appendix the bath correlation function in Eq. (4.14) will be calculated for the idealized physical example of electromagnetic modes in a 1-dimensional cavity. But first it is instructive to think about what kind of correlation there might exist between bath operators that give rise to different noise channels α and β. If for instance α and β represent noise channels to different noise sources originating from distinct sub-baths, it is fairly intuitive to assume that these sub-baths are independent and have no correlation. If however α and β represent different localities within the same bath, then there is no apparent reason why their correlation should vanish. In this case the bath correlation function provides a measure of the spatial as well as a the temporal correlation between the bath operators, and Eq. (4.14) can be thought of as $J_{\alpha\beta}(t-t') = J(r_\alpha - r_\beta, t-t')$. Such a correlation function will be derived here.

B.1 Quantization of the electromagnetic field

This derivation is inspired by Sec. 1.4.2 in [11].

In a 1-dimensional electromagnetic cavity (with no charge or current) the electric field is completely determined by the vector potential $\mathbf{A}(r,t)$ ([11] p. 19). By choosing Coulomb gauge $\nabla \cdot \mathbf{A} = 0$ the vector potential obeys the wave equation ([17] p. 558):

$$\nabla^2 \mathbf{A} - \mu_0 \epsilon_0 \partial_t^2 \mathbf{A} = 0,$$

and the electric and magnetic fields are given by $\mathbf{E} = -\partial_t \mathbf{A}$ and $\mathbf{B} = \nabla \times \mathbf{A}$ respectively.

By assuming the bath to be of finite size L and to have periodic boundary conditions, a solution to this equation is ([11] p. 20):

$$\mathbf{A}(x,t) = \sum_k \left(A_k \mathrm{e}^{i(kx-\omega_k t)} + A_k^* \mathrm{e}^{-i(kx-\omega_k t)} \right) \hat{y}. \tag{B.1}$$

Here A_k are the expansion coefficients determining the field strength, and the field is assumed to be polarized in the y-direction and travelling along the x-direction. The periodic boundaries demand that $k = 2\pi n/L$, where $n \in \mathbb{Z}$, and $\omega_k = c|k|$ with $c = 1/\sqrt{\mu_0 \epsilon_0}$ being the speed of light in vacuum.

From Eq. (B.1) the electric and magnetic fields are determined:

$$\mathbf{E}(x,t) = i \sum_k \omega_k \left(A_k \mathrm{e}^{i(kx-\omega_k t)} - A_k^* \mathrm{e}^{-i(kx-\omega_k t)} \right) \hat{y} \text{ and} \tag{B.2}$$

$$\mathbf{B}(x,t) = i \sum_k k \left(A_k \mathrm{e}^{i(kx-\omega_k t)} - A_k^* \mathrm{e}^{-i(kx-\omega_k t)} \right) \hat{z}. \tag{B.3}$$

Notice that $|\mathbf{B}| = |\mathbf{E}|/c$. Hence, with these expressions the classical Hamiltonian for an electromagnetic field can be found as:

$$H = \frac{1}{2} \int_0^L \mathrm{d}x \left(\epsilon_0 \left| \mathbf{E}(x,t) \right|^2 + \frac{1}{\mu_0} \left| \mathbf{B}(x,t) \right|^2 \right). \tag{B.4}$$

The square of the electric field can be expressed as:

$$|\mathbf{E}(x,t)|^2 = \sum_{kq} \omega_k\omega_q \Big(A_k A_q^* \mathrm{e}^{i[(k-q)x-(\omega_k-\omega_q)t]} - A_k A_q \mathrm{e}^{i[(k+q)x-(\omega_k+\omega_q)t]} \\ - A_k^* A_q^* \mathrm{e}^{-i[(k+q)x-(\omega_k+\omega_q)t]} + A_k^* A_q \mathrm{e}^{-i[(k-q)x-(\omega_k-\omega_q)t]} \Big),$$

and similarly for the magnetic field, except that $\omega_k\omega_q$ is replaced by kq. Hence, the integration over x amounts to solving integrals of the form:

$$\int_0^L \mathrm{d}x \mathrm{e}^{i(k-q)x} = \left[\frac{\mathrm{e}^{i(k-q)x}}{i(k-q)} \right]_0^L = \frac{\mathrm{e}^{i(k-q)L} - 1}{i(k-q)}.$$

Since k and q are both integer multiples of $2\pi/L$ then so is their difference, and so the above vanishes for $k \neq q$. However, for $k = q$ the solution is non-trivial. By defining $\delta \equiv k - q$ this can be solved using l'Hôpital's rule[33]:

$$\lim_{\delta\to 0} \frac{\mathrm{e}^{i\delta L} - 1}{i\delta} = \lim_{\delta\to 0} \frac{iL\mathrm{e}^{i\delta L}}{i} = L, \text{ and hence } \int_0^L \mathrm{d}x \mathrm{e}^{i(k-q)x} = \delta_{k,q} L,$$

where $\delta_{k,q}$ is the Kronecker delta.

Using all this for the Hamiltonian in Eq. (B.4) gives:

$$\begin{aligned} H = \frac{L}{2} \Bigg[& \epsilon_0 \sum_{kq} \omega_k\omega_q \Big(\delta_{k,q} A_k A_q^* \mathrm{e}^{-i(\omega_k-\omega_q)t} - \delta_{k,-q} A_k A_q \mathrm{e}^{-i(\omega_k+\omega_q)t} \\ & - \delta_{k,-q} A_k^* A_q^* \mathrm{e}^{i(\omega_k+\omega_q)t} + \delta_{k,q} A_k^* A_q \mathrm{e}^{i(\omega_k-\omega_q)t} \Big) \\ & + \frac{1}{\mu_0} \sum_{kq} kq \Big(\delta_{k,q} A_k A_q^* \mathrm{e}^{-i(\omega_k-\omega_q)t} - \delta_{k,-q} A_k A_q \mathrm{e}^{-i(\omega_k+\omega_q)t} \\ & - \delta_{k,-q} A_k^* A_q^* \mathrm{e}^{i(\omega_k+\omega_q)t} + \delta_{k,q} A_k^* A_q \mathrm{e}^{i(\omega_k-\omega_q)t} \Big) \Bigg] \\ = \frac{L}{2} \Bigg[& \epsilon_0 \sum_k \omega_k^2 \Big(2|A_k|^2 - A_k A_{-k} \mathrm{e}^{-i2\omega_k t} - A_k^* A_{-k}^* \mathrm{e}^{i2\omega_k t} \Big) \\ & + \frac{1}{\mu_0} \sum_k k^2 \Big(2|A_k|^2 + A_k A_{-k} \mathrm{e}^{-i2\omega_k t} + A_k^* A_{-k}^* \mathrm{e}^{i2\omega_k t} \Big) \Bigg]. \end{aligned}$$

Here it has been used that $\omega_{-k} = \omega_k$, and using that $k = \omega_k/c$ leads to:

$$H = 2\epsilon_0 L \sum_k \omega_k^2 \left(\left[A_k^R\right]^2 + \left[A_k^I\right]^2 \right). \tag{B.5}$$

Here the coefficients have been decomposed into its real and imaginary part: $A_k = A_k^R + iA_k^I$. This shows that the electromagnetic field can be seen as being made up of a collection of harmonic oscillators, where the harmonic oscillator of mode k is given by:

$$H_k = 2\epsilon_0 L \omega_k^2 \left(\left[A_k^R\right]^2 + \left[A_k^I\right]^2 \right). \tag{B.6}$$

Each k then labels an independent degree of freedom for the bath. Now let $A_k(t) = A_k \mathrm{e}^{-i\omega_k t}$, such that:

$$A_k^R(t) = A_k^R \cos(\omega_k t) + A_k^I \sin(\omega_k t), \text{ and } A_k^I(t) = A_k^I \cos(\omega_k t) - A_k^R \sin(\omega_k t).$$

Hence:

$$\partial_t A_k^R(t) = \omega_k A_k^I(t), \text{ and } \partial_t A_k^I(t) = -\omega_k A_k^R(t). \tag{B.7}$$

Eqs. (B.6) and (B.7) suggest that A_k^R and A_k^I are canonically conjugate variables except for some constant λ_k, such that $\tilde{A}_k^I = \lambda_k A_k^I$ is the true canonically conjugate variable to A_k^R. Hence, they obey Hamilton's equations ([18] p. 176):

$$\frac{\partial H_k}{\partial A_k^R} = -\partial_t \tilde{A}_k^I \text{ and } \frac{\partial H_k}{\partial \tilde{A}_k^I} = \partial_t A_k^R. \tag{B.8}$$

These equations provide a solution for H_k given by:

$$H_k = \frac{\lambda_k \omega_k}{2} \left(A_k^R\right)^2 + \frac{\omega_k}{2\lambda_k} \left(\tilde{A}_k^I\right)^2 = \frac{\lambda_k \omega_k}{2} \left(\left[A_k^R\right]^2 + \left[A_k^I\right]^2\right). \tag{B.9}$$

Comparing this with Eq. (B.6) identifies $\lambda_k = 4\epsilon_0 L \omega_k$.

The canonically conjugate variables A_k^R and $\tilde{A}_k^I$ obey the classical relation ([18] p. 198):

$$\left[\tilde{A}_k^I, A_q^R\right]_{PB} = -\delta_{kq}, \tag{B.10}$$

where the subscript PB denotes Poisson brackets ([18] p. 197). The canonical quantization prescription is to replace the Poisson brackets by the quantum mechanical commutator accordingly ([18] p. 201):

$$\left[\tilde{A}_k^I, A_q^R\right]_{PB} \longrightarrow \frac{1}{i\hbar} \left[\tilde{A}_k^I, A_q^R\right]. \tag{B.11}$$

Hence, the commutation relation between the now quantum mechanical operators A_k^R and A_k^I is:

$$\left[A_k^I, A_q^R\right] = -i\delta_{kq} \frac{\hbar}{4\epsilon_0 L \omega_k}. \tag{B.12}$$

By comparing Eq. (B.9) with the usual Hamiltonian for the harmonic oscillator in terms of momentum and position, $H = m\omega^2 x^2/2 + p^2/2m$, the mass of mode k is found as $m_k = \lambda_k/\omega_k$. Hence, the bosonic creation and annihilation operators for the electromagnetic mode k are defined as ([10] p. 89):

$$b_k^\dagger = \sqrt{\frac{\lambda_k}{2\hbar}} \left(A_k^R - i\frac{\tilde{A}_k^I}{\lambda_k}\right) = \sqrt{\frac{2\epsilon_0 L \omega_k}{\hbar}} \left(A_k^R - iA_k^I\right) \text{ and} \tag{B.13}$$

$$b_k = \sqrt{\frac{2\epsilon_0 L \omega_k}{\hbar}} \left(A_k^R + iA_k^I\right). \tag{B.14}$$

In this particular example the creation operator $b_k^\dagger$ represents the creation of a photon in mode k, and the annihilation operator b_k represents the annihilation of a photon in mode k. With these the variables A_k^R and A_k^I can be expressed as:

$$A_k^R = \sqrt{\frac{\hbar}{8\epsilon_0 L\omega_k}}\left(b_k^\dagger + b_k\right) \text{ and} \tag{B.15}$$

$$A_k^I = i\sqrt{\frac{\hbar}{8\epsilon_0 L\omega_k}}\left(b_k^\dagger - b_k\right). \tag{B.16}$$

Hence, the quantized expansion coefficients are given by:

$$A_k = A_k^R + iA_k^I = \sqrt{\frac{\hbar}{2\epsilon_0 L\omega_k}}b_k. \tag{B.17}$$

Finally, plugging this into Eqs. (B.2) and (B.3) gives the quantized electric and magnetic fields:

$$\mathbf{E}(x,t) = i\sum_k \sqrt{\frac{\hbar\omega_k}{2\epsilon_0 L}}\left(b_k \mathrm{e}^{i(kx-\omega_k t)} - b_k^\dagger \mathrm{e}^{-i(kx-\omega_k t)}\right)\hat{y} \text{ and} \tag{B.18}$$

$$\mathbf{B}(x,t) = \frac{i}{c}\sum_k \sqrt{\frac{\hbar\omega_k}{2\epsilon_0 L}}\left(b_k \mathrm{e}^{i(kx-\omega_k t)} - b_k^\dagger \mathrm{e}^{-i(kx-\omega_k t)}\right)\hat{z}. \tag{B.19}$$

Before moving on, observe how the bath Hamiltonian can be expressed in terms of the bosonic creation and annihilation operators:

$$b_k^\dagger b_k = \frac{2\epsilon_0 L\omega_k}{\hbar}\left(\left[A_k^R\right]^2 + \left[A_k^I\right]^2 - i\left[A_k^I, A_k^R\right]\right) = \frac{H_k}{\hbar\omega_k} - \frac{1}{2}.$$

Hence:

$$H_{\mathcal{B}} = \sum_k H_k = \hbar\sum_k \omega_k\left(b_k^\dagger b_k + \frac{1}{2}\right). \tag{B.20}$$

Here the composition $b_k^\dagger b_k$ counts the number of photons in mode k, sometimes called the occupation number n_k ([11] p. 13).

B.2 Derivation of the bath correlation function

Notice that the electric and magnetic fields of Eqs. (B.18) and (B.19) are perpendicularly polarized. Hence, it is trivial to see that their correlation vanishes. It is also apparent that the correlation between magnetic fields will be less than the correlation between electric fields with the same spatial and temporal separation by a factor of c^2, and so it is sufficient to investigate the correlation function for two electric field operators:

$$J_{\alpha\beta}(t-t') = \mathrm{tr}_{\mathcal{B}}\left[\tilde{E}(x_\alpha,t)\tilde{E}(x_\beta,t')\rho_{\mathcal{B}}\right]. \tag{B.21}$$

Observe that the electric field operator in Eq. (B.18) was derived in the Heisenberg picture and so it directly translates into the interaction picture of the system and bath.

The density matrix can be written, with reference to statistical mechanics, as $\rho_{\mathcal{B}} = \mathrm{e}^{-\beta H_{\mathcal{B}}}/Z$, where $Z = \mathrm{tr}_{\mathcal{B}}(\mathrm{e}^{-\beta H_{\mathcal{B}}})$ is the partition function for the bath ([10] p. 189 and [19] p. 178). Before moving on a convenient property of the partition function is presented here. First of all, the degrees of freedom of the bath are given by the modes k and the occupation number of each mode n_k. Hence, the eigenstates of the bath are conveniently expressed in the occupation number basis which span out the Fock space $|n_1, n_2, n_3, ..., n_k, ...\rangle$, such that([11] ps. 10-13):

$$b_k^\dagger b_k \left|n_1, n_2, n_3, ..., n_k, ...\right\rangle = n_k \left|n_1, n_2, n_3, ..., n_k, ...\right\rangle . \tag{B.22}$$

Thus, the partition function can be expressed as:

$$\begin{aligned}
Z &= \sum_{n_1 n_2 ...} \langle n_1, n_2, n_3, ..., n_k, ...| \, \mathrm{e}^{-\beta \sum_k H_k} \left|n_1, n_2, n_3, ..., n_k, ...\right\rangle \\
&= \sum_{n_1 n_2 ...} \langle n_1, n_2, n_3, ..., n_k, ...| \prod_k \mathrm{e}^{-\beta H_k} \left|n_1, n_2, n_3, ..., n_k, ...\right\rangle \\
&= \sum_{n_1 n_2 ...} \prod_k \langle n_k| \, \mathrm{e}^{-\beta H_k} \left|n_k\right\rangle \\
&= \prod_k \sum_{n_k=0}^{\infty} \langle n_k| \, \mathrm{e}^{-\beta H_k} \left|n_k\right\rangle \\
&= \prod_k Z_k,
\end{aligned}$$

where $Z_k \equiv \sum_{n_k} \langle n_k| \, \mathrm{e}^{-\beta H_k} \left|n_k\right\rangle$ traces over the degrees of freedom solely in mode k. Hence, the partition function can be expressed as a product of the partition functions for the independent degrees of freedom of the bath ([19] pp. 122-3 and 180). Observe furthermore, that([19] p. 181):

$$Z_k = \sum_{n_k=0}^{\infty} \mathrm{e}^{-\beta\hbar\omega_k\left(n_k+\frac{1}{2}\right)} = \mathrm{e}^{-\beta\hbar\omega_k/2} \sum_{n_k=0}^{\infty} \left(\mathrm{e}^{-\beta\hbar\omega_k}\right)^{n_k} = \frac{\mathrm{e}^{-\beta\hbar\omega_k/2}}{1-\mathrm{e}^{-\beta\hbar\omega_k}}. \tag{B.23}$$

For the last equality it has been used that the sum is a convergent geometric series, because the value of the exponential is always less than one, as ω_k is positive for all k.

The product of the electromagnetic field operators can be written as:

$$\begin{aligned}
E(x_\alpha, t)E(x_\beta, t') = \frac{\hbar}{2\epsilon_0 L} \sum_{kq} \sqrt{\omega_k \omega_q} \Big[& b_k b_q^\dagger \mathrm{e}^{i\left(kx_\alpha - qx_\beta - \omega_k t + \omega_q t'\right)} + b_k^\dagger b_q \mathrm{e}^{-i\left(kx_\alpha - qx_\beta - \omega_k t + \omega_q t'\right)} \\
& - b_k b_q \mathrm{e}^{i\left(kx_\alpha + qx_\beta - \omega_k t - \omega_q t'\right)} - b_k^\dagger b_q^\dagger \mathrm{e}^{-i\left(kx_\alpha + qx_\beta - \omega_k t - \omega_q t'\right)} \Big]
\end{aligned}$$

When tracing over the bath degrees of freedom the last two terms inside the sum vanish, and the first two terms only contribute for $k = q$. This and the commutation relation

of the annihilation and creation operators lead to:

$$J_{\alpha\beta}(t-t') = \frac{\hbar}{2\epsilon_0 LZ}\mathrm{tr}_{\mathcal{B}}\Bigg(\sum_k \omega_k \Big[\mathrm{e}^{i\left(k[x_\alpha - x_\beta]-\omega_k[t-t']\right)} + 2\cos\left(k[x_\alpha - x_\beta]-\omega_k[t-t']\right) b_k^\dagger b_k\Big]\mathrm{e}^{-\beta H_{\mathcal{B}}}\Bigg)$$

Taking the trace yields:

$$J_{\alpha\beta}(t-t') = \frac{\hbar}{2\epsilon_0 LZ}\sum_{n_1 n_2 \ldots}\sum_k \omega_k \Big[\mathrm{e}^{i\left(k[x_\alpha - x_\beta]-\omega_k[t-t']\right)} + 2\cos\left(k[x_\alpha - x_\beta]-\omega_k[t-t']\right) n_k\Big] \times \prod_{k'} \mathrm{e}^{-\beta\hbar\omega_{k'}\left(n_{k'}+\frac{1}{2}\right)}.$$

Here emerges a sum similar to the geometric series evaluated above:

$$\sum_{n_k} n_k \mathrm{e}^{-\beta\hbar\omega_k\left(n_k+\frac{1}{2}\right)} = \mathrm{e}^{-\beta\hbar\omega_k/2}\sum_{n_k} n_k \mathrm{e}^{-\beta\hbar\omega_k n_k}.$$

In fact its value can be found via the derivative of the geometric series:

$$\frac{\partial}{\partial a}\left(\sum_n \mathrm{e}^{-an}\right) = \frac{\partial}{\partial a}\left(\frac{1}{1-\mathrm{e}^{-a}}\right) \Rightarrow \sum_n n\mathrm{e}^{-an} = \frac{\mathrm{e}^{-a}}{(1-\mathrm{e}^{-a})^2}. \tag{B.24}$$

Hence, using Eq. (B.23) gives:

$$\sum_{n_k} n_k \mathrm{e}^{-\beta\hbar\omega_k\left(n_k+\frac{1}{2}\right)} = \mathrm{e}^{-\beta\hbar\omega_k/2} Z_k^2.$$

Plugging this into the correlation function leads to:

$$J_{\alpha\beta}(t-t') = \frac{\hbar}{2\epsilon_0 L}\sum_k \omega_k \left[\mathrm{e}^{i\left(k[x_\alpha - x_\beta]-\omega_k[t-t']\right)} + 2\cos\left(k[x_\alpha - x_\beta]-\omega_k[t-t']\right)\mathrm{e}^{-\beta\hbar\omega_k/2} Z_k\right].$$

Now observe:

$$\mathrm{e}^{-\beta\hbar\omega_k/2} Z_k = \frac{\mathrm{e}^{-\beta\hbar\omega_k}}{1-\mathrm{e}^{-\beta\hbar\omega_k}} = \frac{1}{\mathrm{e}^{\beta\hbar\omega_k}-1} \equiv n_B(\beta\hbar\omega_k),$$

where $n_B(\beta\hbar\omega_k)$ is the Bose occupation factor for mode k. It is interpreted as the number of photons occupying the kth mode([20] p. 8).

This gives the final expression for the correlation function of a bath of finite size L:

$$J_{\alpha\beta}(t-t') = \frac{\hbar}{2\epsilon_0 L}\sum_k \omega_k \left[\mathrm{e}^{i\left(k[x_\alpha - x_\beta]-\omega_k[t-t']\right)} + 2\cos\left(k[x_\alpha - x_\beta]-\omega_k[t-t']\right) n_B\left(\beta\hbar\omega_k\right)\right]. \tag{B.25}$$

B.3 The bath spectral function

Before finding the bath spectral function as the Fourier transform of Eq. (B.25) it is convenient to split the sum over k into positive and negative k:

$$J_{\alpha\beta}(t-t') = \frac{\hbar}{2\epsilon_0 L}\left(\sum_{k=0}^{\infty}\omega_k\left[\mathrm{e}^{i\left(k[x_\alpha-x_\beta]-\omega_k[t-t']\right)}+2\cos\left(k[x_\alpha-x_\beta]-\omega_k[t-t']\right)n_B\left(\beta\hbar\omega_k\right)\right]\right.$$
$$\left.+\sum_{k=-\infty}^{0}\omega_k\left[\mathrm{e}^{i\left(-|k|[x_\alpha-x_\beta]-\omega_k[t-t']\right)}+2\cos\left(-|k|[x_\alpha-x_\beta]-\omega_k[t-t']\right)n_B\left(\beta\hbar\omega_k\right)\right]\right).$$

By using that $\omega_k = |k|c$ and defining $\tilde{t} \equiv t - t'$ and $\tilde{x} \equiv x_\alpha - x_\beta$ the above can be rewritten as:

$$J_{\alpha\beta}\left(\tilde{t}\right) = \frac{\hbar}{2\epsilon_0 L}\sum_{k=0}^{\infty}\omega_k\left[\mathrm{e}^{-i\omega_k\left(\tilde{t}-\frac{\tilde{x}}{c}\right)}+2\cos\left(\omega_k\left[\tilde{t}-\frac{\tilde{x}}{c}\right]\right)n_B\left(\beta\hbar\omega_k\right)\right.$$
$$\left.+\,\mathrm{e}^{-i\omega_k\left(\tilde{t}+\frac{\tilde{x}}{c}\right)}+2\cos\left(\omega_k\left[\tilde{t}+\frac{\tilde{x}}{c}\right]\right)n_B\left(\beta\hbar\omega_k\right)\right].$$

Hence, the bath spectral function is given by:

$$J_{\alpha\beta}(\omega) = \frac{\hbar}{\epsilon_0 L}\sum_{k=0}^{\infty}\omega_k\cos\left(\frac{\omega_k\tilde{x}}{c}\right)\Big\{\delta(\omega+\omega_k)n_B(\beta\hbar\omega_k)+\delta(\omega-\omega_k)\big[1+n_B(\beta\hbar\omega_k)\big]\Big\}. \tag{B.26}$$

This function can be interpreted as a measure of how well the bath exchanges energy with the system, where the argument ω is the energy received by the bath. Notice that it has peaks only at $\omega = \pm\omega_k$ and is zero otherwise, i.e. it can only exchange and amount of energy that corresponds to a valid photonic mode in the bath. Let ω_i be a positive energy corresponding to the ith mode and observe that:

$$\frac{J(\omega_i)}{J(-\omega_i)} = \frac{1+n_B(\beta\hbar\omega_i)}{n_B(\beta\hbar\omega_i)} = \mathrm{e}^{\beta\hbar\omega_i}.$$

Hence can be concluded that it is more likely that the system emits energy into the bath rather than absorbs energy from the bath, especially in the case of a very cold bath where $\beta \to \infty$. In fact $T = 0$ yields $n_B(\beta\hbar\omega_i) = 0$, and Eq. (B.26) shows that the bath can only receive energy in that case. Conversely, for $T \to \infty$ the system emits and absorbs energy at an equal rate.

B.4 Continuous spectrum of modes

In most physical cases the bath is much larger than the system, and so it is natural to allow the size of the bath to go to infinity: $L \to \infty$. When this happens the photonic

modes approach a continuum, and the sum over k can be converted into an integral according to the prescription ([20] p. 10):

$$\sum_{k=0}^{\infty} \to \frac{1}{\Delta k}\int_0^{\infty} \mathrm{d}k, \tag{B.27}$$

where Δk is the distance between adjacent modes in k-space giving $\Delta k = \pi/L$. Additionally, the variable of integration is conveniently changed using $k = \omega_k/c$:

$$\begin{aligned} J_{\alpha\beta}(\omega) &= \frac{\hbar}{\pi\epsilon_0 c}\int_0^{\infty} \mathrm{d}\omega_k \omega_k \cos\left(\frac{\omega_k \tilde{x}}{c}\right)\Big\{\delta(\omega+\omega_k)n_B(\beta\hbar\omega_k) + \delta(\omega-\omega_k)\big[1+n_B(\beta\hbar\omega_k)\big]\Big\} \\ &= \frac{\hbar\omega}{\pi\epsilon_0 c}\cos\left(\frac{\omega\tilde{x}}{c}\right)\Big\{ -\theta(-\omega)n_B(-\beta\hbar\omega) + \theta(\omega)\big[1+n_B(\beta\hbar\omega)\big]\Big\}. \end{aligned}$$

Here once again the step function $\theta(\omega)$ has been introduced. The expression in the curly brackets might suggest that the bath spectral function is not continuous in $\omega = 0$, but observe:

$$\begin{aligned} \lim_{\omega\to 0^+} J_{\alpha\beta}(\omega) &= \frac{\hbar}{\pi\epsilon_0 c}\lim_{\omega\to 0^+}\frac{\omega \mathrm{e}^{\beta\hbar\omega}}{\mathrm{e}^{\beta\hbar\omega}-1} = \frac{\hbar}{\pi\epsilon_0 c}\lim_{\omega\to 0^+}\frac{\mathrm{e}^{\beta\hbar\omega}+\beta\hbar\omega\mathrm{e}^{\beta\hbar\omega}}{\beta\hbar\mathrm{e}^{\beta\hbar\omega}} = \frac{1}{\pi\epsilon_0 c\beta} \text{ and} \\ \lim_{\omega\to 0^-} J_{\alpha\beta}(\omega) &= -\frac{\hbar}{\pi\epsilon_0 c}\lim_{\omega\to 0^-}\frac{\omega}{\mathrm{e}^{-\beta\hbar\omega}-1} = -\frac{\hbar}{\pi\epsilon_0 c}\lim_{\omega\to 0^-}\frac{1}{-\beta\hbar\mathrm{e}^{-\beta\hbar\omega}} = \frac{1}{\pi\epsilon_0 c\beta}. \end{aligned}$$

Since these two limits are equal the step functions in the spectral function can be replaced with an overall factor of $1/2$. With that, the bath spectral function reduces to:

$$J_{\alpha\beta}(\omega) = \frac{\hbar\omega}{\pi\epsilon_0 c}\frac{\cos\left(\frac{\omega\tilde{x}}{c}\right)}{1-\mathrm{e}^{-\beta\hbar\omega}}. \tag{B.28}$$

Now the correlation function for a continuous spectrum can be found as the Fourier transform of the above, but this function clearly diverges for large ω, and so the immediate Fourier transform will yield an unphysical result. It is therefore necessary to define a cutoff frequency ω_c, such that the spectral function is suppressed for frequencies above this. Instead of a sharp cutoff in the limits of integration of the Fourier transform it will be introduced as a smooth cutoff like so:

$$J_{\alpha\beta}(\omega) \to \frac{\omega_c^2}{\omega^2+\omega_c^2}J_{\alpha\beta}(\omega). \tag{B.29}$$

This is not only analytically convenient, there is also physical justification for such a procedure. As the frequency of a mode increases, its wavelength decreases, and the wavelength determines what the mode can interact with. If the system interacting with the bath is a hydrogen atom, then when the wavelength of the modes become smaller than the diameter of the atom its interaction starts to decrease. If a denotes the diameter of the atom, then the cutoff frequency can be estimated as $\omega_c = 2\pi c/a$.

The correlation function is thus given by:

$$J_{\alpha\beta}\left(\tilde{t}\right) = \frac{\hbar\omega_c^2}{2\pi\epsilon_0 c}\int_{-\infty}^{\infty}\mathrm{d}\omega\left[f(\omega,s_+)+f(\omega,s_-)\right], \text{ where } f(\omega,s_\pm) = \frac{\omega}{\omega^2+\omega_c^2}\frac{\mathrm{e}^{-i\omega s_\pm}}{1-\mathrm{e}^{-\beta\hbar\omega}}, \tag{B.30}$$

and $s_\pm \equiv \tilde{t} \pm \tilde{x}/c$. As such the integral can be evaluated simultaneously for s_- and s_+.

For $s_\pm < 0$ $f(\omega, s_\pm)$ tends to zero on a semi-circular contour in the *upper* half-plane, in which case the value of the integral can be found by *counter-clockwise* integration along this semi-circular contour. Its value is given by $2\pi i$ times the sum of the residues of the poles in the upper half-plane([21] p. 592). In this region the integrand has simple poles at $\omega = i\omega_c$ and $\omega = i2\pi n/\beta\hbar$ for $n \in \{1, 2, 3, ...\}$(recall that $f(\omega, s_\pm)$ is analytical in $\omega = 0$). The values of these residues are given by([21] p. 573):

$$R(i\omega_c) = \lim_{\omega \to i\omega_c} [(\omega - i\omega_c) f(\omega, s_\pm)] = \frac{1}{2} \frac{\mathrm{e}^{\omega_c s_\pm}}{1 - \mathrm{e}^{-i\beta\hbar\omega_c}} \text{ and}$$
$$R\left(i\frac{2\pi n}{\beta\hbar}\right) = \lim_{\omega \to i\frac{2\pi n}{\beta\hbar}} \left[\left(\omega - i\frac{2\pi n}{\beta\hbar}\right) f(\omega, s_\pm)\right].$$

This last limit can be found by defining $\delta \equiv \omega - i2\pi n/\beta\hbar$, so that $\omega = \delta + i2\pi n/\beta\hbar$. Hence:

$$\begin{aligned} R\left(i\frac{2\pi n}{\beta\hbar}\right) &= \frac{i\frac{2\pi n}{\beta\hbar}}{-\frac{4\pi^2 n^2}{\beta^2\hbar^2} + \omega_c^2} \mathrm{e}^{\frac{2\pi n s_\pm}{\beta\hbar}} \lim_{\delta \to 0} \frac{\delta}{1 - \mathrm{e}^{-\beta\hbar\left(\delta + i\frac{2\pi n}{\beta\hbar}\right)}} \\ &= \frac{i2\pi n}{\beta^2\hbar^2\omega_c^2 - 4\pi^2 n^2} \mathrm{e}^{\frac{2\pi n s_\pm}{\beta\hbar}}. \end{aligned}$$

And so the integral for $s_\pm < 0$ is:

$$\begin{aligned} \int_{-\infty}^{\infty} \mathrm{d}\omega f(\omega, s_\pm) &= 2\pi i \left[\frac{1}{2} \frac{\mathrm{e}^{\omega_c s_\pm}}{1 - \mathrm{e}^{-i\beta\hbar\omega_c}} + \sum_{n=1}^{\infty} \frac{i2\pi n}{\beta^2\hbar^2\omega_c^2 - 4\pi^2 n^2} \mathrm{e}^{\frac{2\pi n s_\pm}{\beta\hbar}}\right] \\ &= 2\pi \left[\frac{i}{2} \frac{\mathrm{e}^{\omega_c s_\pm}}{1 - \mathrm{e}^{-i\beta\hbar\omega_c}} - \sum_{n=1}^{\infty} \frac{2\pi n}{\beta^2\hbar^2\omega_c^2 - 4\pi^2 n^2} \mathrm{e}^{\frac{2\pi n s_\pm}{\beta\hbar}}\right]. \end{aligned}$$

For $s_\pm > 0$ $f(\omega, s_\pm)$ tends to zero on a semi-circular contour in the *lower* half-plane, and so the integral can be evaluated by *clockwise* contour integration along this semi-circle. In this case its value is given by $-2\pi i$ times the residues of the poles in the lower half-plane. The poles here are at $\omega = -i\omega_c$ and $\omega = -i2\pi n/\beta\hbar$. Similarly to before, the residues are given by:

$$R(-i\omega_c) = \frac{1}{2} \frac{\mathrm{e}^{-\omega_c s_\pm}}{1 - \mathrm{e}^{i\beta\hbar\omega_c}} \text{ and}$$
$$R\left(-i\frac{2\pi n}{\beta\hbar}\right) = \frac{-i2\pi n}{\beta^2\hbar^2\omega_c^2 - 4\pi^2 n^2} \mathrm{e}^{-\frac{2\pi n s_\pm}{\beta\hbar}}.$$

Hence the integral for $s_\pm > 0$ is:

$$\int_{-\infty}^{\infty} \mathrm{d}\omega f(\omega, s_\pm) = 2\pi \left[\frac{-i}{2} \frac{\mathrm{e}^{-\omega_c s_\pm}}{1 - \mathrm{e}^{i\beta\hbar\omega_c}} - \sum_{n=1}^{\infty} \frac{2\pi n}{\beta^2\hbar^2\omega_c^2 - 4\pi^2 n^2} \mathrm{e}^{-\frac{2\pi n s_\pm}{\beta\hbar}}\right].$$

Now the cutoff frequency can be got rid off again by allowing $\omega_c \to \infty$. In both cases, $s_\pm > 0$ and $s_\pm < 0$, the first term in the brackets above vanishes due to the exponential

decay with ω_c. The sum is not so trivial. For terms with small n it is straight forward to find the limit:

$$\lim_{\omega_c\to\infty}\frac{2\pi n\omega_c^2}{\beta^2\hbar^2\omega_c^2-4\pi^2n^2}\mathrm{e}^{-\frac{2\pi n s_\pm}{\beta\hbar}}=\lim_{\omega_c\to\infty}\frac{2\pi n}{\beta^2\hbar^2-4\pi^2n^2/\omega_c^2}\mathrm{e}^{-\frac{2\pi n s_\pm}{\beta\hbar}}=\frac{2\pi n}{\beta^2\hbar^2}\mathrm{e}^{-\frac{2\pi n s_\pm}{\beta\hbar}}.$$

Here the factor of ω_c^2 in the numerator comes from the correlation function as can be seen in Eq. (B.30). For terms with large n, such that $n\approx\beta\hbar\omega_c$, the limit above is not valid. However, in that case there is another exponential decay with ω_c, and so these terms have a vanishing contribution to the sum.

Using all this for the correlation function yields:

$$J_{\alpha\beta}(\tilde{t})=-\frac{2\pi}{\beta^2\hbar\epsilon_0 c}\sum_{n=1}^{\infty}\left(n\mathrm{e}^{-\frac{2\pi n|s_-|}{\beta\hbar}}+n\mathrm{e}^{-\frac{2\pi n|s_+|}{\beta\hbar}}\right).$$

Adding the term where $n=0$ to the sum contributes nothing, and so it can be evaluated according to Eq. (B.24):

$$\sum_{n=0}^{\infty}n\mathrm{e}^{-\frac{2\pi n|s_\pm|}{\beta\hbar}}=\frac{\mathrm{e}^{-\frac{2\pi|s_\pm|}{\beta\hbar}}}{\left(1-\mathrm{e}^{-\frac{2\pi|s_\pm|}{\beta\hbar}}\right)^2}=\frac{1}{\left(\mathrm{e}^{\frac{\pi|s_\pm|}{\beta\hbar}}-\mathrm{e}^{-\frac{\pi|s_\pm|}{\beta\hbar}}\right)^2}=\frac{1}{4\sinh^2\left(\frac{\pi}{\beta\hbar}|s_\pm|\right)}.$$

Finally, the correlation function is derived:

$$J_{\alpha\beta}(t-t')=-\frac{\pi}{2\beta^2\hbar\epsilon_0 c}\left(\frac{1}{\sinh^2\left(\frac{\pi}{\beta\hbar}\left|t-t'-\frac{x_\alpha-x_\beta}{c}\right|\right)}+\frac{1}{\sinh^2\left(\frac{\pi}{\beta\hbar}\left|t-t'+\frac{x_\alpha-x_\beta}{c}\right|\right)}\right). \tag{B.31}$$

An important observation to make here is, that this correlation function diverges at $t-t'=\pm(x_\alpha-x_\beta)/c$. In other words, when the temporal separation of the electromagnetic field operators is equal to the time it takes for a photon to traverse the spatial separation of the field operators, then the correlation of the field operators diverges. This is in fact perfectly natural, as what is being measured is the correlation of an electromagnetic field operator with itself only some time and distance apart. This is a consequence of the idealized model, namely a 1-dimensional cavity of electromagnetic modes, because the fields transmit perfectly across a line without loss no matter the distance they travel. This poses a problem for the ULE since for large spatial separations the bath will have perfect correlations at non-zero times $(x_\alpha-x_\beta)/c$, and so the bath correlations cannot be said to decay rapidly on the timescale of system-bath interactions Γ^{-1}. Hence, the correlation function in Eq. (B.31) represents a "bad" Markovian bath.

In a more realistic physical setting, such as two superconducting qubits on a metallic chip (the one located at $\mathbf{r}_\alpha$, the other at $\mathbf{r}_\beta$), the space is first of all 3-dimensional. Hence, when an electromagnetic wave scatters off the one qubit, its amplitude will have decreased by a factor of $|\mathbf{r}_\alpha-\mathbf{r}_\beta|$ by the time it reaches the second qubit[22]. Besides, there will typically be other impurities in the chip, which the wave will scatter off further

weakening its field strength. For simplicity, in this thesis the correlation between bath operators at different localities will on the basis of the arguments above be assumed to have decayed so much with the distance that they are virtually uncorrelated compared to the correlation of bath operators at the same locality. This assumption is the same as the approximation that $J_{\alpha\beta}(t-t') = 0$ for $\alpha \neq \beta$, which means that the matrix $\mathbf{J}(t)$ is diagonal, which in turn means that $\mathbf{g}(t)$ is diagonal. This greatly simplifies the expression for the jump operator, as the sum over noise channels in Eq. (4.19) only has one term, which is the term corresponding to the noise channel that the jump operator is itself representing. This approximation is further supported by the fact, that for $t - t' = 0$ and large spatial separation $|x_\alpha - x_\beta|$ the correlation function in Eq. (B.31) decays exponentially with the separation on a characteristic decay length of $\beta\hbar c/2\pi$, which for room temperature is on the order of micrometers.